AN ABSTRACT OF THE THESIS OF

Witawat Wijaranakula for the degree of Doctor of Philosophy

in Mechanical Engineering presented on April 21, 1986

Title : Heat Treatment Characteristics of Heavily Doped Epitaxial Silicon Materials

Redacted for privacy

Abstract approved: _____
Peter M. Burke

Nucleation and growth kinetics of oxygen precipitates and bulk defects in epitaxial silicon wafers were investigated. Low temperature nucleation heat treatments were applied to the well characterized epitaxial silicon wafers before and after the epitaxial deposition processing. Subsequently the wafers were heat treated at a high temperature.

In the case of post-epitaxial nucleation heat treatment it was found that the heat treatment ambients have an effect on the growth of oxygen precipitates. However, the application of nucleation heat treatment can suppress this effect. The maximum bulk defect density in as-received epitaxial materials is limited by the epitaxial deposition process.

In the case of pre-epitaxial annealing the effect of the epitaxial deposition heat treatment can be retarded and a higher bulk defect density can be achieved. The effects of thermal history were also observed.

The results indicate that the heterogeneous nucleation process is predominant in epitaxial silicon materials.

Heat Treatment Characteristics of Heavily Doped Epitaxial Silicon Materials

by

Witawat Wijaranakula

A THESIS

submitted to

Oregon State University

in partial fulfillment of
the requirements for the
degree of

Doctor of Philosophy

Completed April 21, 1986
Commencement June 1986

APPROVED:

Redacted for privacy

Associate Professor in Mechanical Engineering in Charge of Major

Redacted for privacy

Head of Mechanical Engineering

Redacted for privacy

Dean of Graduate School

Date thesis is presented April 21, 1986

Typed by researcher for Witawat Wijaranakula

ACKNOWLEDGMENT

I extend my sincere appreciation to Dr. Peter M. Burke for his guidance and support during this investigation. Also to be thanked is Professor Len Forbes for his encouragement and help.

I am grateful to Dr. John H. Matlock at SEH America, Inc. for his valuable contribution and support during the fabrication and heat treatment of the epitaxial wafers. Additional thanks go to Dr. James C. Rawers for his timely and critical reading of this manuscript and to Dr. Howard Mollenkopf at SEH America, Inc. for his helpful discussion.

I am deeply indebted to my parents for their faith and encouragement.

This work was sponsored in part by the Intel Research Council and SEH-America, Inc.

TABLE OF CONTENTS

Table of Contents -- Continued

Table of Contents -- Continued

LIST OF FIGURES

LIST OF FIGURES - continued

LIST OF FIGURES - continued

LIST OF FIGURES - continued

Heat Treatment Characteristics of Heavily Doped Epitaxial Silicon Materials

I. INTRODUCTION

Silicon has been a starting material for fabrication of integrated circuit devices for over 20 years. During these years much research work has been conducted, and most of the basic understanding of heat treatments and defect formation mechanisms found in silicon material is considered to be very satisfactory. However, more research work is still needed because of rapid change in integrated circuit device design and processing procedures. In ultra-large scale integrated circuit (ULSI) fabrication, for example, large silicon wafers, up to 200 mm in diameter, with defect-free surfaces are desired as the starting material. This requirement is very difficult to meet because the wafer thickness for large wafers must be increased so that the wafers can be handled without introducing any damage during device processing. In such silicon wafers the defect-free surface condition can be maintained only by employing effective gettering methods. The currently employed external gettering methods, such as the back-side damage process, may not be effective enough. This is because the diffusion distance between the metallic contaminations at the front side of the wafer and the back-side damages has been significantly increased. Furthermore, back-side damage has its own limitations, because a heavily damaged back-side leads to a warpage control problem of the wafer.

An alternative solution for this problem is internal gettering, ultilizing oxygen precipitation and proper heat treatment cycles. In the past several years oxygen precipitation in silicon material has

become an interesting subject of study. This is because bulk stacking faults originating from the oxide precipitates are believed to have the gettering effect on heavy metal impurities and point defects. However, heavy precipitation in silicon wafers could have negative effects, such as warpage and current leakage. A controllable as well as reproducible internal gettering process is, therefore, the goal of this investigation.

In advanced MOS (Metal-Oxide-Semiconductor) silicon technology, a thin layer (approximately 10 to 15 microns) of silicon with low doping concentration is deposited on a heavily doped silicon substrate wafer by a technique called chemical vapor deposition (CVD). This process is also known as the epitaxial deposition process. Epitaxial silicon wafers are widely used as a starting material for high density CMOS devices because of their superior latch-up characteristics. Furthermore, an epitaxial layer provides good protection against surface defects associated with grown-in defects. The current understanding of oxygen precipitation in heavily doped silicon material used for fabrication of epitaxial silicon wafers is considered to be unsatisfactory. One of the reasons is because point defects which are incorporated into the silicon matrix during crystal growth interact with the dopant atoms and form unknown complexes. The reaction associated with the complexing process results in a reduction and a non-equilibrium condition of the point defect concentration (vacancies and silicon self-interstitials) in the silicon matrix. Reduction in this manner could lead to either enhancement or retardation of the oxygen precipitate process. Secondly, the epitaxial deposition process normally involves high temperature processing steps

which can have an enormous impact on the final bulk defect density of the epitaxial wafers. It has been found that bulk defect density decreases rapidly after epitaxial deposition processes.

Besides the above mentioned problems in heavily doped silicon material, growth parameters such as pull-rate, length, and thermal history of the crystal ingot also become important factors in oxygen precipitation processes. In order to understand this complicated process all of the possibilities and factors described above have been included in this study.

In the first part of this research work, the effect of heat treatment ambients on nucleation and growth processes of the bulk defects in as-received epitaxial silicon wafers was investigated. The effect of ambients on oxygen out-diffusion and the so called denuded zone or defect free zone formation has been included. The major goal of these studies was to obtain a basis of understanding for the nucleation and growth process of the bulk defects as well as the interaction mechanisms between the point defects and defect nuclei (oxide precipitates) in as-received epitaxial silicon wafers.

In the second part the effect of oxygen concentration, length of the ingot and the thermal history of the substrate wafers were investigated. The impact of epitaxial deposition on nucleation and growth processes of the bulk defects was also included. In order to perform these experiments on the effects of heat treatment, two well characterized silicon crystal ingots, with known oxygen concentration and growth parameters, were grown. Silicon substrate wafers were taken from the different sections of the crystal ingots. Various preanneal heat treatment periods prior to the epitaxial deposition processs were used to nucleate preexisting and additional precipitate nuclei. A test

heat treatment cycle was selected to simulate the heat treatment cycles used in integrated circuit device fabrication processes (CMOS drive-in process). The effect of nucleation heat treatment prior to the heat treatment cycles was also studied.

II. POINT DEFECTS, INTERSTITIAL OXYGEN ATOMS AND OTHER IMPURITIES IN CZ-SILICON CRYSTAL

In silicon material point defects play a major role in the formation of crystal defects and oxygen precipitation during heat treatment. These defects include vacancies, silicon self-interstitials, interstitial oxygen atoms and other impurities such as carbon. They believed to be incorporated into the silicon crystal during the growth process. There is, however, no satisfactory explanation of the incorporation mechanism of self-interstitials and vacancies. One of the reasons is that they can be incorporated in many forms such as single defects or complexes. On the other hand, the incorporation mechanisms of oxygen atoms and other impurities such as carbon seem to be well understood. In the study of the nucleation and growth process of the crystal defects or thermal process induced defects in silicon, the type of point defects and impurities as well as their initial concentrations in an as-grown stage must be identified.

A. Point Defects.

It is well accepted that the intrinsic point defects present in silicon materials are the silicon self-interstitial Si_i and the vacancy V_{Si}. Figures 1 and 2 show the configuration of the intrinsic point defects postulated by Seeger [1]-[2]. In these figures the configuration of the point defects varies with the degree of lattice distortion and the tempurature at which the defects are formed.

To understand how the intrinsic point defects are incorporated into the silicon crystal one should consider the boundary condition at

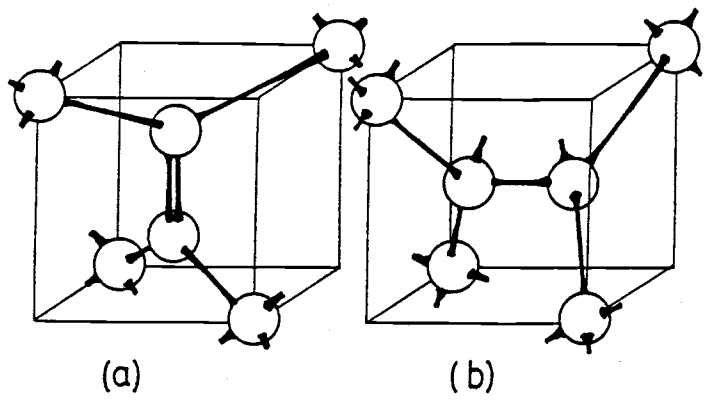

Figure 1: Silicon Sublattice containing Silicon Self-Interstitial
a) Formed at Low Temperature
b) Formed at High Temperature

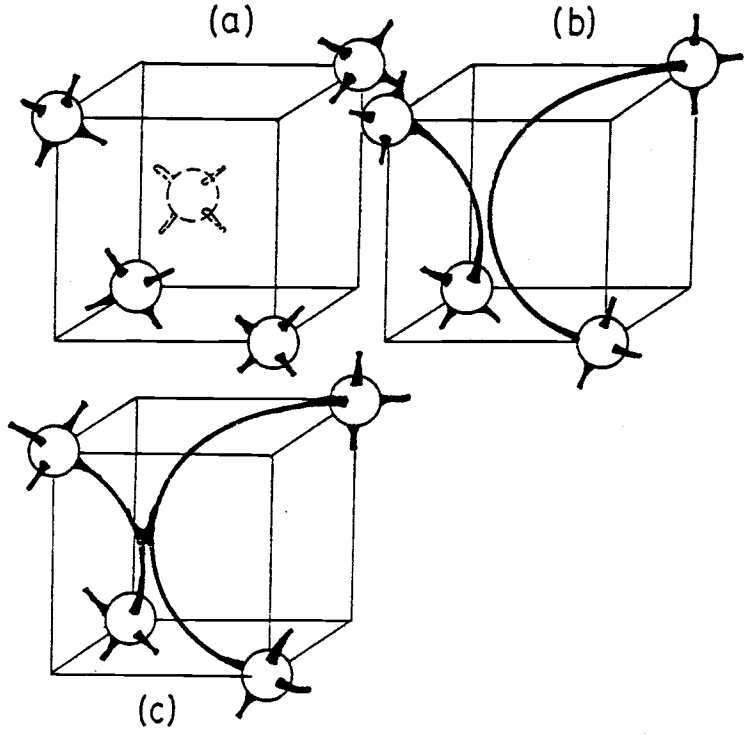

Figure 2: Silicon Sublattice containing Vacancy a) Neutral Vacancy, b) Single-Positive Charged Vacancy and c) Double-Positive Charged Vacancy.

the interface between the silicon melt and the solid crystal. It is presumed that the boundary layer is formed at that interface due to the rotation of the crystal ingot and counter-rotation of the quartz crucible. Here the growth of the silicon crystal proceeds by the transport of silicon atoms from the melt to the edge of the boundary layer, through which it must diffuse before it can be absorbed on the surface. In this case silicon atoms encounter two major problems before they can be attached to the surface:

(a) Effect of Boundary Layer Thickness: Non-uniform boundary layer thickness has an effect on the incorporation rate of the point defects. The boundary layer thickness depends directly upon the relative angular rotation of the crystal and the quartz crucible. Figure 3 shows the simple case of the flow field along the liquid-solid interface during crystal growth. It should be pointed out that at the center of the ingot the boundary layer is considered to be zero due to zero angular velocity, and the laminar boundary layer thickness will increase gradually toward the periphery of the ingot.

Under this condition it can be assumed that the flux of silicon atoms diffusing from the melt into the solid at the center of the crystal ingot is higher than that at the outer periphery of the crystal. Therefore, it is presumed that the possibility of self-interstitials incorporating into the ingot at the center is higher than that at another position on the solid-melt interface.

b) Effect of Crystal Pull-Rate: Swirl-A defects are generated after condensation of the silicon self-interstitials. The formation mecanism of the swirl is already explained elsewhere [5]. It has been found that swirl-A density can be suppressed when the crystal pull-rate is increased [4]. Therefore incorporation of silicon self-

interstitials decreases with increasing crystal pull-rate. From this observation it can be presumed that the crystal pull-rate controls the incorporation rate of the point defects from the melt into the silicon ingot. In the case where commercial silicon crystal ingot is grown it is believed that the pull-rate of the crystal is high enough (approximately 2-3" per hour) to suppress condensation of self-interstitials and therefore swirl-A formation. From this observation it may be reasonable to assume that vacancies predominate the overall point defects which incorporate into the silicon crystal during the growth process. Figure 4 demonstrates the model of point defect incorporation mechanism during the crystal growth process. It should be mentioned that change in crystal pull-rate during the crystal growth process , e.g. the pull-rate has to be decreased due to loss of crystal diameter, will also have an impact on incorporation of the point defects. As mentioned earlier, point defects can incorporate into crystal ingot in various forms, e.g. as a single defect or as a complex. In the case of vacancies the most favorable form of complex is the vacancy-oxygen complex. Figure 5 shows a silicon sublattice containing the vacancy-oxygen complex [6]. From the figure, an oxygen atom occupies the substitutional site of the silicon lattice and is off center in a $\langle 100 \rangle$ direction. The incorporation of oxygen atoms will be discussed in the next chapter.

T. Abe, et.al. [7] have studied the point defect in FZ (Float Zone) silicon and concluded that the point defects existing in an as-grown silicon crystal are vacancies, and their concentration near the center of the crystal ingot is higher than that near the periphery. Figure 6 shows the point defect concentration according to T. Abe.

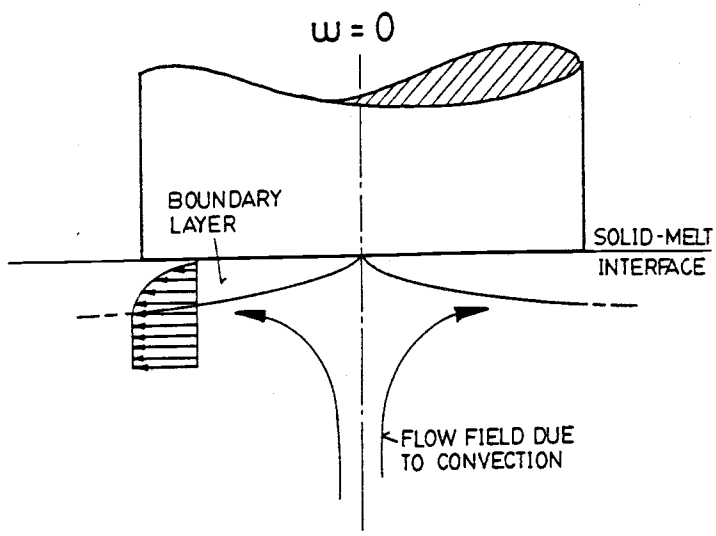

Figure 3: Flow Field along the Solid-Melt Interface during Crystal Growth.

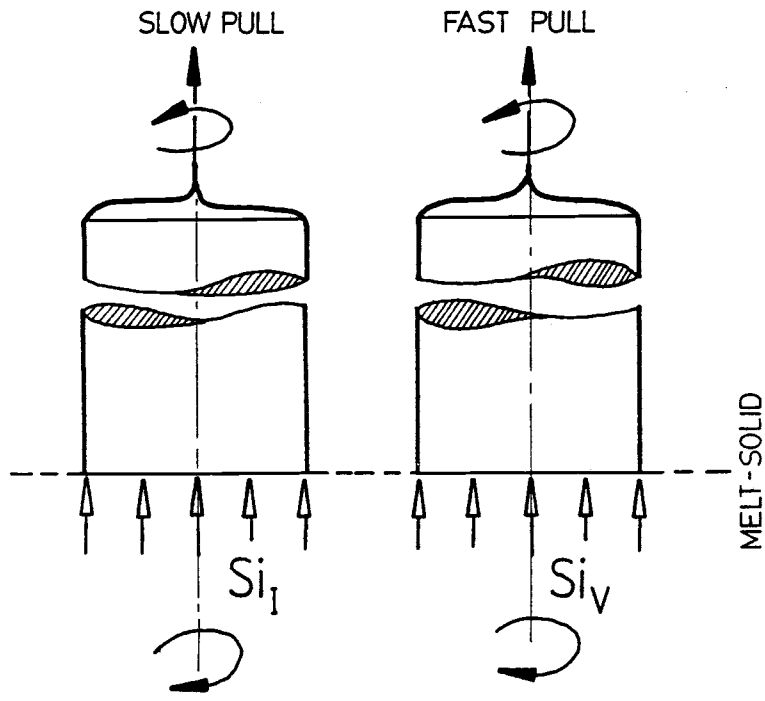

Figure 4: Model of the Point Defect Incorporation into the Growing Crystal
a) With Slow Crystal Pull-Rate
b) With Fast Crystal Pull-Rate

From their results and also from another observation it was found that the effect of the boundary layer on incorparation of the point defects can be neglected and only the effect of crystal pull-rate should be considered. From Figure 6 vacancy concentration is the highest at the center of the crystal. This is because the diffusion-rate of the vacancies in growth crystal is controlled by the temperature gradient. During the crystal growth process, at a certain portion of the crystal ingot, temperature near the center of the crystal ingot is higher than that at the periphery, due to heat lost from the crystal surface. Simultaneously, vacancies at the growth interface are supersaturated and diffuse rapidly uphill into the crystal. At the crystal periphery where temperature is low, the incorporation rate of supersaturated vacancies is also low. Another possibility that causes a decrease in vacancy concentration at the crystal pheriphery is the out-diffusion of the vacancies [7]. Vacancies can out-diffuse from the crystal outer surface due to the surface tension of the growing crystal ingot.

B. Interstitial Oxygen Atoms.

Until today it was not clear in what manner the oxygen is incorporated into the Si-melt: as dissolved $[SiO]_{Si}$ or as dissolved $[O]_{Si}$ [8]. However it is well-known that the oxygen originates from the quartz crucible which is partly dissolved by the molten silicon [9]. Dissolved oxygen atoms incorporate into the silicon ingot and occupy the interstitial sites of the silicon lattice [10]. In the incorporation mechanism two factors play a significant role:

a) Behavior of oxygen segregation at the growth interface differs from that of other impurities. Yatsurugi, et al [11] measured the equilibrium segregation coefficient

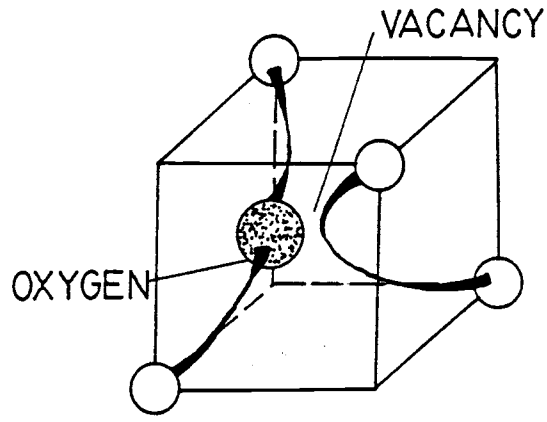

Figure 5: Silicon Sublattice containing Vacancy-Oxygen Complex after Watkins [6]

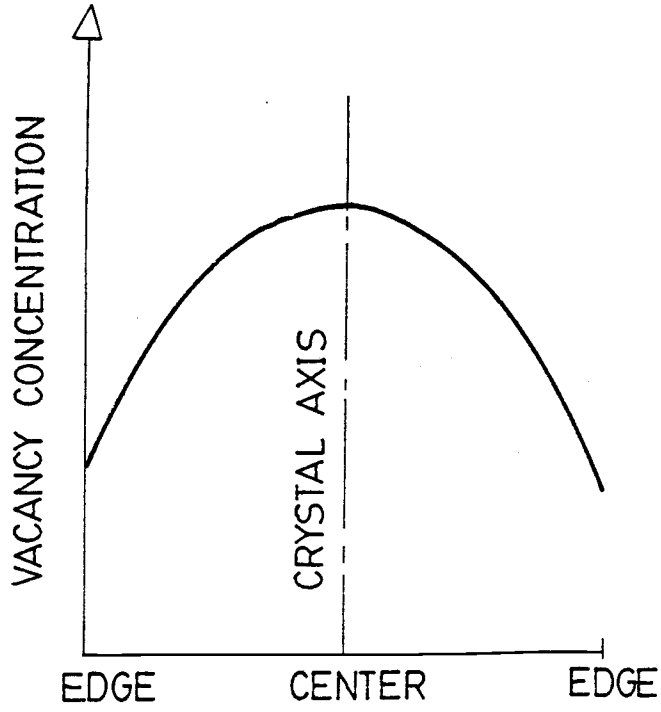

Figure 6: Vacancy Distribution across the Crystal Ingot after Abe [7]

k_o of oxygen and obtained a value larger than unity, i.e., $k_o = 1.25$. They also found by both infra-red and radioactive analysis that the segregation coefficient of interstitial oxygen atoms is unity and suggested that excess oxygen atoms are incorporated as amorphous SiO which is formed at the interface. Due to the large atomic radius of oxygen, SiO complexes can exist only in the form of SiO-Vacancy complexes. This is because vacancies will relieve the lattice stress mismatch generated by SiO complexes. This type of complex (SiO complex surrounded by vacancies) is considered to be the heterogeneous nucleation site of the oxygen precipitates [7].

b) Oxygen concentrations in the melt vary with the conditions of the melt flows which carry oxygen from the inner surface of the quartz crucible. Crucible rotation change, therefore, affects the melt flow pattern and the dissolution rate of oxygen.

Typical oxygen concentrations for a single crystal are between 25 to 32 ppmA. The oxygen is present initially in Si-O-Si bound interstitial form, which gives an infra-red absorption band at 9 microns [12]-[18]. Figure 7 shows an interstitial oxygen atom in the silicon lattice.

Normally, oxygen concentration in the seed-end section of the crystal, which is the highest, decreases gradually toward the tang-end section of the crystal ingot. This is because at the beginning of the crystal growth process the crucible-melt interface area is the

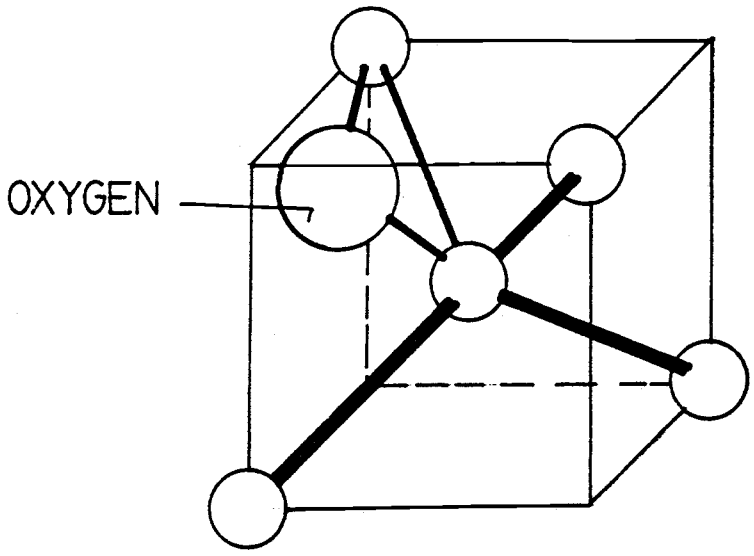

Figure 7: Silicon Sublattice with Oxygen Atom in an Interstitial Position

largest. As a result the oxygen dissolution rate (from the crucible into the silicon melt) will be high, and therefore, so will the oxygen content in the melt. As the crystal growth process continues, the volume of the melt in the quartz crucible decreases. This leads to a decrease in the crucible-melt interface area and consequently the oxygen content in the melt.

From the above explanation, the oxygen dissolution rate will depend upon crucible-melt interface area. However, another growth parameter, such as crucible rotation velocity, can also influence the dissolution rate of oxygen from the quartz crucible into the melt. Therefore it will become possible to grow crystal ingot with relatively uniform oxygen concentration from the seed-end to the tang-end section of the crystal ingot. This is done by, for example, increasing the crucible rotation speed toward the end of the crystal growth process.

In polished silicon wafers, oxygen concentration can be measured by FTIR (Fourier Tranform Infra-Red) spectrometry. However, in heavily doped substrate wafers, which are used in fabrication of epitaxial silicon wafers, this method can not be applied. This is because the absorption band of oxygen is interfered with the free carriers. SIMS (Secondary Ion Mass Spectroscopy) is, therefore, used to analyze the oxygen concentration in heavily doped materials, for example, epitaxial silicon substrate.

Unlike other impurities, such as boron or phosphorus, interstitial oxygen atoms do not play any role in integrated circuit device performance, but have other important effects during device processing:

a) Oxygen impurity suppresses dislocation motion and prevents dislocation generation in device processing. Once oxygen precipitates are formed in the crystal, Cz crystal becomes weaker than Fz crystal for the warpage formation during the heat cycle [19]-[20].

   This is not alway true, because other factors such as backside damage and deposited film stresses also play a significant role in warpage of the silicon wafers.

b) Oxygen atoms are formed by annealing at about 450^{o}C, and new donors [21] - [23] by annealing in a range of 550 to 800^{o}C [24] - [25]. The thermal donor formation can affect the device characteristics. However in heavily doped silicon material, such as epitaxial substrate wafers, this effect can be neglected.

c) Oxygen precipitates which have gettering effects are formed

by the post growth heat treatment (internal gettering). For an effective gettering it is desired to control oxygen concentration, uniformity and precipitation in Cz crystals. Oxygen precipitation mechanisms and the internal gettering processes will be explained in detail later.

C. Other Impurities.

Carbon contamination in Czochralski silicon originates from starting polycrystalline material and also from graphite components in the crystal growth chamber [26]. The typical concentration range of the carbon atoms can be from 0.05 to 5 ppmA, with levels usually rising throughout the length of an ingot [27]. Carbon contamination normally depends upon the starting material as well as growth procedures. The presence of carbon, and its influence on the electrical properties of silicon is still not well understood. However, it was found that the nucleation and growth process of oxygen precipitates can be influenced by carbon impurities [28]. This may be because carbon atoms are relatively small compared to silicon and oxygen atoms. They normally occupy the substitutional site of the silicon lattice. Under a transmission electron microscope, a strain field develops around a silicon lattice containing carbon atoms similar to that around the vacancy defects. As a result the free energy change due to formation of oxygen precipitate nuclei will be reduced at a silicon lattice containing carbon atoms.

So far, no direct evidence of improvement performance in silicon wafers containing some amount of carbon during heat treatment cycles has been found. However, low carbon levels are of considerable importance for yield and performance of very large scale integrated

circuit devices [29].

Other impurities found in silicon wafers are transition metals, for example, copper or nickel. Transition metal impurities are believed to originate from starting polycrystalline silicon and from the crystal puller parts and heating components. They can also be introduced during the wafer processing. This is because contamination can be introduced during the slicing process, and polishing slurry normally contains a certain amount of heavy metal.

If the concentration of heavy metal contamination is high enough, it will precipitate. Precipitates in the form of metal silicide, which are referred to as " hazes", are often found on the wafer surface.

III. DEFECT NUCLEATION AND GROWTH MECHANISMS

In general, microdefects which are introduced into silicon materials can be divided into two types. The first type of defect is found on the surface of the silicon wafers and the second type in the silicon bulk. Both types are primarily nucleated from the same sources, namely at the grown-in defects. The growth of the surface defects is known to be strongly dependent upon the heat treatment ambients, while ambients seem to have less effect on the growth of the bulk defects. In this chapter the nucleation and growth of the microdefects during heat treatment will be discussed.

A. Grown-in Defects.

In dislocation-free silicon crystals microdefects or grown-in defects can be revealed and studied by techniques such as preferential etching, TEM (Transmission Electron Microscopy) or by copper decoration. The defects are normally small in size and can be observed when some special preparation or heat treatment is performed on the material to be studied. For a TEM study, the silicon sample must undergo a considerably long period of low temperature annealing (between 600 and 750^{o}C), so that the grown-in defects can become visible. Another technique, such as copper decoration, can also create a good overview of the defects close to as-grown condition, because no long annealing process is required. However, the common method used to study the defects is preferential etching because this technique is fast and does not require complicated sample preparations.

One of the common types of grown-in defects is swirl. A swirl test is normally performed by oxidizing silicon slugs or wafers in a wet oxygen ambient at a temperature between 1000 and 1100^{o}C. Following the oxidation process, the samples are preferentially etched. A swirl pattern can be observed on the front- and back-side of the wafers under a high intensity light source without any magnification. From observation, the distribution pattern of the swirl is generally in the form of a spiral across the surface and through the thickness of the wafer. A swirl pattern can be found in both Czochralski and floating zone crystal irrespective of their crystallographic orientation [30].

Two types of swirls have been identified in both Czochralski and floating zone silicon crystals. The larger of the two types is called an A type defect and the other is called a B type defect [31]. A type defects are found to occur predominantly in the regions removed from the outer periphery of the crystals. The defects are suppressed by controlling growth rate of the crystal ingot. Because these defects are found at the outer periphery of the crystal, some of them will be removed during the ingot gridding operation. The second type of swirl defect is the B type. B type defects normally distribute over the entire crystal extending to the outer surface.

As first proposed by deKock, [31]-[33] the formation of swirl defects proceeds by the association of excess vacancies and oxygen atoms in the crystal, with the oxygen acting as a nucleation center for precipitation of excess vacancies. His observation comes from the fact that a high density of swirl defects can be observed more frequently in the crystal ingot containing high oxygen. From his model, various vacancy-oxygen complexes are formed during the cool-down stage from the solidification temperature. These vacancy-oxygen

complexes will grow to a larger size and act as nuclei for the condensation of more vacancies.

The model proposed by deKock was very controversial and inaccurate. Later studies of the defects using a high resolution transmission electron microscope show that type A swirl defects are interstitial dislocation loops approximately 1 to 3 microns in size [34]-[40]. B type defects could not be observed by transmission electron microscopy, although copper decorated B types have been reported as being very small dislocation loops (approximatelt 600 to 800 Å in diameter) [38].

At this point the nucleation mechanism of those swirl defects is still unclear. So far it is known that A type defects are interstitial dislocation loops which form at a lower temperature than the B type defects. Furthermore it is also beleived that A type defects are a product of the transformation of a B type defect. This transformation can proceed by an increase in the size of B defects as the crystal cools to about 1050°C, at which point the largest of the B defects becomes unstable and collapses on (111) close packed planes in the form of an interstitial dislocation loop [41].

B. Oxidation Induced Stacking Faults.

Oxidation induced stacking faults (OSFs) are the crystallographic defects which are observed to be generated in the surface regions of the silicon wafers after oxidizing at elevated temperatures [42]-[47]. A typical temperature range is between 900 to 1250°C. OSFs are also observed in silicon wafers which have been oxidized in a dry oxygen ambient, but the density of the faults obtained from wet oxygen or

steam ambients is the highest.

In some literature, stacking faults may be called line defects because of their appearance under the optical light microscope. But in general, stacking faults are two-dimensional defects that are formed by either removing (intrinsic stacking fault) or inserting (extrinsic stacking fault) an extra plane of atoms between close packed (111) planes [48]. In silicon, stacking faults are always found to be extrinsic in nature, and the extra plane of silicon atoms is bound by Frank partial dislocations of the type a/3{111} [49]-[50]. Figure 8 shows the photomicrograph of oxidation induced stacking faults. The photo was taken after the silicon oxide layer was removed and the wafer was preferentially etched.

1. Nucleation Mechanisms.

First one should consider the nucleation site of the oxidation induced stacking faults. The possible nucleation sites of OSFs are found to be:

i) At the region on the wafer surface that has been mechanically damaged [51].

ii) At the swirl defects [50]

iii) At heavy metal precipitates [52].

As mentioned earlier, the OSF is extrinsic in nature, therefore an excess amount of silicon atoms is required to nucleate the stacking fault. To achieve this, the nucleation and growth process of OSFs must involve generation of excess silicon atoms near the surface. Studies of oxidation enhanced diffusion of phosphorus in silicon shows that excess self-interstitials are generated at the wafer surface during the oxidation process [43], [53]-[60]. According to the model, during

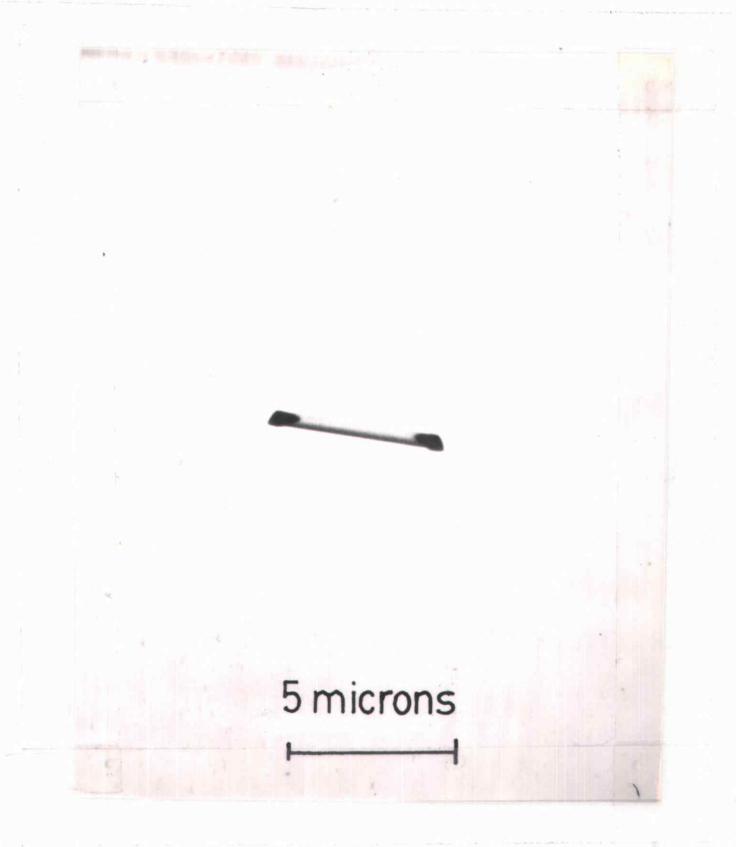

Figure 8: Photograph of Oxidation Induced Stacking Fault (OSF)

thermal oxidation, oxygen atoms diffuse through the growing oxide layer and react with silicon atoms at the oxide-silicon interface to form silicon oxide. Reaction can take place when oxygen atoms occupy the vacancy sites of the silicon lattice and/or displace the substitutional silicon atoms. Displacement of substitutional silicon atoms by oxygen atoms can result in generation of excess silicon atoms. Excess silicon atoms generated at the oxide-silicon interface diffuse rapidly into the silicon matrix and occupy the interstitial sites of the silicon lattice by forming an extra plane between the (111) close packed plane of silicon.

2. Growth Kinetics.

Besides the visual observation of the size and density of OSFs, study of OSF growth mechanisms is also done by observing the enhancement or retardation of the diffusion rate of impurities such as boron, [53]-[54] phosphorus [53]-[57] or arsenic [61]. Since the diffusion mechanism of those impurities under the influence of thermal point defects (vacancies and silicon self-interstitials) is well understood, the growth of OSFs under the same influence can be compared and analyzed.

As first pointed out by Hu, [43] these effects are closely related to each other as can be seen by the result that under the same oxidation conditions both the diffusion of boron and the growth rate of oxidation-induced stacking faults increases with the surface orientation in the order (111), (110), (100). From observation, growth kinetics of OSFs can be summarized as follows:

i) The length (or radius) of an OSF depends on oxidation time with an exponent between 0.5 and 1, depending on the oxidation conditions [43]-[44], [62]-[64].

ii) Stacking fault size usually increases with increasing oxidation time, while the density of the OSFs decreases.

iii) During oxidation at temperatures above 1200^{o}C, OSFs first grow and then start to shrink away. This phenomenon was first observed by Lawrence [65] and later independently by Hu [66], who termed it "retrogrowth". A small percentage of chlorine in the oxidizing atmosphere leads to the same behavior at much lower temperatures [67]-[72].

3. Growth and Shrinkage of Faults.

The growth and shrinkage of stacking faults is governed by the concentration of thermal point defects (vacancies and silicon self-interstitials) in the vicinity of the faults. Extrinsic stacking faults can grow by emission of vacancies or by the absorption of interstitials from the surrounding area.

The basic formula for the shrinkage and growth of the stacking faults via the emission or absorption of point defects [73]-[75] is given by

$$dr_{SF}/dt = -\alpha_{eff} D_I C_I^{eq} [\exp(\Delta G/kt) - C_I/C_I^{eq}] A/\Omega \qquad (1)$$

for an interstitial model and by

$$dr_{SF}/dt = -\alpha_{eff} D_V C_V^{eq} [C_V/C_V^{eq} - \exp(-\Delta G/kt)] A/\Omega \qquad (2)$$

for a vacancy model.

C_I and C_V are the point defect concentrations far away from the partial dislocation bordering the OSF. A is the area per atom in the stacking fault, Ω is the atomic volume and ΔG is the positive free enthalphy increase due to taking away one self-interstitial from the OSF (or adding one vacancy), and α_{eff} is the stacking fault energy determined by the line tension.

From the equations, the fault will shrink when C_V/C_V^{eq} is greater than 1. This situation can take place when silicon wafers are annealed in vacuum or argon [76]. It should be noted that during annealing in a vacuum or argon ambient, vacancies are generated at the wafer surface and in turn cause an increase in vacancy concentration.

C. Oxygen Precipitates.

During high temperature heat treatment, oxygen atoms incorporated into the Czochralski-grown silicon matrix can either out diffuse or precipitate. Out-diffusion of oxygen atoms will take place only in the region near the silicon surface, and the process usually takes several hours.

In commercially grown silicon crystal where interstitial oxygen concentration, ranging between 25 - 35 ppmA, already exceeds the solubility limit, oxygen atoms tend to precipitate. Precipitation of silicon oxide from supersaturated oxygen occurs by a nucleation and growth process [77]. Nucleation of oxygen precipitates can occur by means of composition fluctuations of the oxygen atoms in the silicon matrix (homogeneous nucleation) or at the internal lattice defects (heterogeneous nucleation). These two types of nucleation processes in silicon materials will be discussed later.

Up to this point the nucleation of oxygen precipitaes in silicon materials can only be understood mathematically, when the homogeneous case is considered. In general, the heterogeneous nucleation can not be included because the number of preexisting nucleation sites is unknown and unpredictable.

1. Mathematical Model for the Homogeneous Nucleation Process.

Like nucleation processes of impurities in other materials, homogeneous nucleation can be treated using Volmer-Weber-Becker-Doring assumptions. From their model it is assumed that an equilibrium distribution of particle sizes exists, and the nucleation rate of those particles must be slow compared to the growth rate of

subcritical particles [78]. A high growth rate can result in non-uniform growth of the nuclei and ,therefore, shrinkage of the subcritical particles. The Volmer-Weber-Becker-Doring expression for the rate of nucleation per unit volume , J_V , is then given by

$$J_V = N_{r^*} R^+_{r^*} Z \qquad (3)$$

where N_{r^*} is the equilibrium concentration of the critical particle size r^* . Below the critical particle size the particle lowers its free energy by decreasing its size, so that particles with radii smaller than r* tend to dissolve and go back into solution. On the other hand, particles with radii larger than r* undergo a decrease in free energy with increasing radius. For this reason they are stable and should continue to grow. $R^+_{r^*}$ is the rate at which monomers join the critical cluster, and Z is the so called Zeldovich factor which takes into account the fact that only a certain fraction of the critical concentration of particles N_{r^*} will grow; others will shrink [79]. The factor Z is a constant on the order of a few percent.

Nucleation and growth of oxide precipitate particles normally involves a change of volume and therefore the free energy. This free energy change may be expressed by the following equation:

$$\Delta F = -\Delta F_V + \Delta F_S + \Delta F_M \qquad (4)$$

where ΔF_V is the free energy associated with the formation of the volume of silicon oxide. The second term, ΔF_S , is the energy of the surface created between the silicon oxide and silicon matrix, and is always positive. The last term, ΔF_M represents the strain energy

arising from the formation of the oxide particle. This includes the strain energy in the silicon matrix and in the oxide particle and is caused by the fact that the volume of the silicon oxide particle is approximately 2.3 times larger than the volume of silicon that it displaces [80]. The strain energy term varies directly as the volume of the precipitate particle. For a simple mathmatical model, however, ΔF_M is assumed to be zero. It is reasonable to assume that at the growth temperature strain energy due to volume expansion of the oxide is normally low. Figure 9 shows the free energy of precipitate as a function of its radius.

In the case of spherical nuclei, the free energy for critical nucleus formation can be written as [81]:

$$\Delta F = 4/3\pi(r^*)^3\Delta F_V + 4\pi(r^*)^3\Delta F_S \qquad (5)$$

where ΔF_S is the surface free energy of the precipitate.

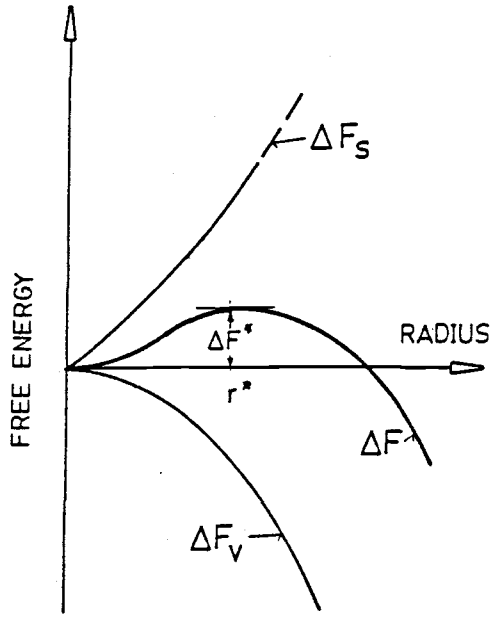

Figure 9:

Free-Energy of Precipitate as a Function of the Radius

With

$$r^* = -2 \Delta F_S / \Delta F_V \quad (6)$$

the free energy for critical nucleus formation becomes:

$$F^* = -(2/3) \pi r^{*3} \Delta F_V \quad (7)$$

From thermodynamics, the volume free energy change of the precipitate nuclei can be expressed as

$$F_V = \Delta H (\Delta T/T) \quad (8)$$

where ΔH is the enthalpy change of the $Si + 2O \rightleftharpoons SiO_2$ reaction which is 22 kCal/mol [82].

It is also known that the equilibrium concentration, N_{r^*}, of the critical particle size r^* is a function of the diffusing species concentration N_i (in this case the interstitial oxygen concentration) and can be expressed by:

$$N_{r^*} = N_i \exp (- \Delta F^*/ kT) \quad (9)$$

The nucleation rate, J_V, from equation (3), can be rewritten more explicity as

$$J_V = Z (4\pi r^{*2}) (2D/\alpha^2) N_i \exp (- \Delta F^*/ kT) \quad (10)$$

where $2D/\alpha^2$ is the frequency factor involving the diffusion coefficient D and the atomic jump distance α. Using equation (10) the nucleation rate of oxygen precipitates can be calculated.

Figure 10 shows the theoretical nucleation rate of oxygen precipitates as a function of temperature. The detailed mathematical treatment of this problem can be found in reference [83].

It should be mentioned that no precipitation can occur until nucleation begins, but once it has started the silicon matrix lose its oxygen atoms in two ways. First, to the growing particles already formed (preexisting precipitate nuclei), and second, to the formation of additional nuclei. In other words, nucleation may continue simultaneously with the growth of preexisting precipitate nuclei. The progress of precipitation at a given temperature is shown in Figure 11, where the amount of precipitate, as a percentage of the maximum, is plotted as a function of time. Logarithmic units are used for the time scale because spontaneous reactions of this nature usually start rapidly and finish slowly.

Because precipitate particle size varies, and precipitation does not begin immediately, a finite time t_o is required before it can be detectaed. This time interval is called the incubation period and represents the time necessary to form stable visible nuclei. The curve in Figure 10 shows that the precipitation process finishes very slowly, an effect that is to be expected in light of the continued loss of oxygen atoms from the silicon matrix.

The speed at which the formation of precipitate nuclei occurs varies with temperature. This is already shown qualitatively in Figure 10. At very low temperatures (less than $500^{\circ}C$), long periods are required to nucleate precipitate nuclei because the diffusion rate is

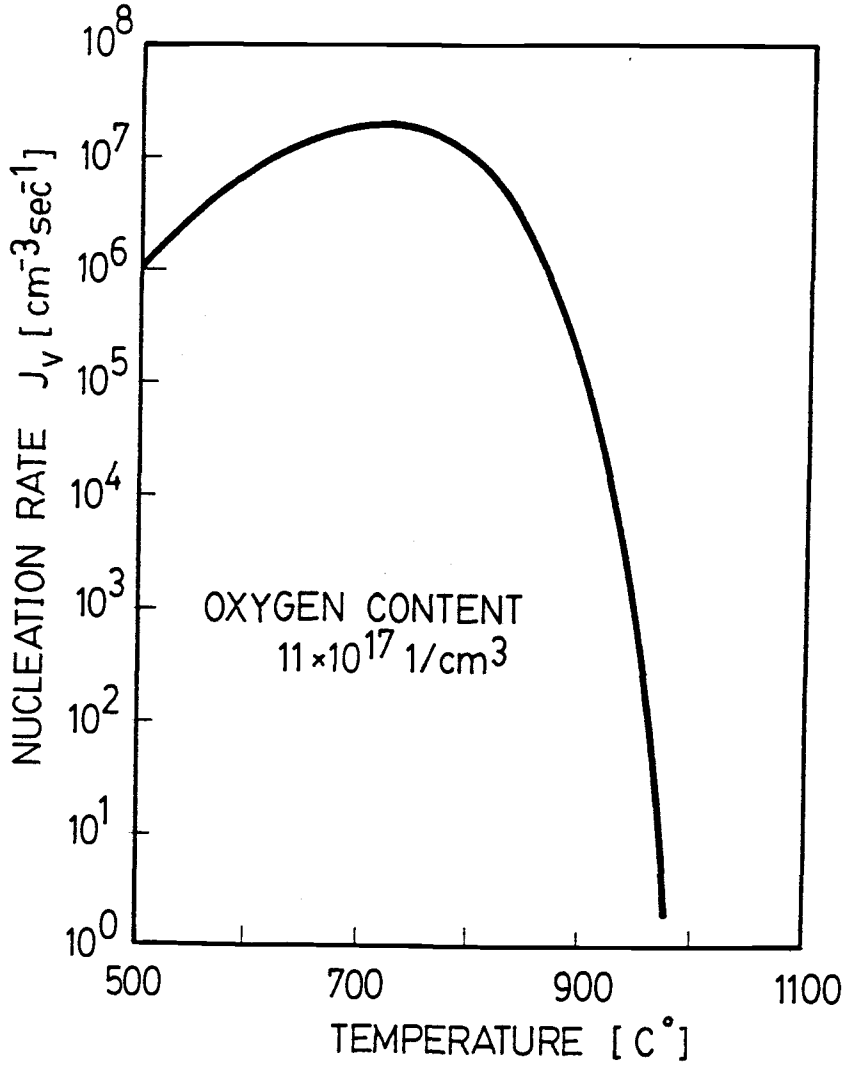

Figure 10: Calculated Nucleation Rate of Oxygen Precipitates as the Function of Temperature [83]

very slow. Here the rate of the reaction is controlled by the rate at which atoms can migrate. The nucleation rate is also very slow at temperatures just above 850 ^{o} C. In this case, the free-energy decrease resulting from precipitation is very small. Nucleation is accordingly slow, and precipitation is controlled by the rate at which nuclei can form. The high diffusion rates that exist at these temperautres can do little if nuclei do not form.

At intermediate temperatures, between the two above-mentioned extremes, the nucleation rate increases to a maximum, and therefore the time to complete the precipitation is very short. In this range, the combination of moderate diffusion and nucleation rates makes precipitation rapid. Usually the precipitate particles only become visible in an optical microscope when oxide precipitates grow to a sufficiently large size.

2. Heterogeneous versus Homogeneous Nucleation.

As mentioned earlier, precipitate particles can be nucleated in two basic ways. They can form at internal lattice defects such as dislocations, dislocation nodes (intersections of two or more dislocations), impurity particles, or discontinuities in grain boundaries. This process is known as heterogeneous nucleation, wherein the formation of a second-phase particle is made easier by lattice defects. Homogeneous nucleation, on the other hand, is the spontaneous formation of nuclei through composition fluctuations of the solute. Here oxygen atoms cluster in the lattice of the matrix and start a second-phase of oxide particles growing in an otherwise perfect crystal. Homogeneous nucleation occurs only with considerable

difficulty. The principal difficulty is that a surface is created when a second-phase particle is nucleated.

In silicon crystal ingot, the bulk silicon usually contains a certain amount of grown-in defects or impurities such as carbon. These grown-in defects and impurities are considered to be ideal nucleation sites for oxide precipitates. Following nucleation, oxide particles grow in size as a result of the diffusion of oxygen from the surrounding silicon matrix toward the particles. The growth of the precipitate particles is directly related to the surface tension at the interface between the matrix and the particles. Because of the boundary-surface energy, the free energy per atom in a large precipitate particle is lower than that in a small particle. This free-energy difference is the driving force that causes the dissolution of small particles and the growth of large ones.

It should be pointed out that precipitate particles are not always spherical in shape. Frequently, the precipitate has a plate like, or even a needle like form. In many cases, plate- or needle-shaped precipitate particles grow in such a manner that they are aligned along specific crystallographic planes [77].

3. Effect of the Doping Concentration on Oxygen Precipitation.

The effect of doping concentration on oxygen precipitation has been studied by many reseachers. However, they still can not agree on many points, and therefore the conclusions are still controversial.

DeKock et al have studied the effect of the doping concentration from crystal quenching experiments. They have concluded that the point defects (vacancies and silicon interstitials) interact with the dopant to form complexes. Later, T. Abe pointed out that the retardation of

the oxygen precipitation process in n-type silicon material heavily doped with arsenic is due to the atomic radii of arsenic. The arsenic atomic radius is large compared to the spacing in the silicon lattice. When silicon material is heavily doped with arsenic, arsenic atoms will occupy most of the lattice space. This reaction can lead to a decrease in vacancy concentration in the silicon matrix and ,therefore, retardation of the oxygen precipitate process.

4. Effect of Spatial Location in the Crystal Ingot on Oxygen Precipitation.

During the crystal growth and cooling period, different sections of the crystal ingot undergo different temperature changes that cause nucleation and growth of oxide precipitates. The seed-end, for example, spent a much longer time in the crystal growth chamber. Consequently in the case of homogeneous nucleation, a high density of precipitate nuclei is expected at the seed-end section. On the other hand, if a heterogeneous case is considered and constant grown-in defect density throughout the crystal ingot is assumed, the nuclei size at the seed-end section must be larger than that in the tang-end section due to a longer incubation period.

As mentioned, the heterogeneous case can not be simulated by a mathematical model because the initial size and density of grown-in defects or heterogeneous nucleation sites are unknown and depend strongly on the growth parameters. Therefore the most convenient way of studying the effect of spatial location is to perform the experiments, rather than attempt theoretical calculation.

D. Bulk Stacking Faults.

After oxide precipitates are formed in the bulk of the silicon wafer, bulk stacking faults can be induced. The nucleation and growth of the bulk stacking faults are different from the stacking faults induced by oxidation processes. The significant differences between both types of stacking faults are listed as follows:

1) The nucleation site: Mechanically damaged silicon surface, swirl defects and heavy metal precipitates are considered to be the nucleation sites of the oxidation induced stacking faults. On the other hand, bulk stacking faults are believed to be nucleated only at the oxide precipitate.
2) Growth Kinetics: Oxidation induced or surface stacking faults normally grow in an oxidizing ambient or during wet oxidation. In neutral ambients, like in nitrogen, OSFs will not grow, or in some cases will start to shrink. Bulk stacking faults, however, can grow in all ambients.

Figure 12 shows the nucleation and growth of the bulk stacking faults, according to Freeland, et al [84]. As mentioned earlier, that high tensile stresses can develop around the precipitate particle because the lattice parameter of the oxide precipitate is different from that of the silicon matrix. At high temperatures the misfit stresses in the lattice can easily exceed the yield strength of the silicon material. As a result, a dislocation will punch out from the precipitate particle, see Figure 12a. As the heat treatment continues, excess oxygen atoms in the silicon matrix will diffuse toward the precipitate particle. During the incorporation process of oxygen atoms into the precipitate particle, silicon atoms are forced to move away

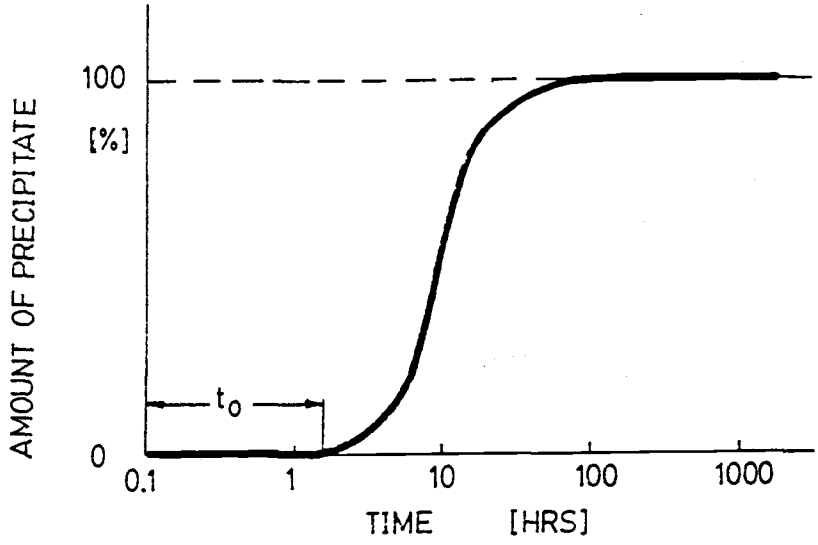

Figure 11: Amount of Precipitate as a Function of Time

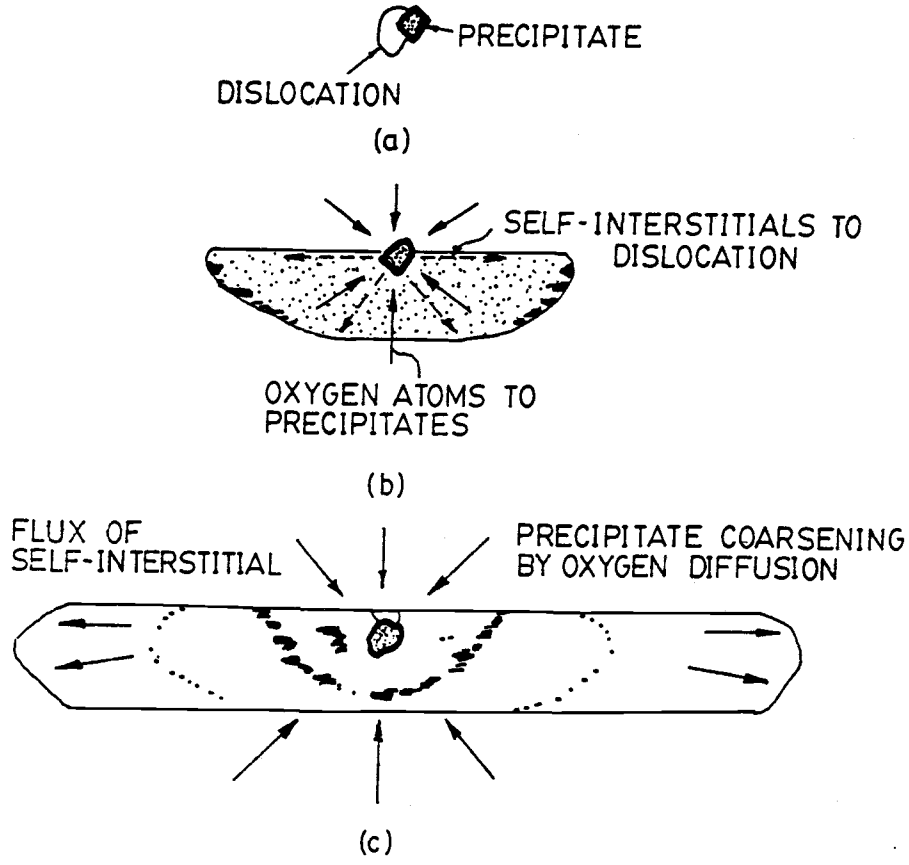

Figure 12: Nucleation and Growth of Bulk Stacking Fault after Freeland et al [84]: a) Nucleation Site at Non-Coherent Precipitate, b) Early Stage of Formation, and c) Growth of Bulk Stacking Fault.

from the particle. This reaction takes place during precipitate growth because the composition of the oxide precipitate has to be maintained.

As a consequence, the misfit stresses at the precipitate and silicon matrix interface will be constantly built-up, and the silicon matrix adjacent to the oxide precipitate particle will be supersaturated by excess interstitial silicon atoms. To relieve the high misfit stresses, the dislocation loop will continue to grow. Growth of the loop can result in extrinsic stacking fault formation due to supersaturation of excess interstitial silicon atoms. Figure 12b shows the early stage of formation of extrinsic faults.

According to Freeland et al [84], in the later stage (see Figure 12c) the oxide precipitate can be homogeneously nucleated in the fault. Therefore, under a transmission electron microscope extrinsic stacking faults decorated with precipitate particles can be observed [85]. It was , however, found later that decorated precipitate particles in the faults are not oxide precipitate particles as reported by Freeland, but heavy metals such as Cu and Ni [86]. It is believed that the only bulk defects that act as the gettering sites for heavy metals are the bulk stacking faults. The subject of internal gettering will be discussed later.

IV GETTERING TECHNIQUES.

Heavy metals and other impurities are known to contribute to leakage related yield losses in state-of-the-art VLSI circuits. It is, therefore, required that some type of getter system be included. In general, gettering techniques can be divided into two groups; a) external gettering and b) internal gettering.

A. External Gettering.

External gettering is a process in which gettering sites are located at the back-side of the wafer [87]. One of the external gettering techniques is the mechanical backside damaging method. Mechanical backside damage can be introduced by several techniques such as sand blasting. During subsequent high temperature processing, step crystal defects such as stacking faults and dislocation loops are generated at the damage site and extend a few microns into the wafer volume. Stacking faults as well as dislocation loops are known to be effective gettering sites for heavy metal impurities and point defects. The gettering effect can, however, lose its strength if the temperature of the subsequent processing step is too high (above 1150^{o} C). This is because at that temperature dislocation loops and stacking faults can be annealed out [88].

A poorly controlled sand blasting process can give occasional contamination and warpage problems. Another major problem associated with sand blasting is silicon particulates. Silicon particulates generated during sand blasting are left behind at the mechanical damage sites. They can eventually be annealed out by a low temperature heat treatment process. If silicon particulates are not removed during

the annealing step, they might migrate to the wafer backside surface during the device processing. This may result in cross contamination of the front-side of adjacent silicon wafers.

Due to the problems described above, other external gettering techniques are developed and widely used instead of mechanical backside damage. They are:

a) Phosphorus diffusion into the backside of a silicon wafer.

b) Controlled pattern of laser damage on the backside of the wafers [89] and

c) Polysilicon backside layer [90] - [91]

Phosphorus diffusion has been used for a long time. In this method, phosphorus atoms at a high concentration are incorporated into the silicon lattice and precipitated with excess silicon self-interstitials. SiP precipitate particles penetrate deeper into the backside surface during the subsequent high temperature process and generate the dislocation networks. These dislocation networks will act as sinks for heavy metal impurities.

The second method is known as controlled pattern laser damage. The aim of laser irradiation is to generate thermally stable dislocation networks acting as sinks for heavy meatl impurities and point defects. In this method, a high intensity laser beam is applied to the backside of the wafer, creating localized melting spots. During solidification of the melting zone a strain field is developed around the spots. During the subsequent high temperature heat treatment, a high strain field will induce dislocation networks on the backside of the wafer [92].

In the last method, a polysilicon layer is deposited using Low Pressure Chemical Vapor Deposition at temperatures ranging between 600

and 650°C. The purpose of depositing a polysilicon layer is to create misfit stresses between the polysilicon and monocrystalline silicon lattice. This causes a formation of dislocation networks. Moreover, the grain boundary of polysilicon is an ideal site for the gettering of heavy metal impurities. Normally after the polysilicon layer is deposited, the wafers are annealed at a high temperature in a nitrogen ambient to ensure the uniformity of the polysilicon grains. It was also observed that the gettering effect is enhanced by the polysilicon backside process in oxygen rich silicon material. This may be because the temperature of the polysilicon process is similar to that of the oxygen nucleation process. Therefore, it is believed that a link between the polysilicon backside and the internal gettering processes must exist. Internal gettering processes will be discussed in detail in the next section.

The polysilicon back-side and laser damage processes are claimed to be much cleaner in processing than mechanical damage, and much more stable in repeated thermal cycling. The laser backside method allows one to have a great deal of control over the exact amount of damage done, while the polysilicon layer provides less of a problem with in-process warpage.

B. Internal Gettering.

This method is considered to be the cleanest gettering method, but requires a lot of knowledge concerning the heat treatment of silicon material in order to control the process. In this method, oxygen atoms incorporated into the silicon matrix during the crystal growth process are nucleated to form precipitate nuclei. The oxygen

nucleation process is normally performed at low temperatures, ranging between 650 and 800°C. However, the optimal nucleation heat treatment temperature was found to be around 750°C. The next step is the high temperature heat treatment. During this step some oxygen precipitate nuclei will grow, while the rest will shrink or be dissolved. Oxide precipitate particles are known to induce the secondary defects (bulk stacking faults and dislocation loops) which act as prime gettering centers.

In oxygen rich silicon wafers, oxide precipitates can form at the device active region close to the wafer surface and in turn cause damage to the devices. In this case, a high temperature heat treatment prior to the nucleation heat treatment is required. During this heat treatment step, out diffusion of oxygen atoms near the wafer surface takes place . This results in a decrease in oxygen concentration at the surface region. A denuded, or defect free, zone is formed when oxygen concentration in that region drops below the precipitation threshold level. Therefore, no oxygen precipitate can be nucleated close to the surface region during the subsequent nucleation heat treatment. In general, the depth of the defect free or denuded zone depends upon the denuding temperature and the oxygen concentration. Figure 13 shows the fundamental heat treatment steps of the internal gettering process.

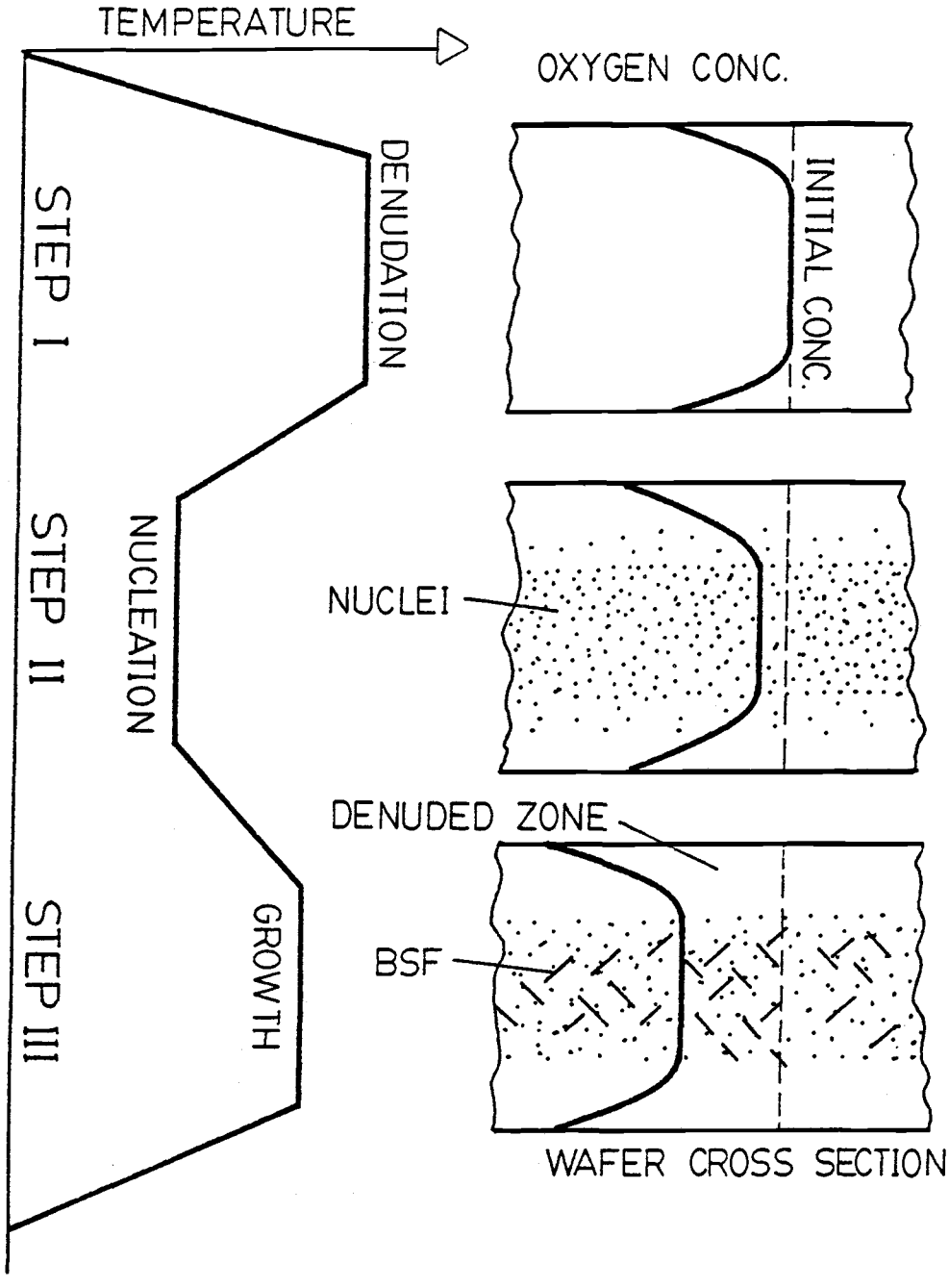

Figure 13: Fundamental Heat Treatment Steps of Internal Gettering Process

V. EXPERIMENTAL PROCEDURES.

A. Post-Epitaxial Deposition Heat Treatment.

1. Isothermal Heat Treatment.

The samples used were prepared from one hundred and fifty 4" P/P+(100) epitaxial silicon wafers of resisitivity between 0.01 and 0.03 ohm-cm. They were between 500 and 525 microns thick and originated from different lots of materials. The wafers were mechanically backside damaged . A thin chemical vapor deposition (CVD) oxide layer of 4500 Angstrom was deposited on the backside of the wafers. The epitaxial layer on the front side was approximately 13.5 microns thick. The epitaxial silicon layer had a resistivity between 30 to 50 ohm-cm. Each wafer was first cleaved into four quarter-sections. The silicon particulates resulting from cleaving were removed. Subsequently, organic substances were removed by dipping the samples for approximately 10 mintues each in TCE, acetone, and methanol. After these cleaning procedures, the samples were rinsed in deionized (DI) water. The hydrous oxide film on the front side of the samples were removed by dipping the samples for between 2 to 5 seconds in HF acid - water solution (1:50). The samples were then rinsed in DI water for 20 minutes and blown dry with nitrogen gas.

One- and two-step isothermal heat treatment cycles as shown in Figure 14 were used. The summary of the experimental procedures is shown in Figure 15. It should be noted that before the high temperature heat treatment step in the N_2 ambient, a thin layer of silicon oxide was thermally grown on the sample surface to protect the surface from "N_2 pitting". This was done by heat treating the samples

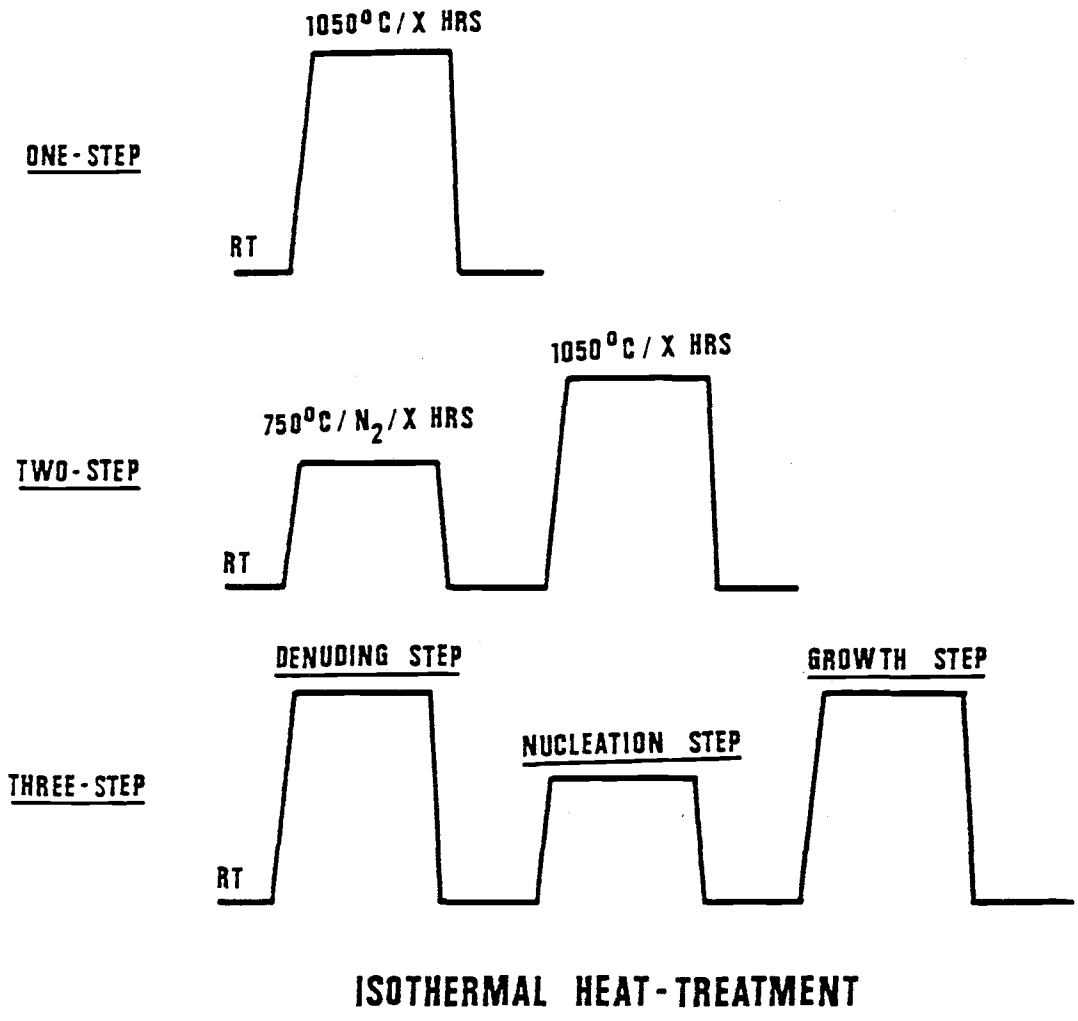

Figure 14: Isothermal Heat Treatment Cycles

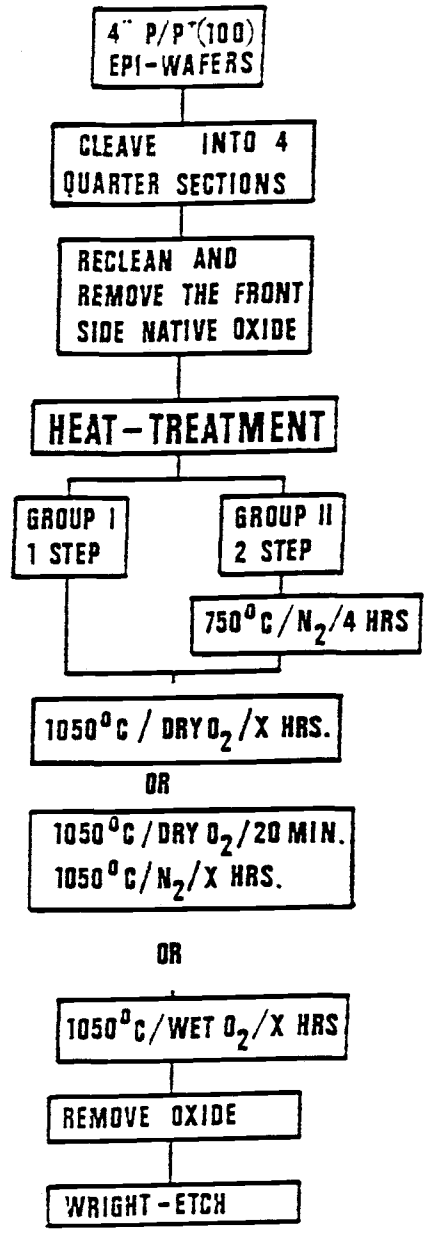

Figure 15: Summary of the Experimental Procedures.

in dry O_2 for 20 mintues after the boat was pushed in. Subsequently, the ambient was switched to N_2 ambient. Samples were normally pushed and pulled only in dry O_2 ambient.

Surface stacking faults were revealed by etching the sample for 3 mintues in Wright etch [93] and examining at 200X magnification. Cross section examination was done by cleaving the sample and etching in Wright etch for 1-1/2 minutes. A shorter etching period than 1-1/2 minutes can be applied, however long etching periods can lead to over-etching and artifacts. Defect counting was done at 150X magnification.

In the case of three-step isothermal heat treatment (see Figure 14), the samples were first heat treated at 1050°C for times ranging between 4 to 16 hrs. in dry O_2 and in N_2 ambients. This step is called the "denuding step". Following this step all samples were combined together to receive a nucleation heat treatment at 750°C for 4 hours in nitrogen ambient. Subsequently the samples were heat treated at 1050 C in wet O_2 ambient for 16 hours. After the heat treatments, the samples were evaluated using the evaluation procedures described above.

2. Heat Treatment with Ramp-Up and Ramp-Down Scheduels.

In this experiment, ninety 4" P/P+(100) epitaxial silicon wafers, similar to those wafers used in the experiments described above were used. First, the sample identification numbers were scribed on the back-side of each wafer. The wafers were then cleaved into four quarter-sections. Subsequently, the quarter-section samples were cleaned using the standard RCA cleaning procedure which consists of DI water, hydrochloric acid and hydrogen peroxide.

The heat treatment cycles similar to those shown in Figure 14 were used. The samples, however, were pushed and pulled into the diffusion furnace at a rate of 3" per minute. Push and pull was performed at a temperature of 800^{O}C in a dry oxygen ambient. The ramp-up rate from 800 to 1050^{O}C was 7 C per minute and the ramp-down rate was 2 ^{O}C per minute. After the heat treatment, the samples were evaluated according to the procedures described in the last section.

B. Pre-Epitaxial Deposition Heat Treatment.

For the experiments, two 4" silicon ingots heavily doped with boron were grown. They were (100) oriented and grown with different growth parameters to obtain different oxygen concentrations. The first crystal ingot was approximately 140 cm long and had a low oxygen concentration, ranging between 25 to 28 ppmA. The second crystal ingot was double-pulled. That means the crystal growth process was prematurely interrupted due to lose of the crystal structure after the crystal ingot reached a length of approximately 60 cm. The first section of the crystal ingot (section A) was then cooled and removed from the crystal growth chamber. The growth process of section B was continued by dipping a new crystal seed into the remaining silicon melt. A silicon ingot section approximately 71 cm long was pulled from the remaining melt. The second ingot had medium oxygen content, ranging between 29 and 31 ppmA. The oxygen concentration of both crystal ingots was determined by secondary ion mass spectrometry analysis and calibrated to ASTM 1979 standard.

From the first crystal ingot one 20 cm sections was selected from the section close to the seed-end, the tang-end and the center section of the crystal ingot. From section A of the second crystal ingot only

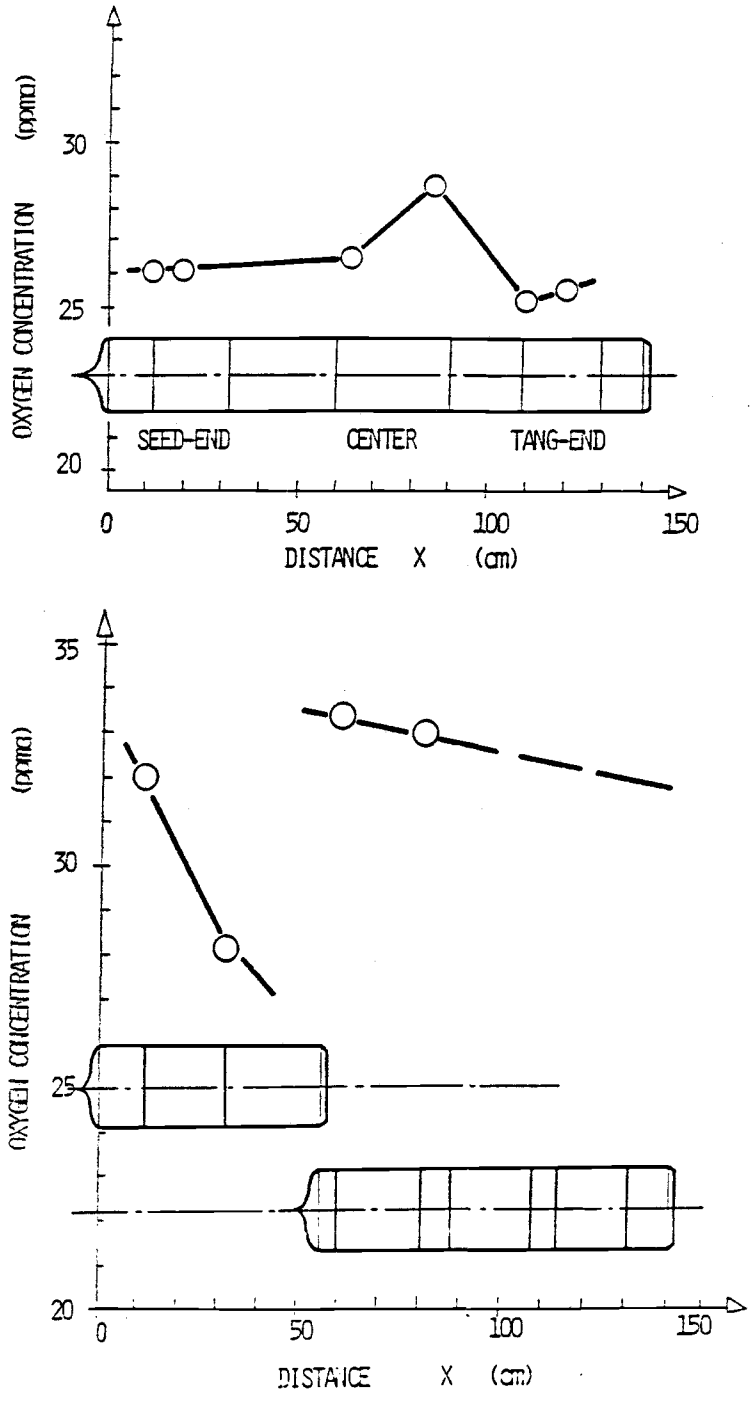

Figure 16: Position of the Ingot Sections and Oxygen Distribution in the Crystal Ingot
a) Containing Low Oxygen Concentration
b) Containing Medium Oxygen Concentration

one section, 20 cm long, close to the seed-end was selected for study. From section B, three 20 cm long sections were selected. They were from the section close to the seed-end, center, and tang-end, respectively. Figures 16a and 16b show the positions of those ingot sections. Also plotted in the figures is the oxygen distribution along the crystal ingot axis.

First, the ingot sections were sliced and the silicon slices were processed according to the standard chemical wafer (CW) procedures. The procedures involve a chemical etching process to remove the mechanical damage generated during the slicing processes, and a mechanical backside damage process for external gettering purposes. To identify the wafers the front side of each wafer was laser marked. After the CW processing steps, 28 silicon wafers were selected randomly from each section. The total number of the wafers was 196.

First, the 28 substrate wafers from each section of the crystal ingots were divided into 4 groups of 7 wafers. One group was set aside and the rest were preanneal heat treated at 650^{o}C in a nitrogen ambient for 30, 150, and 300 minutes, respectively. After preannealing, the wafers were recleaned. Subsequently, the backside of the wafers was encapsulated with 4500 angstroms of thin CVD silicon dioxide film. CVD silicon dioxide deposition was performed by SiH_4 injection onto the backside of the wafer. After the CVD process, the wafers were recleaned. Subsequently the frontsides of the wafer were polished. Approximately 20 microns were removed from the frontsides of the wafers during the polishing step.

After being polished, the wafers were recleaned and inspected. Subsequently, the epitaxial deposition process was performed. During

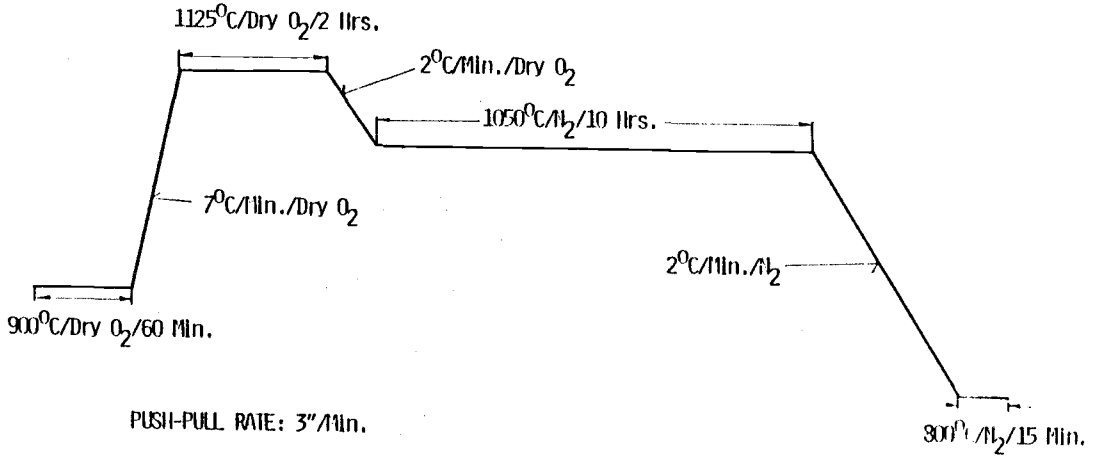

Figure 17: CMOS Short-Loop Cycle

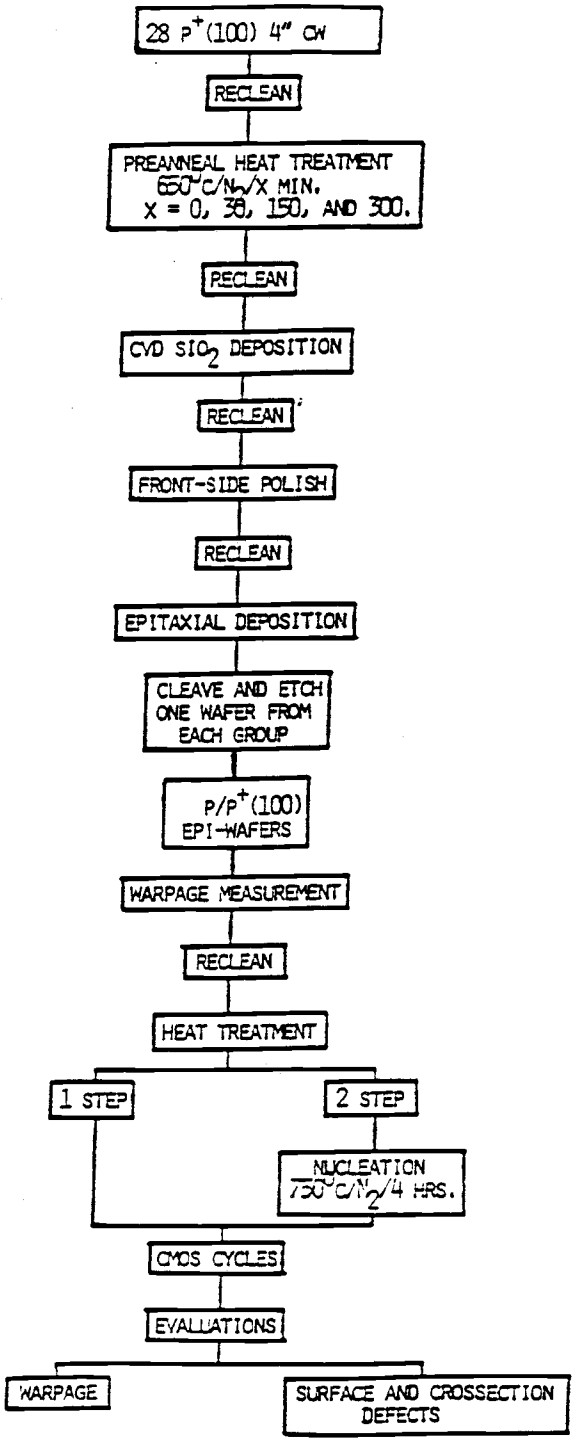

Figure 18: Summary of the Experimental Procedures

this process a high resistivity layer (approximately 30 to 50 ohm-cm) of 13.5 microns was grown on the heavily doped substrate wafers.

The warpage measurement was performed on the Microsense 6034 right after the epitaxial deposition. Subsequently, the wafers were recleaned and inspected. One wafer was taken from each group as a control sample to inspect the bulk defects grown during the epitaxial deposition. Those wafers were cleaved and etched in the Wright etch solution for 1-1/4 minutes.

After final inspection, all wafers were combined and divided into two lots. The wafers from the first lot were nucleation heat treated at 750^{o}C in a nitrogen ambient for 4 hours, and the other lot was set aside. Subsequently, the lots were recombined and the wafers were heat treated according to the short-loop CMOS heat treatment cycles given in Figure 17. After the heat treatment, the warpage measurement was repeated. The experimental procedures are again summarized and shown in Figure 18. The wafers were cleaved and etched in the Wright etch solution for 1-1/4 minutes. The defect count was performed at 200X magnification under the optical light microscope.

C. Impact of the Epitaxial Deposition Process.

In this experiment, two substrate and epitaxial silicon wafers were selected from each section of the crystal ingots. The epitaxial silicon wafers were not preanneal heat treated. The wafers were first cleaved into quarter sections. Only two quarter sections were used in this experiment. The first and second quarter sections were heat treated using heat treatment process A and B, respectively. Heat treatment process A consisted of a nucleation heat treatment at 750^{o}C in a nitrogen ambient for 4 hours, followed by a high temperature heat

treatment at 1050°C in a dry O_2 ambient for 16 hours. Heat treatment process B consisted only of a high temperature heat treatment step at 1050°C in a dry O_2 ambient for 24 hours. Figures 19a and 19b show both heat treatment processes. After being heat treated, the wafers were cleaved and etched in the Wright etch solution for 1-1/4 minutes. The bulk defects were counted under the optical light microscope at 200 X magnification.

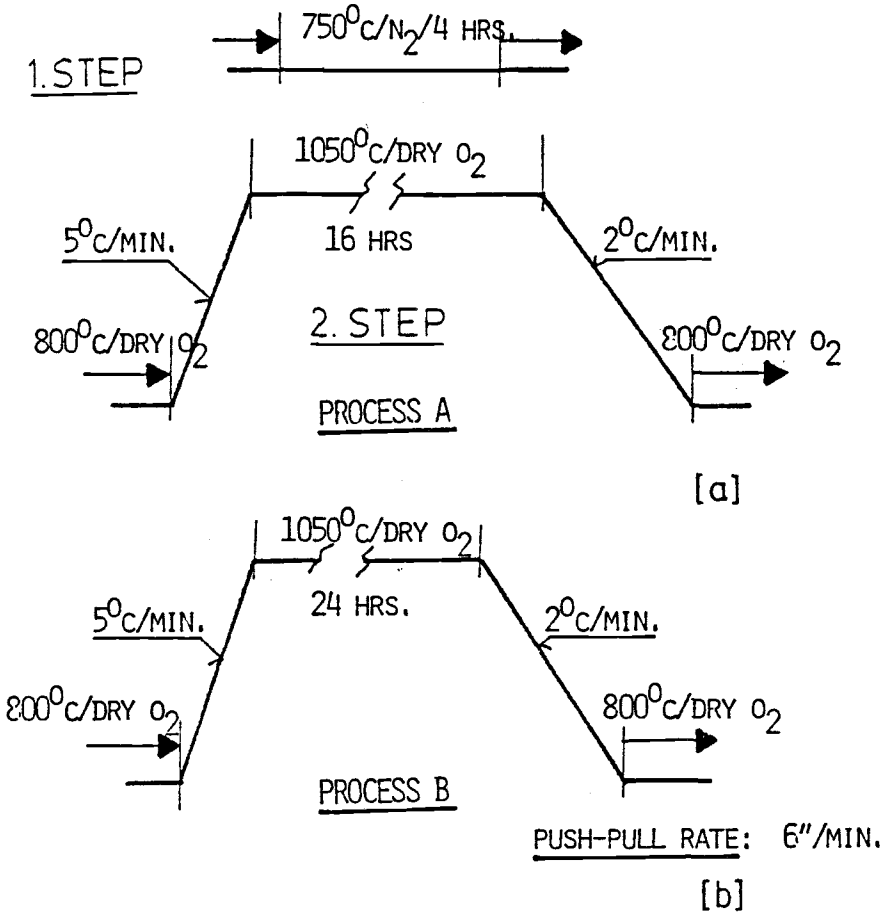

Figure 19: One- and Two-Step Heat Treatment Cycles
a) Process A: Two-Step Heat Treatment Cycle
b) Process B: One-Step Heat Treatment Cycle

VI RESULTS

A. Post-Epitaxial Deposition Heat Treatments.

In this experiment, no surface defects related to the grown-in defects were observed. Upon examination of the cross section at 200X magnification, bulk stacking faults with sizes between 5 and 15 microns were observed, see Figure 20. Also observed were other micro-defects which are identified as microstacking faults under a scanning electron microscope at 2000x magnification. The size of a microstacking fault is under 2 micron. Figures 21a and 21b show the SEM photos of the bulk defects.

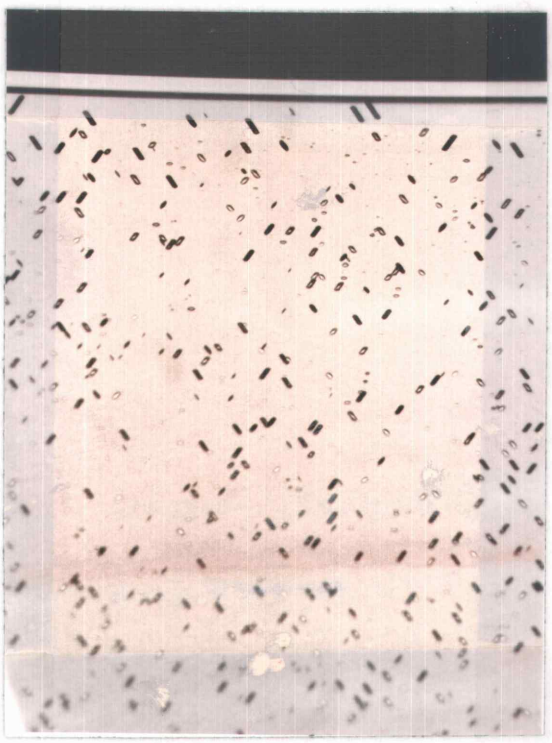

Figure 20: Optical Micrograph of the Cross Section at 200X Magnification

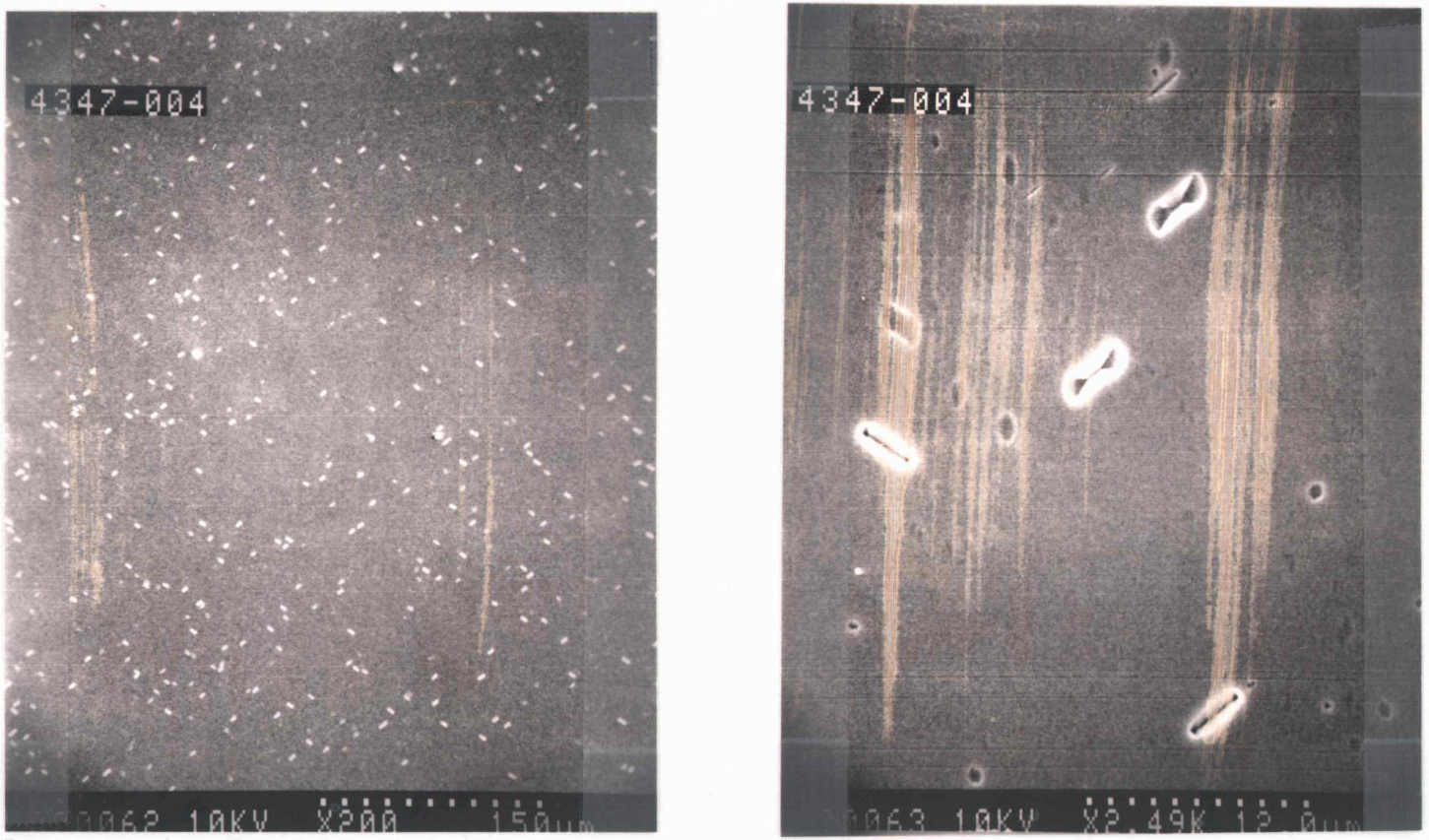

(a) (b)

Figure 21: Scanning Electron Micrographs. a) Bulk Defects at 200X Magnification and b) at 2490X Magnification.

1. Effect of Heat Treatment Ambients on Growth Kinetics of the Bulk Defects.

All bulk defects between 20 to 25 mm from the edge of the wafer were counted and plotted in Figures 22a to 22c. The data obtained from samples heat treated with ramp-up and ramp-down scheduels are shown as closed symbols. In the figures it can be observed that bulk defect density increases with increasing post-epitaxial deposition heat treatment period. In general, bulk defect density in the samples heat treated with a two-step cycle have a higher bulk defect density those that with one-step.

Another observation shows that in the samples heat treated with a one-step cycle, the standard deviation of the bulk defect density is relatively large. (Standard deviation shows as the broken line in the figures.) In some cases, a high bulk defect density in one epitaxial wafer was observed, but no defects in another wafer after a split run using a one-step heat treatment cycle. This phenomenon is believed to be related to the thermal history and to the spatial location of the wafers from the crystal ingot, but not to the heat treatment ambients.

In Figures 23a and 23b bulk defect density in the samples that were heat treated with one- and two-step cycles is plotted. From Figure 23a it can be observed that bulk defect density in the samples heat treated with a one-step cycle in nitrogen ambient is higher than that in wet oxygen and dry oxygen ambients. The bulk defect density in the samples heat treated in wet oxygen and dry oxygen ambients is comparable. We believed that this phenomenon is related to the heat treatment ambient as reported by S.M. Hu [94]. In his model, vacancy-oxygen complexes in the as-grown stage will be annihilated during the oxidation process by silicon self-interstitials generated at the

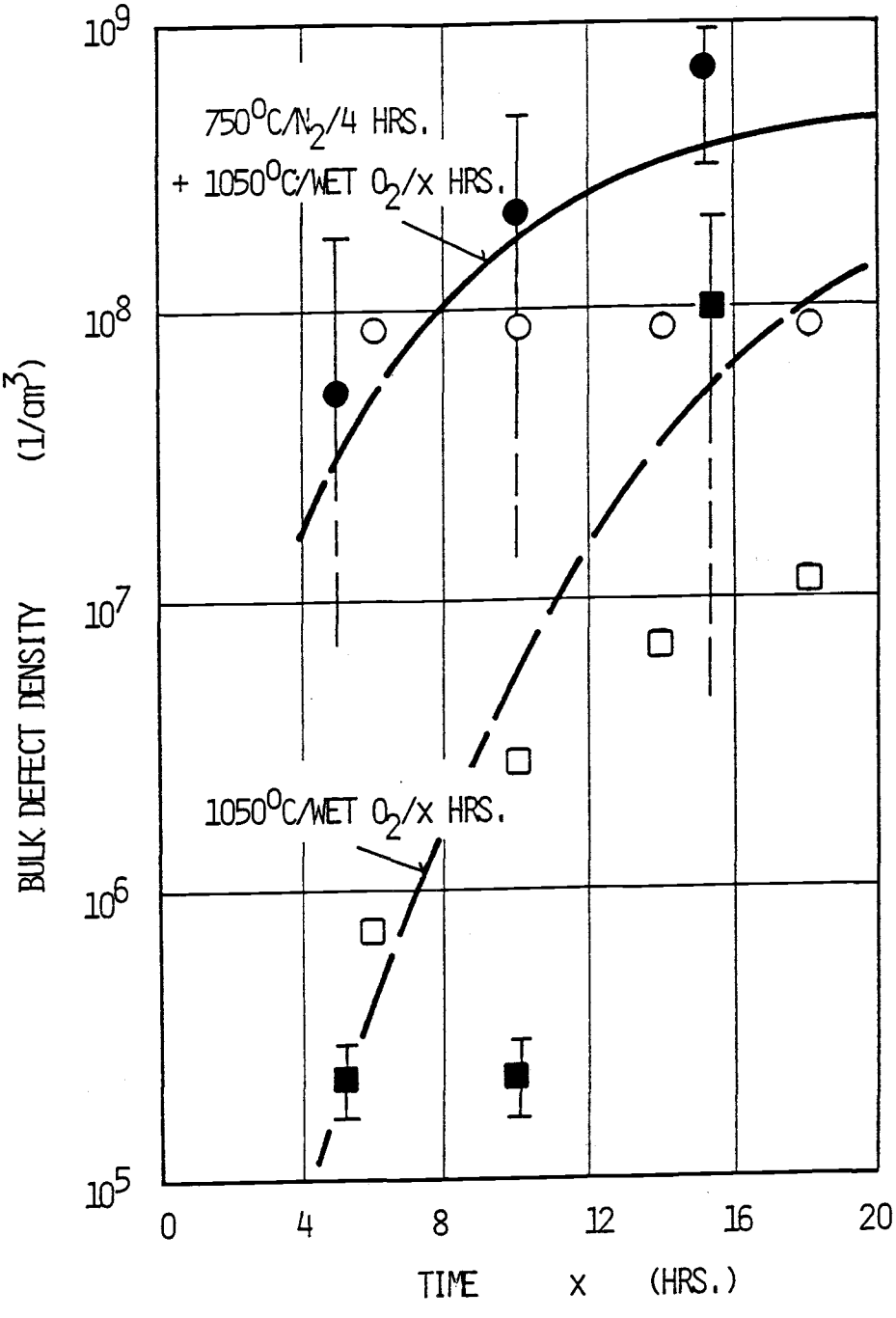

Figure 22: Relationship between Bulk Defect Density and Heat Treatment Time
a) In Wet O2 Ambient
b) In Dry O2 Ambient
c) In Nitrogen Ambient

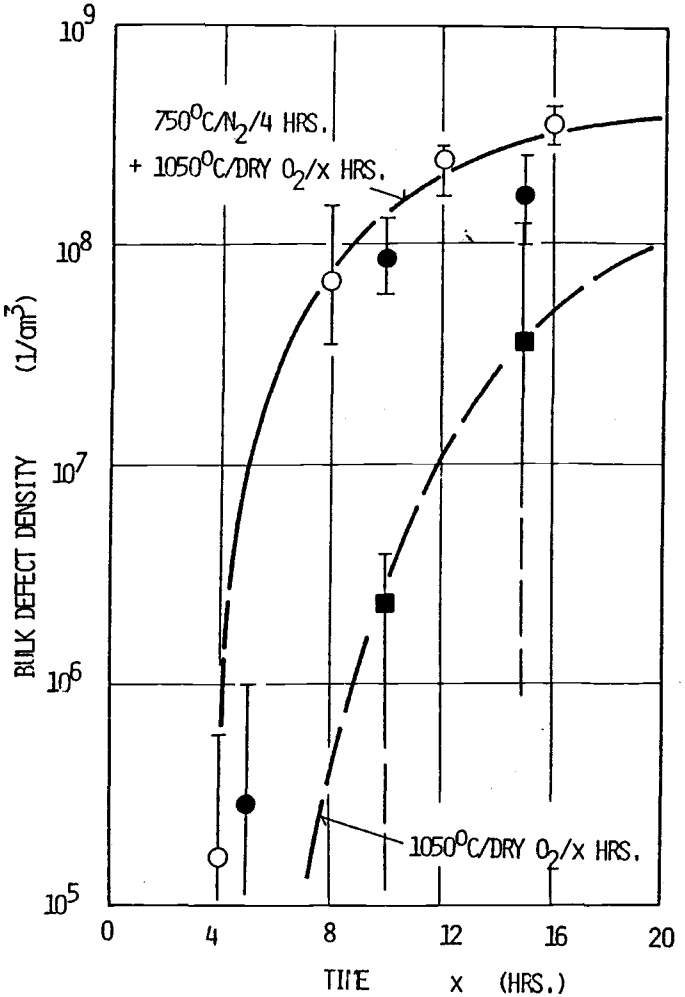

Figure 22b:

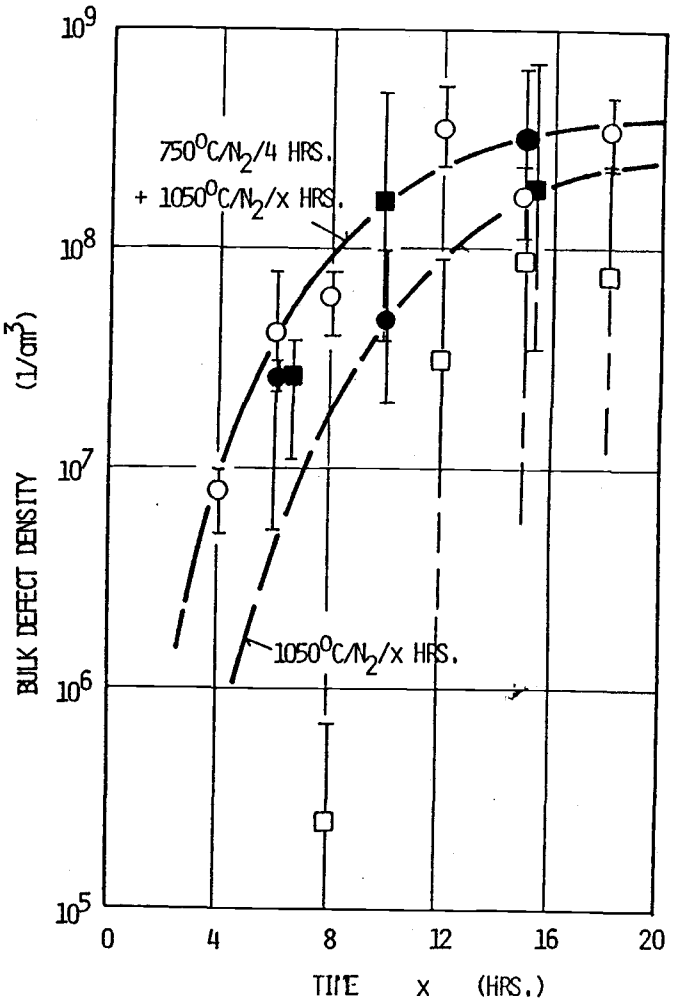

Figure 22C:

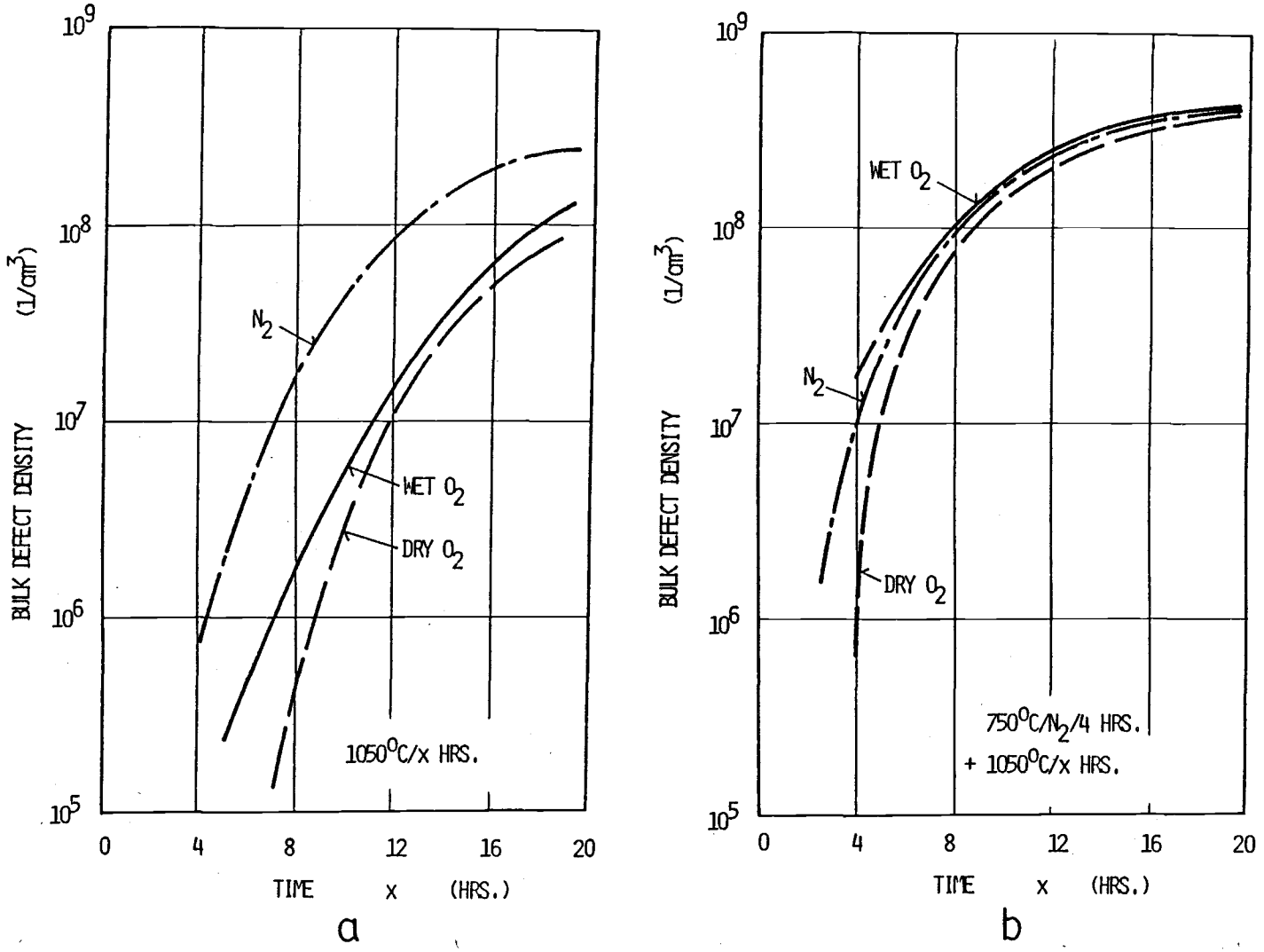

Figure 23: Effect of Heat Treatment Ambients on Bulk Defect Density
a) One-Step Heat Treatment b) Two-Step Heat Treatment

silicon surface.

From Figure 23b, bulk defect density in the samples heat treated using a two-step cycle in all ambients is comparable. It is suggested that this phenomenon may be caused by heterogeneous nucleation at the preexisting precipitate nuclei. In as-received silicon wafers, oxygen precipitate nuclei exist in various forms [7], [95]. Nuclei can be dissolved partially or completely during the epitaxial depostion process and during subsequent heat treatment. The amount of dissolution depends upon the initial size of the nuclei. Large nuclei will remain in the silicon after the epitaxial deposition process. Subsequent low temperature annealing will cause heterogeneous nucleation and in turn cause an increase in nuclei size. Large nuclei are normally stable, and consequently, the effect of the ambients (induced point defects) becomes negligible.

Figures 24a and 24b show the defect density distibution from the edge to the center of the wafer. It can be seen that the bulk defect density at the edge of the wafer is lower than that at the center of the wafer. These results agree with the point defect distribution model proposed by T. Abe, which was described in detail earlier. From observation bulk defect density increases exponentially from the edge to the center of the wafer. In the case where no nucleation heat treatment was applied prior to post-epitaxial heat treatment, the slope of the curve increases with increasing post-epitaxial heat treatment period (see Figure 24a). No significant increase was observed when nucleation heat treatment was applied.

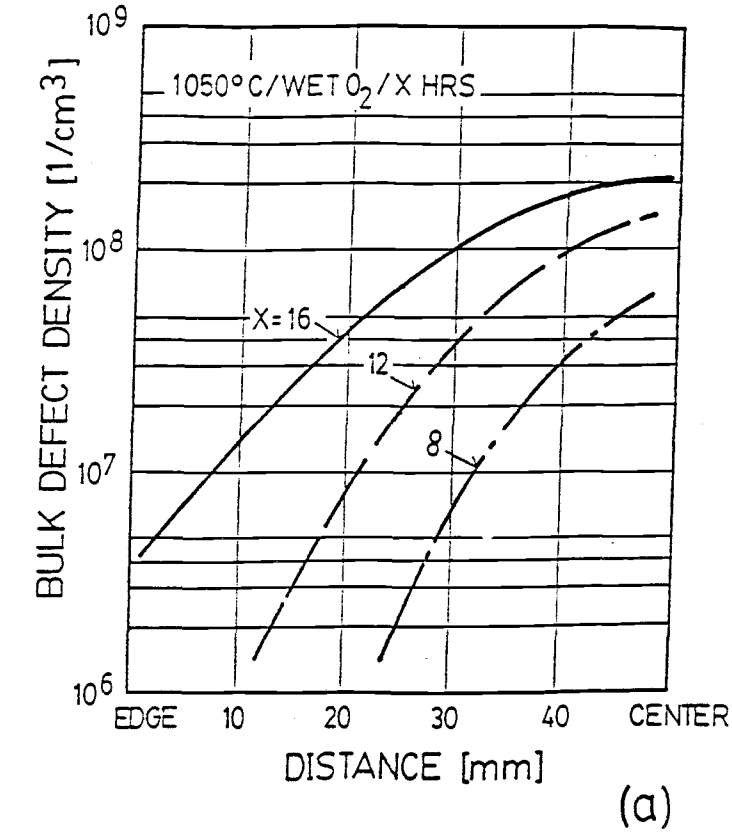

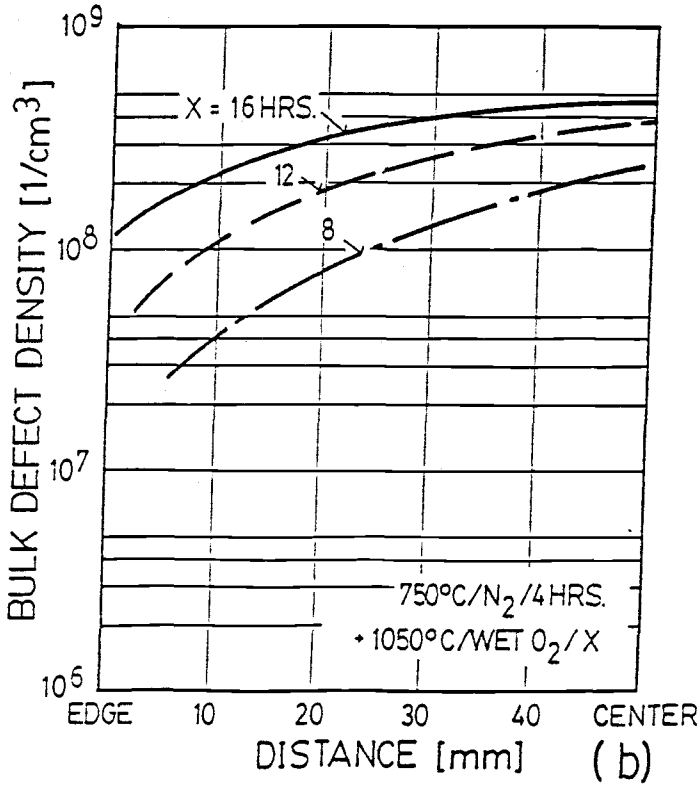

Figure 24: Bulk Defect Density Distribution across the Epitaxial Wafers a) One-Step Heat Treatment b) Two-Step Heat Treatment.

2. Effect of Ambients on the Denuded Zone Formation.

It is known that oxygen atoms diffuse out when the wafer is subjected to high temperature heat treatment. Therefore, during the epitaxial deposition process, oxygen atoms diffuse into the growing epitaxial layer and in turn cause a decrease in oxygen concentration at the surface region of the substrate wafer. If the initial oxygen concentration in the substrate wafers was low, a denuded zone will form underneath the epitaxial layer after subsequent high temperature heat treatment.

Figure 25 shows the relationship between denuding time in nitrogen and in dry oxygen ambients and denuded zone width (DZW). It can be seen that in the nitrogen ambient the denuded zone width increases with increasing denuding time, while in dry oxygen ambient it remains

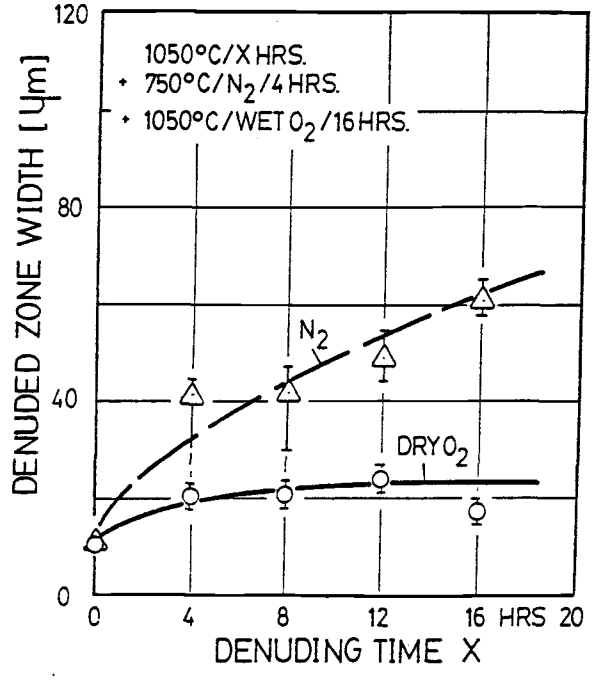

Figure 25: Relationship between Denuding Time and Denuded Zone Width

constant. Monkowski, et al [96] measured the diffusivity of oxygen atoms during out-diffusion from the silicon substrate in various ambients. From their measurements, the out-diffusion rate of oxygen in a nitrogen ambient is higher than that in a dry oxygen ambient. It was suggested that during heat treatment of silicon in nitrogen ambient, vacancies are introduced into the silicon substrate. Oxygen atoms do not diffuse via substitutional sites of the silicon lattice, however vacancies ease out-diffusion process of oxygen. Their results also seem to explain the results shown in Figure 25, where denuded zone width formed in nitrogen ambient is larger than that in dry oxygen ambient.

Andrews [97] calculated the denuded zone width formed in dry oxygen ambient using a Laplace transformation equation and an oxygen supersaturation ratio s = 4.7. From his results, denuded zone width in dry oxygen ambient increases with increasing denuding time. The experimental results in dry oxygen ambient, however, indicate that Laplace's equation can not be applied for a very long denuding time. It is, therefore, suggested that the denuding mechanism might also involve a point defect interaction. This interaction is not well understood at the present time.

Figure 26 shows the relationship between bulk defect density and denuding time in dry oxygen and nitrogen ambients. It can be seen that denuding in nitrogen ambient causes less reduction in bulk defect density than denuding in dry oxygen. This result agrees with the results shown in Figure 23a. It is believed that during denudation, point defect interaction with precipitate nuclei is similar to that during one-step heat treatment. Ambients of the following heat

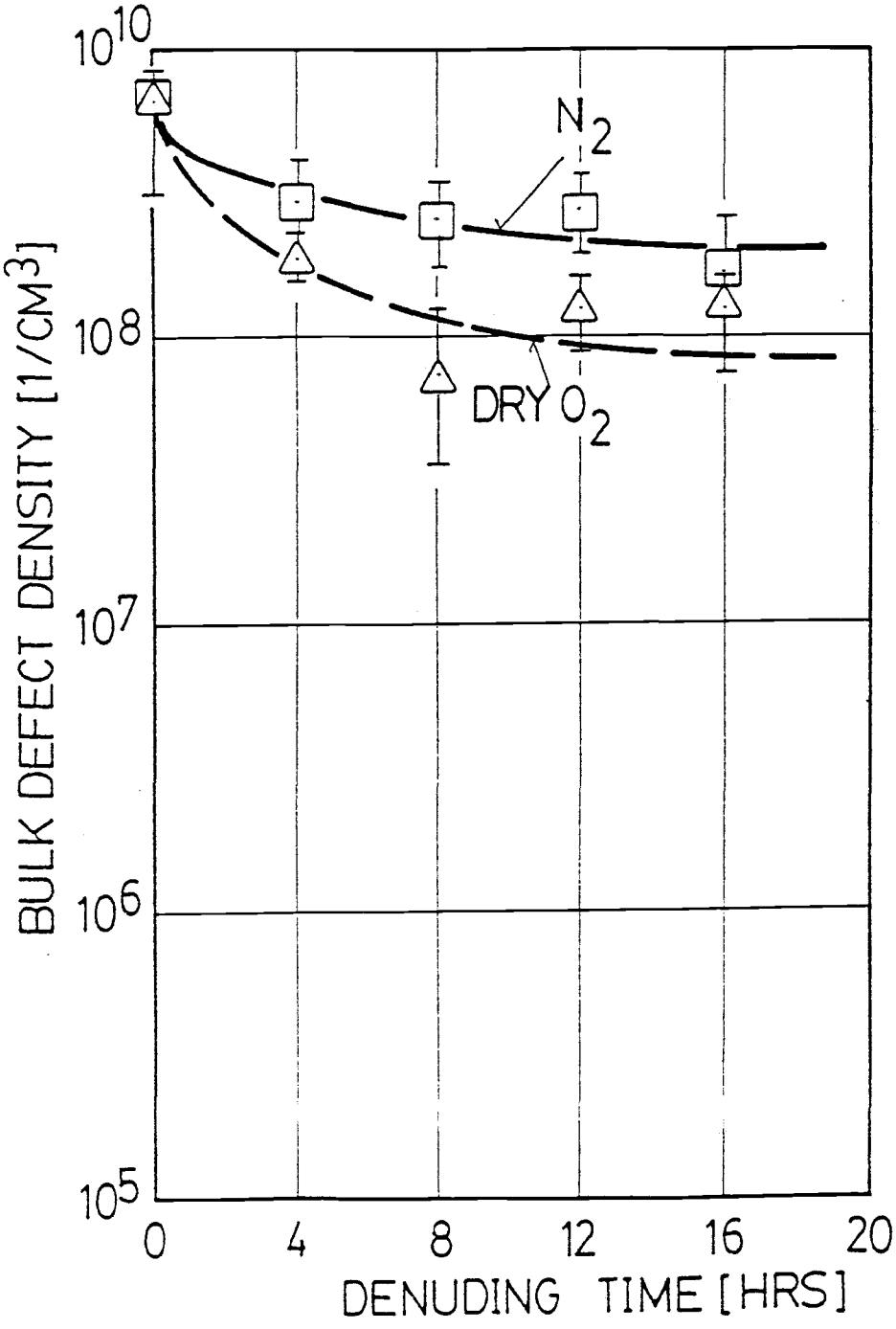

Figure 26: Relationship between Denuding Time and Bulk Defect Density

treatments (nucleation and growth steps) have less effect on the growth of precipitate nuclei.

B. Pre-Epitaxial Deposition Heat Treatment.

1. Warpage.

Figure 27 and 28 show the results of the warpage measurements. It can be seen that warp decreases uniformly after the heat treatment cycles; The linear relationship between initial warp W_i and the final warp W_f can be expressed as follows:

$$W_f = 0.85\, W_i - 2.5 \quad [\text{microns}] \qquad (10)$$

where W_i is the initial warp [microns] measured after the epitaxial deposition process and W_f is the final warp [microns] measured after the CMOS heat treatment. It should be noted that oxide grown on the front-side of the epitaxial wafers after the CMOS heat treatment was not removed before the warpage measurement.

Another observation is that decrease in warp does not depend upon either spatial location in the crystal or the pre- and post-epitaxial deposition annealing. This is because the slopes shown in Figures 27 and 28 are identical.

Figures 29 and 30 show the relationship between change in warp and preannealing time. Change in warp is defined as:

$$\text{Change in Warp} = (W_f - W_i) \times 100 / W_f \quad [\%] \qquad (11)$$

From the figures, no correlation between change in warp and preanneal heat treatment period was found.

In polished silicon wafers there is still controversy over the

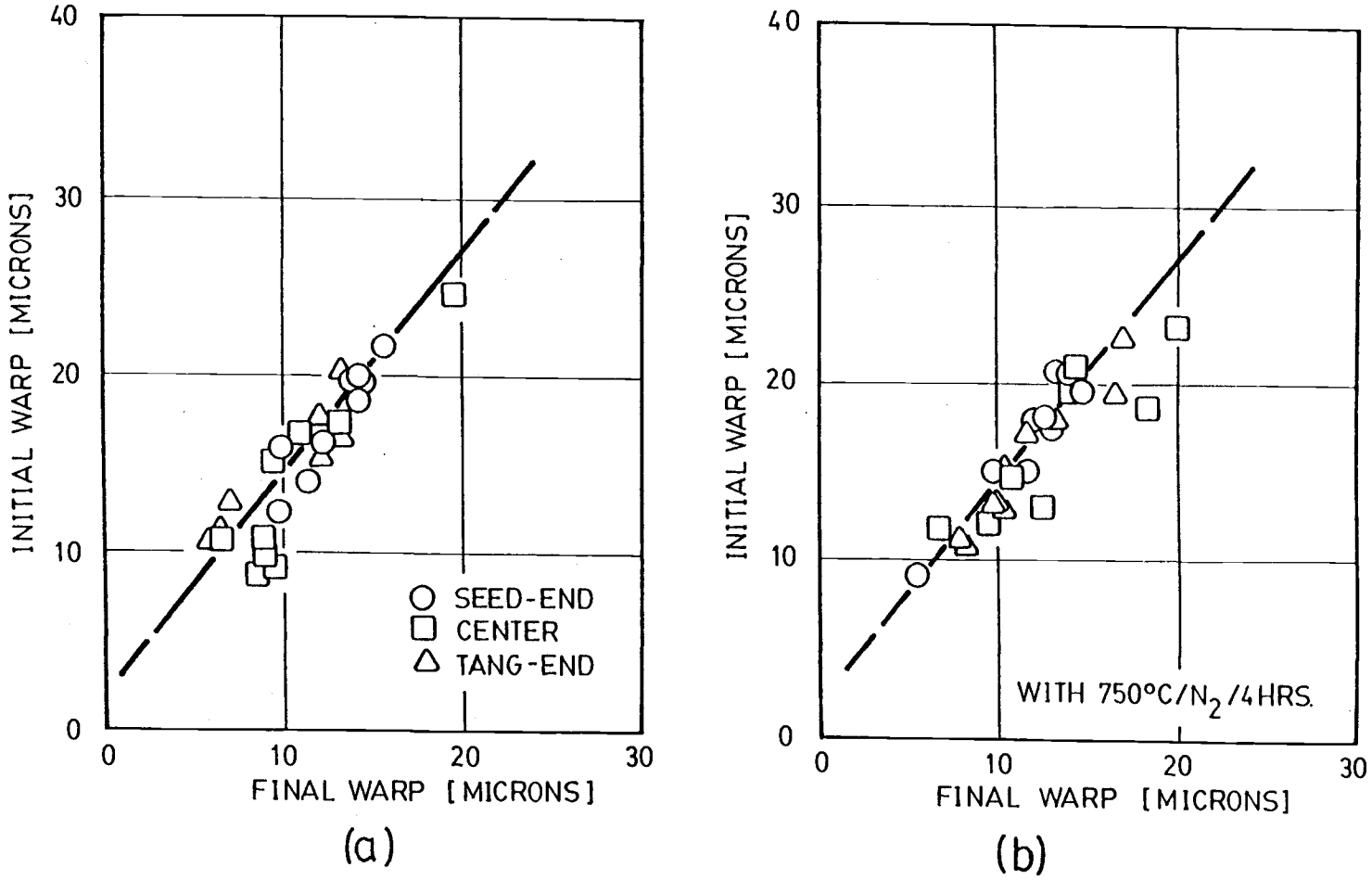

Figure 27: Relationship between Initial and Final Warp in Crystal Ingot containing Low Oxygen Concentration
a) Without Post-Epitaxial Deposition Annealing
b) With Post-Epitaxial Deposition Annealing

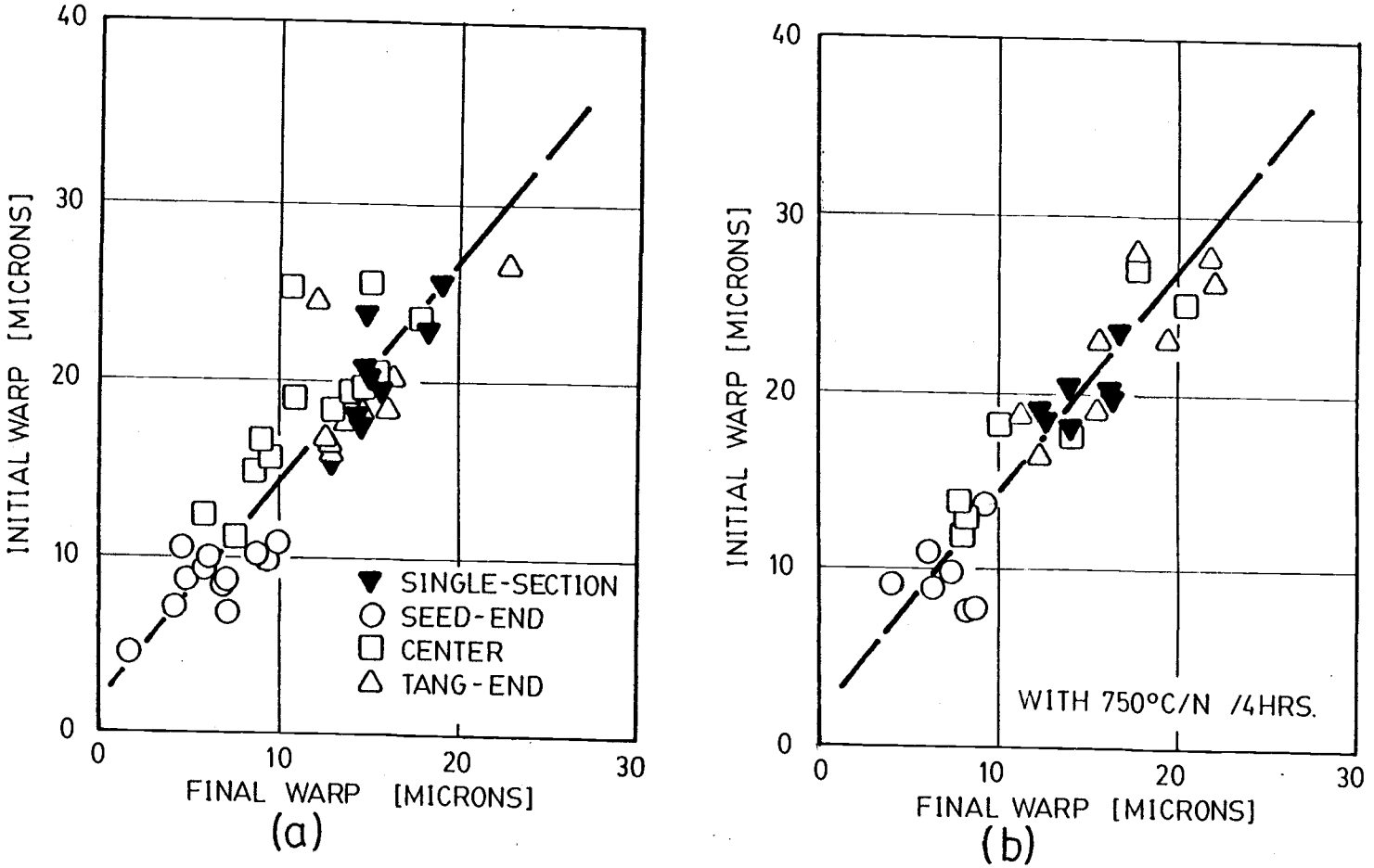

Figure 28: Relationship between Initial and Final Warp in Crystal Ingot containing Medium Oxygen Concentration
a) Without Post-Epitaxial Deposition Annealing
b) With Post-Epitaxial Deposition Annealing

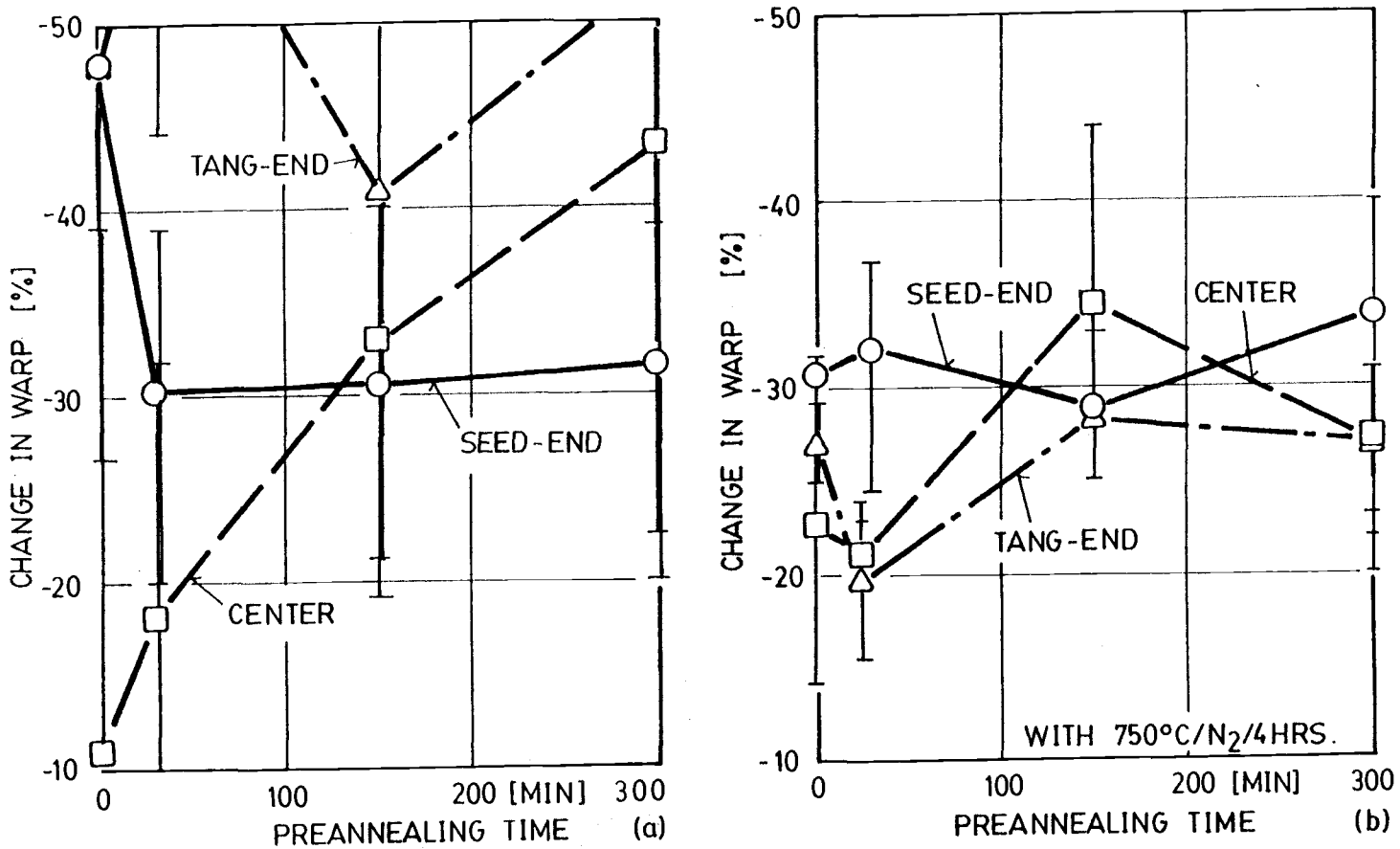

Figure 29: Relationship between Preannealing and Change in Warp in Crystal Ingot Containing Low Oxygen Concentration
a) Without Post-Epitaxial Deposition Annealing
b) With Post-Epitaxial Deposition Annealing

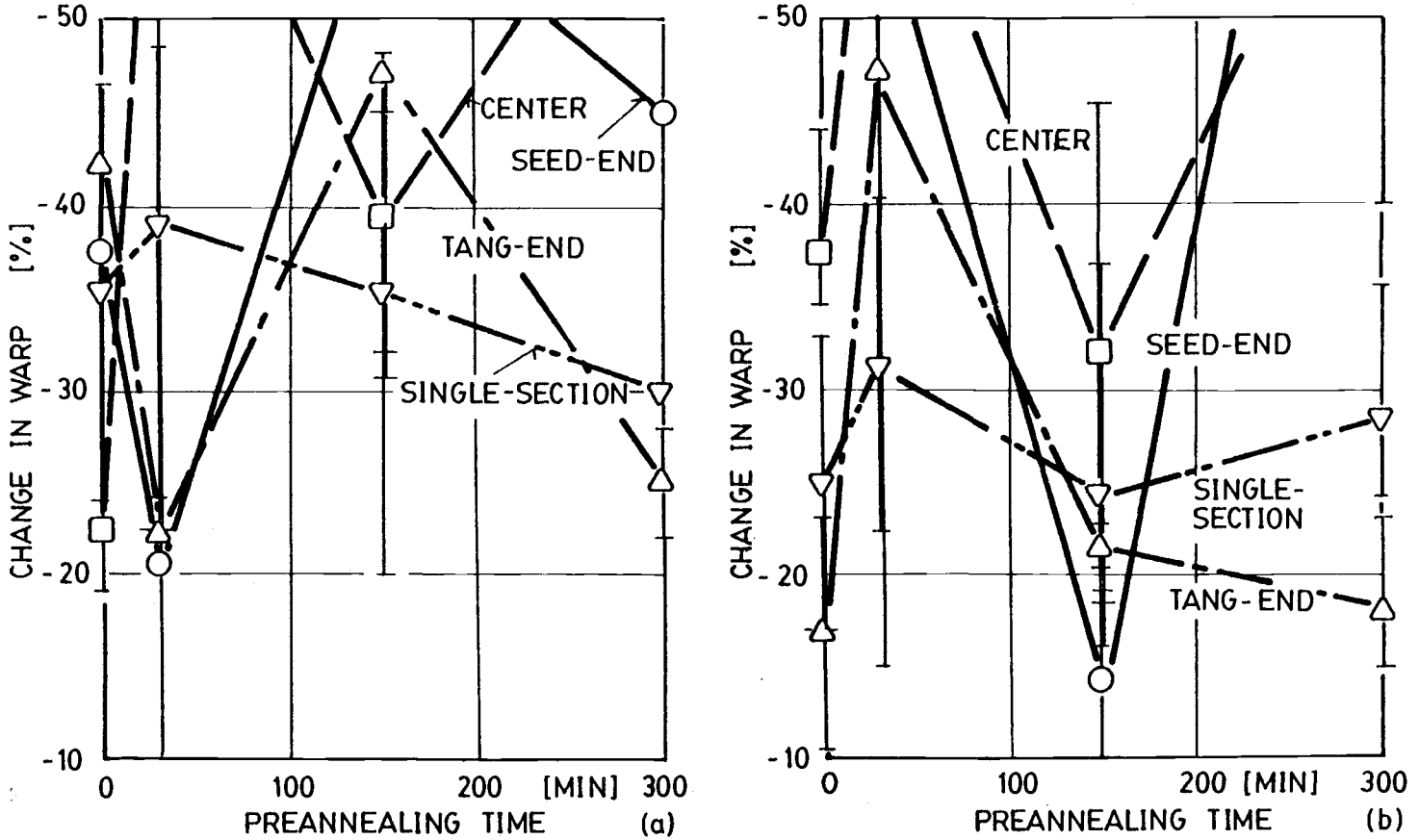

Figure 30: Relationship between Preannealing and Change in Warp in Crystal Ingot Containing Medium Oxygen Concentration
a) Without Post-Epitaxial Deposition Annealing
b) With Post-Epitaxial Deposition Annealing

dependency of warpage on the internal gettering process. Swaroop [98] has reported on his experiment on the internal gettering processes applied to MOS and Bipolar heat treatment cycles. From his experiment he could not observe any correlation between oxygen concentration and the change in warp following the thermal cycles. However, it was pointed out that asymmetrical precipitation of oxygen across the wafer could affect warp [98]. On the other hand, Tarui [99] has shown that dissolved oxygen atoms have the effect of suppressing process-induced warp, and that reduction in oxygen might result in an increase in warp. He noted that warp is also affected by the presence of surface films (SiO_2 or other) and is not influencd by the oxygen concentration in the wafer, especially when the radial oxygen gradient of the wafers is less than 1 ppmA.

The effect of dissolved oxygen atoms on the mechanical properties of silicon has been studied by many researchers. Patel [112] suggested that the yield strength of silicon crystals is decreased when the oxygen atoms form oxide precipitates and this facilitates the nucleation of dislocations. S.M. Hu [19] first claimed that neither interstitially dissolved oxygen nor oxide precipitates have any appreciable dislocation pinning effect, but later reported [20] on a definitive proof of the pinning effect caused by oxygen atoms in silicon. Theoretically, oxygen atoms which have a relatively large size compared to silicon and other impurity atoms will occupy the interstitial site of the silicon lattice [101] and hinder the movement of the silicon lattice under shear stresses. Therefore float-zone silicon wafers which contain oxygen atoms less than the FTIR measureable level are far more susceptible to slip than Czochralski wafers [102].

Blockage of lattice or dislocation movement ultilizing precipitate particles has been employed for many years in the steel industries. Batavin [103] - [104] reported on observing a hardening effect, due to the oxide precipitates. His observation is easy to verify because at room temperature precipitated silicon wafers are much more brittle than unheat treated wafers. However, at device processing temperatures, high tensile stresses develop in the silicon matrix due to precipitation [105] and in turn creating internal stresses in the silicon matrix. As a result, precipitation of oxygen atoms might lead to lowering of the silicon yield strength [106].

In epitaxial silicon material the situation is much more complicated. CVD silicon oxide film deposited at a relatively low temperature is under compressive stresses at room temperature due to a thermal expansion coefficient mismatch between the oxide film and silicon substrate. However, at temperatures above CVD silicon oxide deposition temperature, tensile stresses will develop in the oxide film. The magnitude of the stress depends upon the temperature difference between the device processing temperature and CVD silicon oxide deposition temperature. Therefore, it can be assumed that at the precipitate growth temperature, high stresses could develop in the silicon substrate.

Another important factor which has to be considered in this experiment is the oxide that is thermally grown during the CMOS test cycles. Actually, the effect of thermally grown oxide film stress should be taken into consideration because during the cooling period high compressive stress can develop in the oxide film [107]. Warp can be either a result of a permanent distortion of the silicon lattice or

an elastic deformation which can be recovered after removing the surface film. In this experiment, where oxide film with the same thickness on each wafer was thermally grown on the front-surface, it can be assumed that the effect of oxide film stress will be similar on each wafer. Therefore the warpage measurement results should not be affected when the oxide film was not removed.

As long as the correlation between mechanical behavior of silicon and precipitation phenomenon is not well established, the controversy over the dependency of warp on internal gettering will remain [98].

2. Effect of Preanneal Heat Treatment.

Bulk stacking faults (BSFs) and microstacking faults (MSFs) are shown in Figures 31 and 32. MSFs and BSFs can be distingushed from each other by their size and appearance. A MSF's length is less than 2 microns, while a BSF is normally between 10 and 15 microns long and is found to be decorated with precipitate particles.

A bulk stacking fault decorated with oxide precipitate particles (OXPREP) is shown in Figure 32a. Single precipitate particle was also found outside the fault. Other types of bulk defects could not be found. It is, therefore, concluded that bulk defects consist of bulk stacking faults, microstacking faults and precipitate particles. At 200x magnification only BSFs and MSFs were observed and counted.

The relationship between bulk defect density in the crystal containing low oxygen concentration and preannealing time is shown in Figure 33a. It can be seen that the bulk defect density increases with increasing preannealing time. From observation, the bulk defect density in the seed-end section is higher than that in other sections.

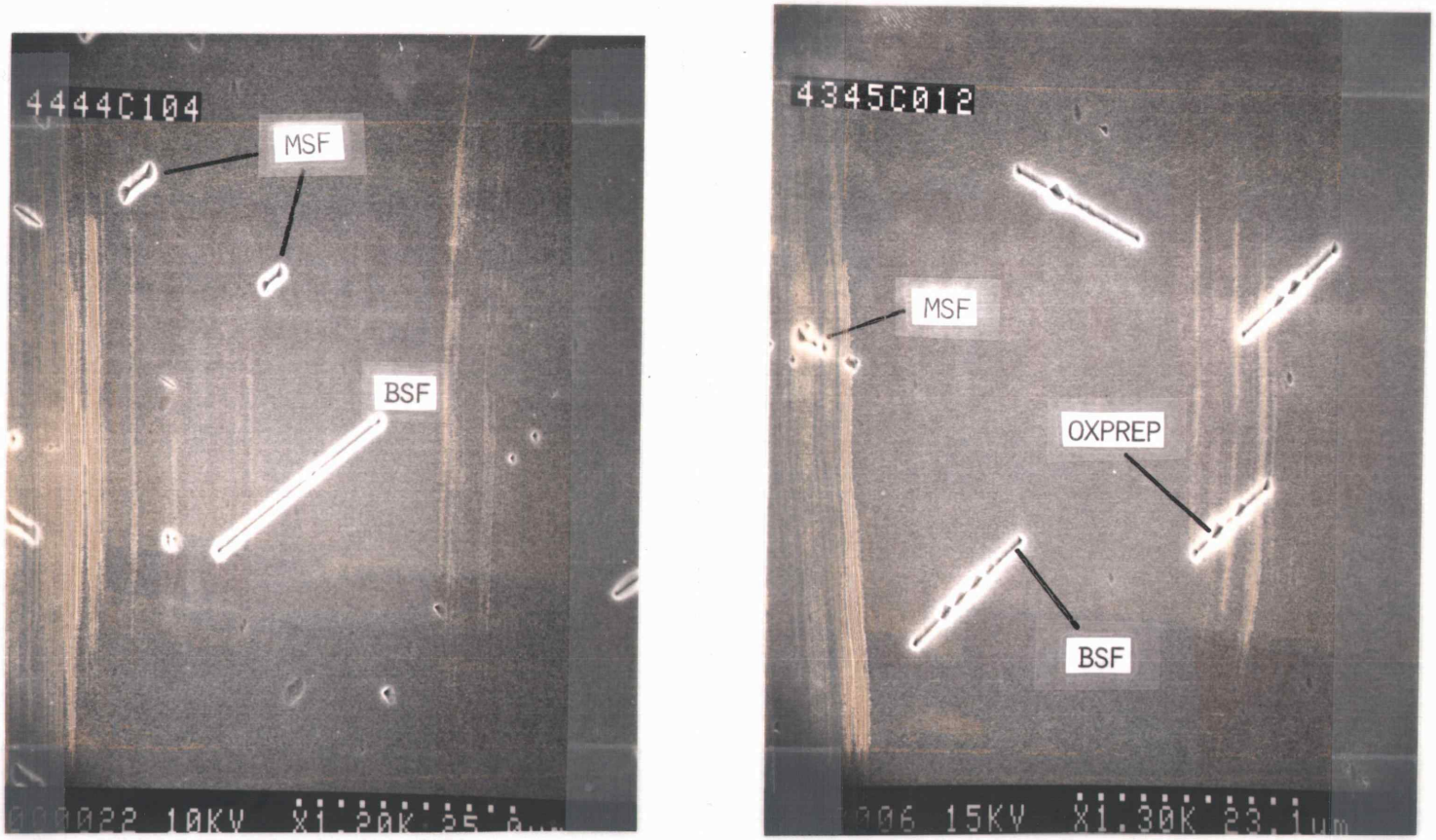

Figure 31: SEM Photomicrograph of the Bulk Defects

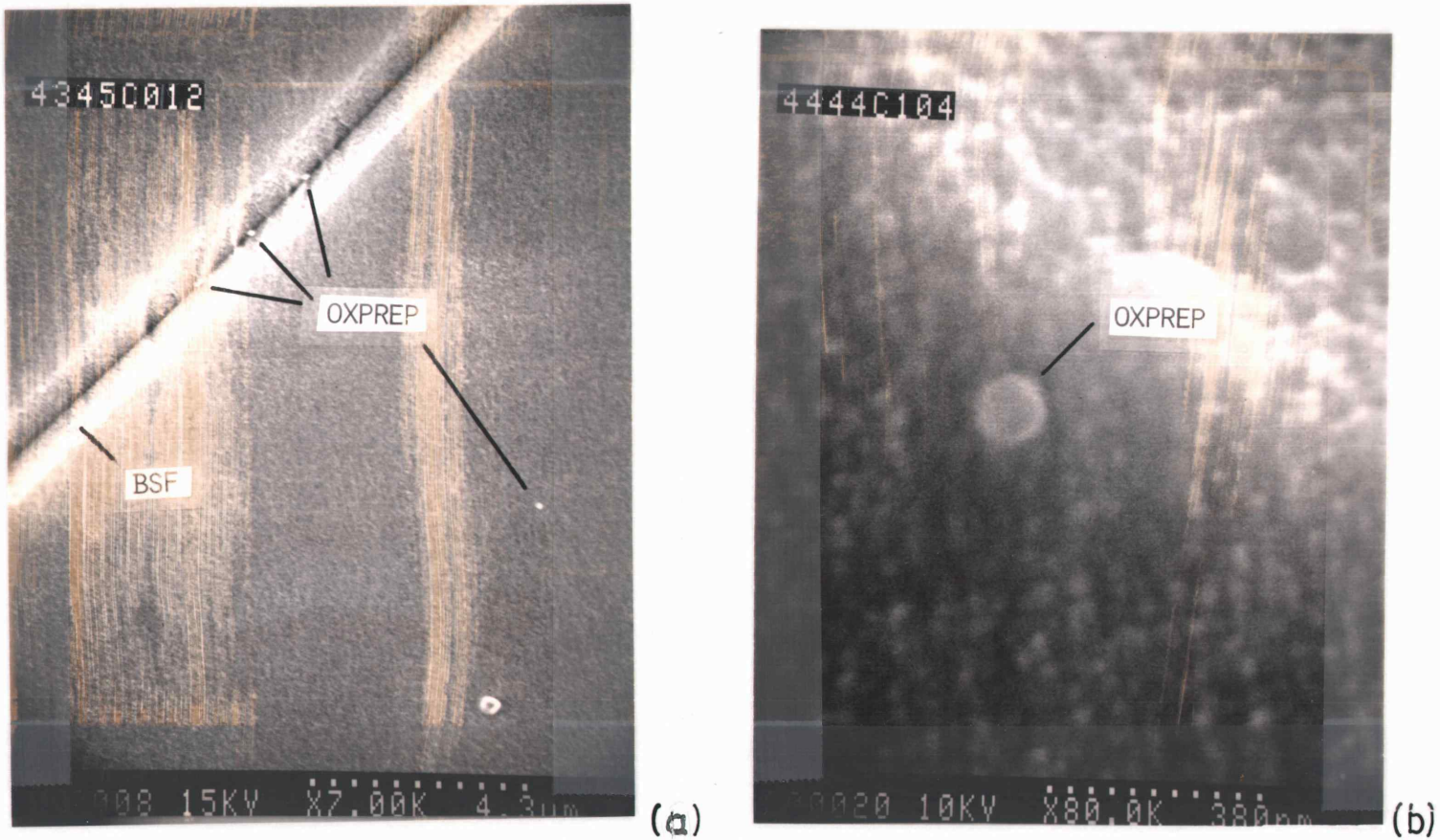

Figure 32: SEM Photomicrographs of the Bulk Defects
a) Bulk Stacking Fault Decorated with Precipitate Particles
b) Precipitate Particle

In the center and tang-end sections, bulk defect density seems to be comparable, except in the case where no preannealing was applied. In that case, no bulk defects can be observed in the tang-end section at 200X magnification.

In the crystal containing medium oxygen concentration, as shown in Figure 34a, bulk defect density increases with increasing preannealing time. The defect density in the single-section, seed-end, and center section seems to be comparable and much higher than that in the tang-end section.

Comparing the relationships plotted in Figures 33a and 34a, it was found that the nucleation and growth behaviors of the bulk defects in both crystals are similar. The differences in bulk defect density are presented as follows: On the seed-end no significant difference in bulk defect density can be observed. On the other hand, bulk defect density in the center section of medium oxygen concentration crystal is much higher than that in low oxygen concentration crystal. At this point it is still not clear whether this effect is related to a difference in oxygen concentration or to the actual length of the crystal. In the tang-end section, bulk defect density is again comparable.

3. Effect of Post-Epitaxial Deposition Annealing.

In Figures 33b and 34b the relationship between bulk defect density and preannealing time is plotted. It should be noted that the wafers were annealed at 750°C prior to the CMOS test cycles.

In the crystal containing low oxygen concentration, bulk defect density in the seed-end section initially increases rapidly with increasing preannealing time and remains unchanged after approximately

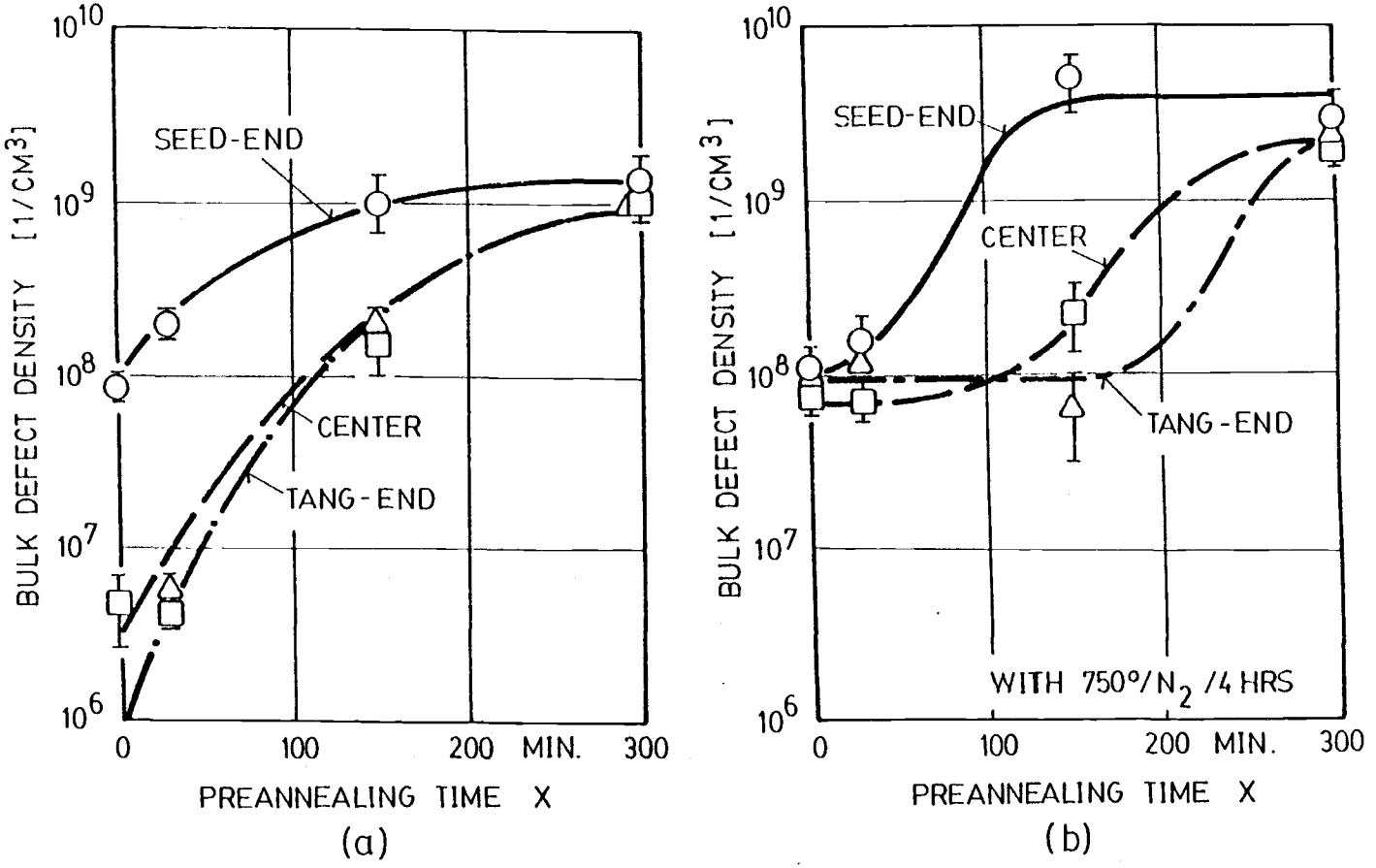

Figure 33: Relationship between Preannealing and Bulk Defect Density in Crystal Ingot containing Low Oxygen Concentration
a) Without Post-Epitaxial Deposition Annealing
b) With Post-Epitaxial Deposition Annealing

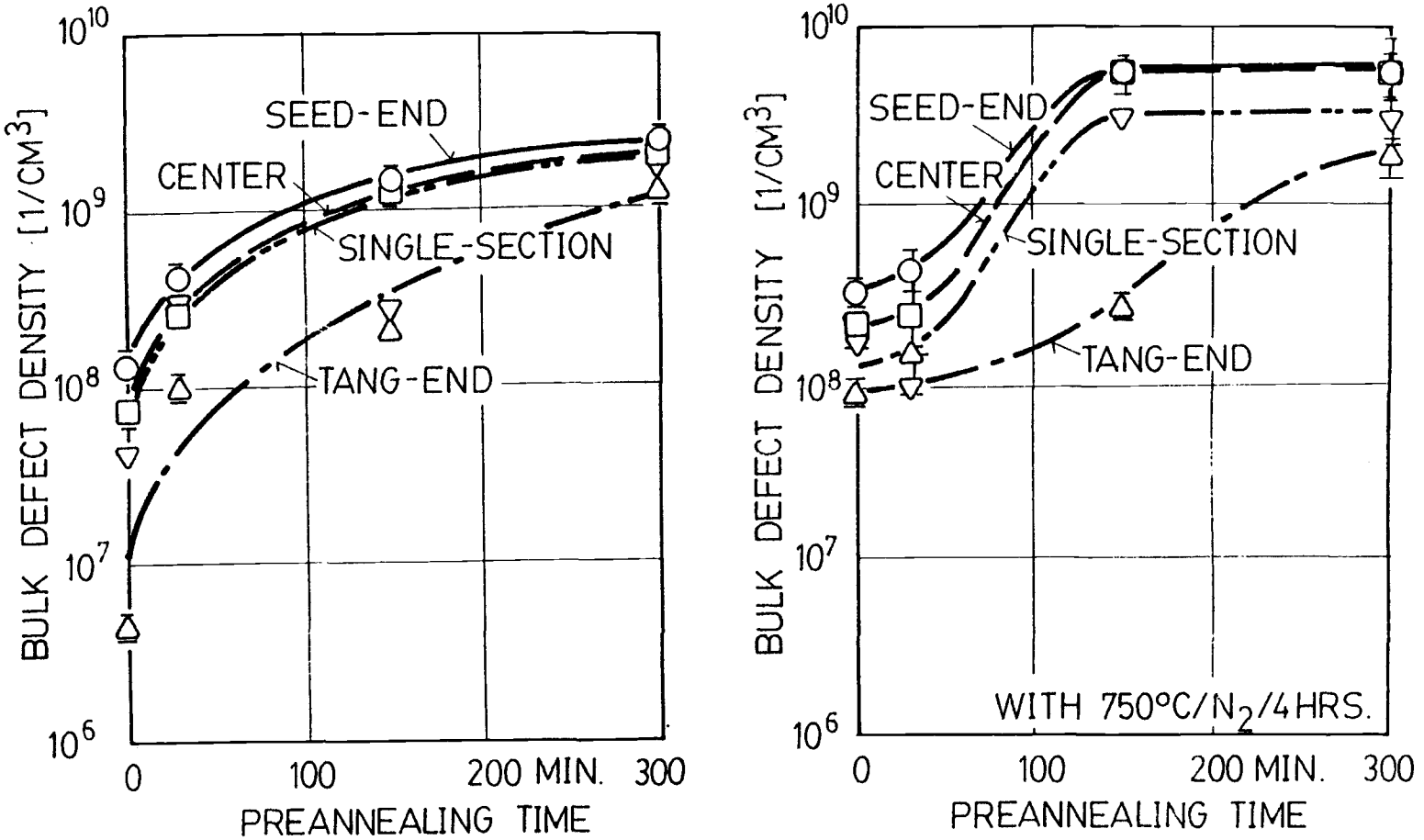

Figure 34: Relationship between Preannealing and Bulk Defect Density in Crystal Ingot Containing Medium Oxygen Concentration
a) Without Post-Epitaxial Deposition Annealing
b) With Post-Epitaxial Deposition Annealing

150 minutes of preannealing (see Figure 33b). Unlike the seed-end , in the center and tang-end sections a certain preannealing period or "incubation time" is required before any increase in the bulk defect density could be observed. From observation, "incubation time" in the tang-end is relatively long compared to the center section.

Similar results, as described above, are also observed in the crystal containing medium oxygen concentration, except in the center section, where bulk defect density initially increases rapidly with increasing preannealing time.

4. Effect of Spatial Location in the Crystal Ingot.

Figures 35a and 35b show the bulk defect distribution in a crystal containing low oxygen concentration. In the case where no preannealing was applied, bulk defect density decreases from the seed-end toward the center section, and no bulk defects were observed in the tang-end section of the crystal. In the case where preannealing was applied, bulk defects were observed in all sections. Prolonged preannealing (more than 150 minutes) can result in almost uniform defect distribution throughout the crystal ingot. It should be noted that a lower bulk defect density in the center section was observed.

Figure 35b shows the bulk defect density distribution along the same crystal. The samples received a post-epitaxial deposition annealing at 750°C. It can be seen that the bulk defect density is relatively uniform in the case where no or only 30 minutes of preannealing was applied. For 150 minutes of preannealing, a high bulk defect density was observed in the seed-end section. For 300 minutes of preannealing, bulk defect density seems to be high and almost

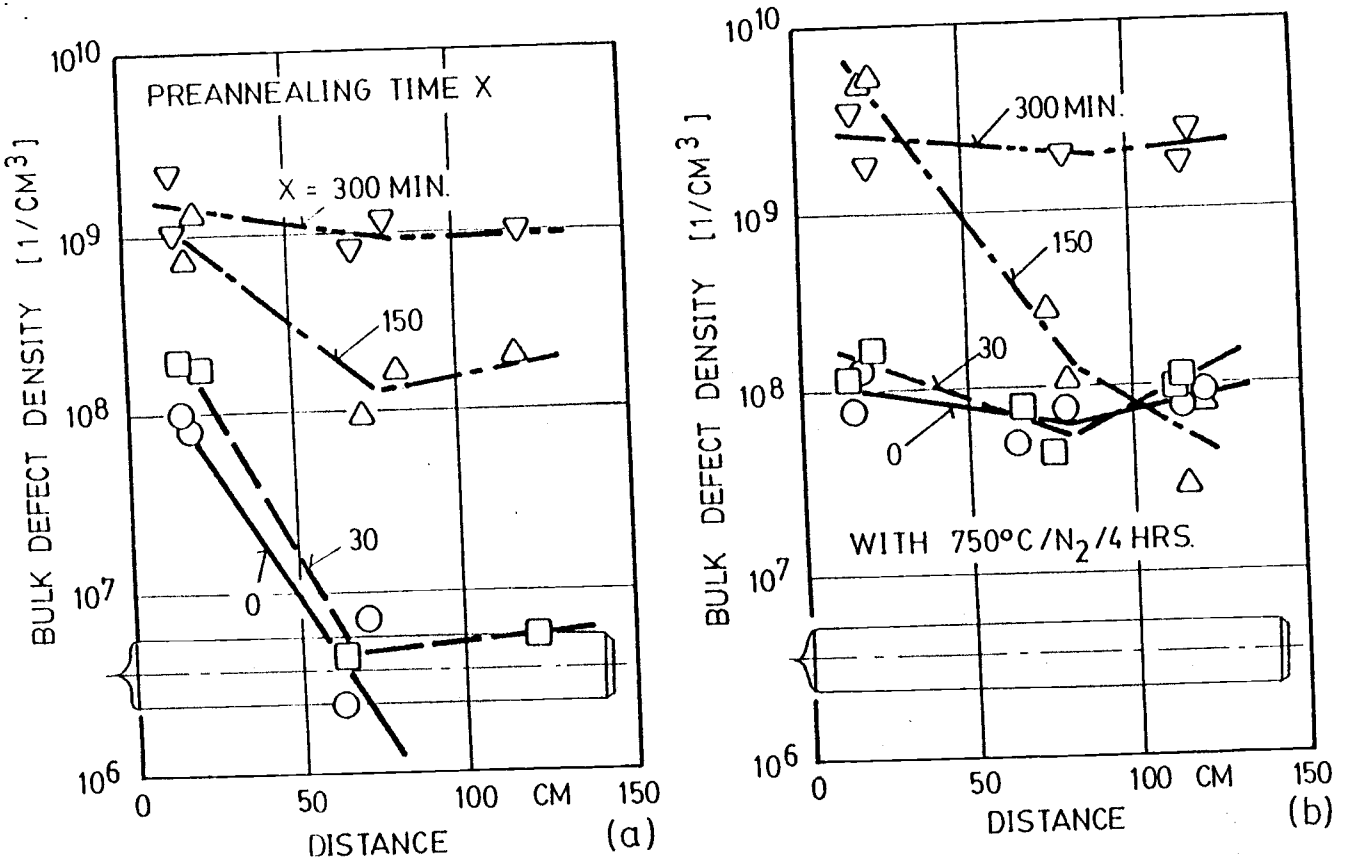

Figure 35: Bulk Defect Distribution in Crystal Ingot containing Low Oxygen Concentration
a) Without Post-Epitaxial Deposition Annealing
b) With Post-Epitaxial Deposition Annealing

uniformly distributed throughout the crystal. Similar to Figure 35a, a kink in defect distribution at the center section was again observed.

From the oxygen concentration profile, shown in Figure 16a, a kink has already been observed at the center section of the ingot. This kink could be caused by changing a crystal growth parameter such as the crucible rotation or crystal pull-rate. Change in growth parameters can cause an increase or decrease in the incorporation rate of the point defects, and therefore the grown-in defect density. The mechanism was already explained earlier. It is believed that this change caused a significant drop in bulk defect density, despite relatively high oxygen concentration in that section. From observation, pre- and post-epitaxial deposition annealing could not correct this growth procedure related effect.

Figures 36a and 36b show the defect density distribution in the crystal containing medium oxygen concentration. From Figure 36a it can be seen that the bulk defect density decreases from the seed-end toward the tang-end section. After 30 minutes of preannealing, bulk defect density in the tang-end section seems to increase significantly. For 300 minutes of preannealing it can be observed that the bulk defect density distribution is almost uniform throughout the crystal.

In the case where the wafers have been annealed at 750° C in nitrogen ambient (see Figure 36b), no significant change in the defect distribution was observed when no or 30 minutes of preannealing was applied. Significant increase in defect density was observed after the wafers had been preannealed for 150 minutes or longer.

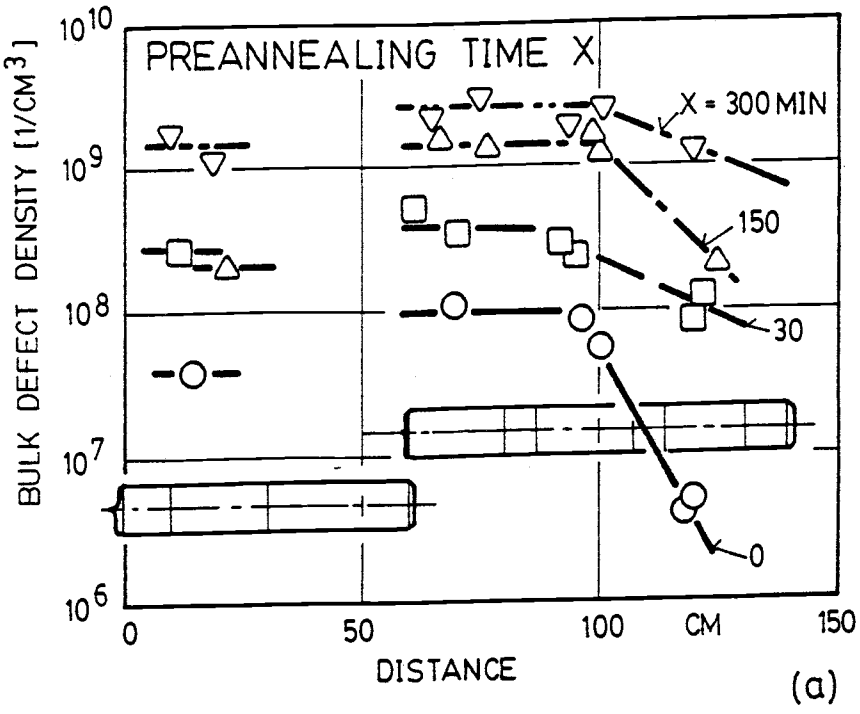

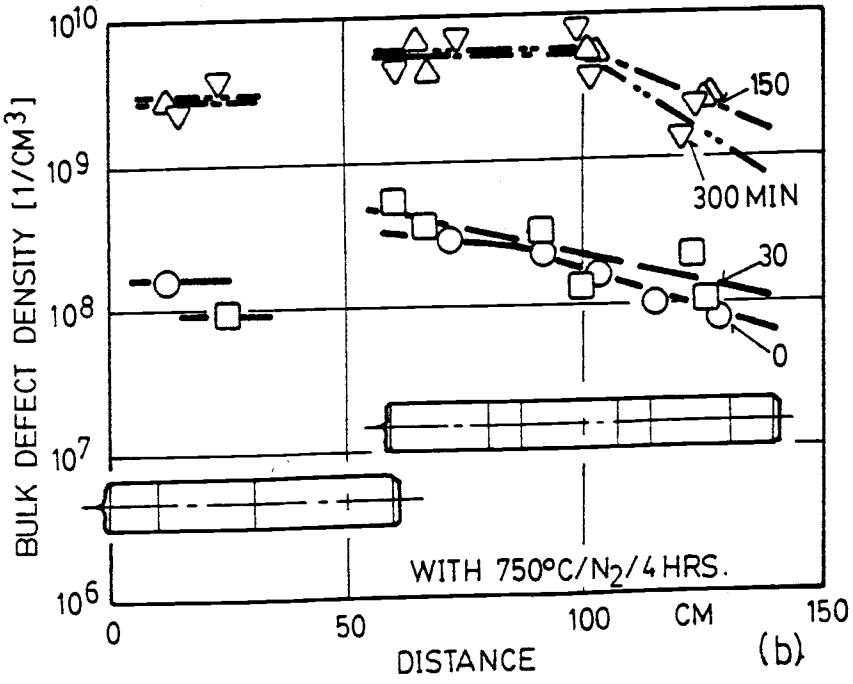

Figure 36: Bulk Defect Distribution in Crystal Ingot Containing Medium Oxygen Concentration: a) Without and b) With Post-Epitaxial Deposition Annealing

5. Growth Kinetics of the Bulk Defects.

T. Abe, et al [7] have studied the microdefects and impurities in dislocation-free silicon crystals. In FZ-silicon it was found that D-defects [108], which are generated at relatively low temperatures, are grown-in microprecipitates. They are formed by precipitation of residual oxygen atoms and surrounded by a cloud of vacancies. This type of microprecipitate is dissolved when the vacancies around them have been annihilated. Annihilation can be caused by out-diffusion of vacancies or by vacancy and silicon self-interstitial recombination. For this reason, retardation of the oxygen precipitation process in silicon is due to oxidation induced self-interstitials, as observed by Hu [94]and Rozgonyi [109].

a. Bulk Defect Density Distribution.

Microprecipitates, as characterized by T. Abe, are the heterogeneous nucleation sites for oxide precipitates. It is assumed that microprecipitate density along the crystal axis depends upon crystal growth parameters such as crystal pull-rate. If there is no fluctuation in pull-rate the microprecipitates must be uniformly distributed throughout the crystal ingot. Up to this point, the microprecipitate size in an as-grown silicon crystal has not been well characterized. However, it is possible that microprecipitates located in the seed-end of the crystal are much larger than those in other sections. This is because the seed-end section spent much more time in the crystal growth chamber than the other sections. During that period, the section undergoes a temperature change which results in growth of microprecipitates. For this reason, bulk defects in that

section are more stable and can withstand the dissolution during the epitaxial deposition process and subsequent heat treatment.

During preannealing, residual oxygen atoms form precipitate nuclei by a homogeneous nucleation process and/or diffuse toward microprecipitates , a heterogeneous nucleation. Homogeneous nucleation can cause the formation of additional precipitate nuclei, while during the heterogeneous nucleation process, microprecipitates will increase their size. A prolonged preannealing process leads to a significant increase in microprecipitate size, which may eventually exceed the critical nuclei size. Since a higher bulk defect density in crystal containing medium oxygen concentration was observed, homogeneous nucleation should also be considered here. Figure 37 shows the model for microprecipitate density and size distribution along the crystal axis.

In the case where post-epitaxial deposition annealing at 750° C was applied, higher defect density was observed. This is because during the 750° C annealing process heterogeneous nucleation takes place at the microprecipitates which remain from the epitaxial deposition process. Some of those microprecipitates would be completely dissolved during the subsequent CMOS process if this 750° C annealing was not applied. Therefore, post-epitaxial deposition annealing is very effective where no, or a short, preannealing time was applied.

b. Bulk Defect Size.

As is known, the growth of precipitates requires either the presence of vacancies or the generation of silicon self-interstitials. If silicon self-interstitials are generated, they will incorporate

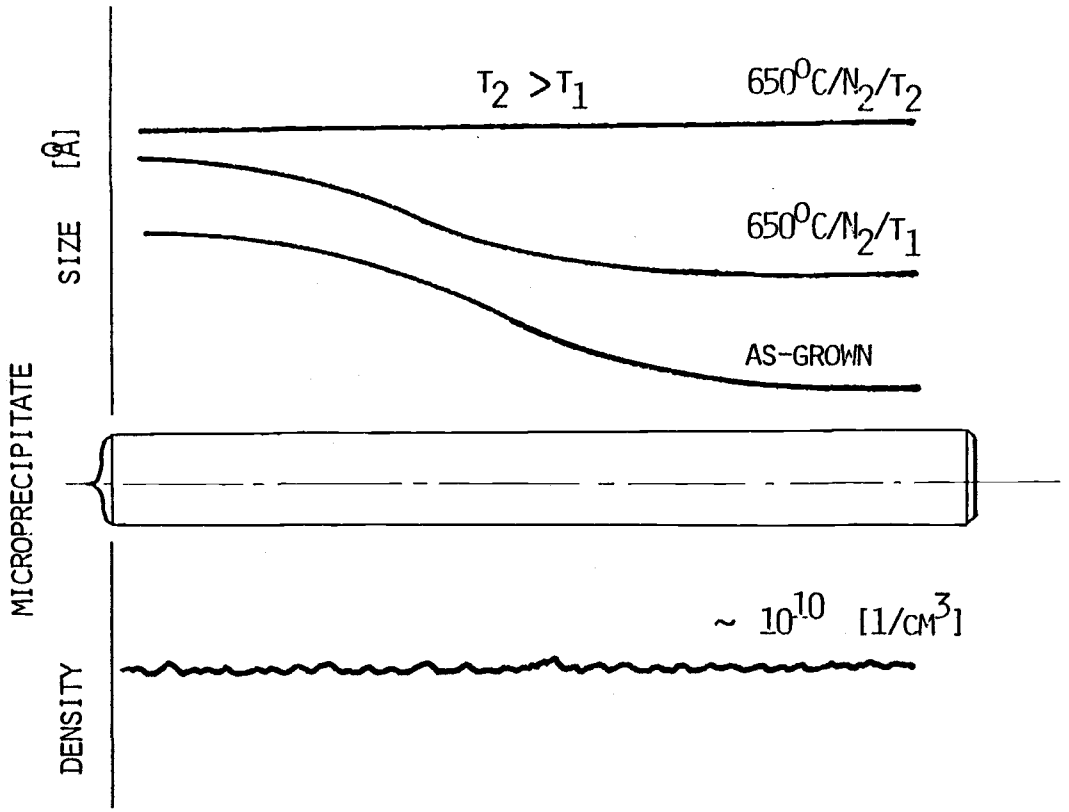

Figure 37: Model for Microprecipitate Size and Density Distribution along the Crystal Axis

into the silicon lattice by formation of an extra plane. This will result in an extrinsic stacking fault and interstitial dislocation loop formation. It is believed that the formation of extrinsic stacking faults as described above is not similar to that proposed by Freeland [84] - [85]. Bourret et al [110] and Ponce, et al [111] reported on microdefects formed after prolonged heat treatment at low temperatures. Under the bright field TEM, those microdefects were identified as a) oxide precipitate platelets and b) small stacking faults lying along (111) planes. Oxide precipitate platelets will grow into small polyhedral precipitates after high temperature heat treatment, and later on induce the bulk stacking faults (BSFs). Small stacking faults will become larger during heat treatment and presumably turn into microstacking faults (MSFs).

As mentioned above, an extended preannealing can cause an increase in the density of stable microprecipitates, which in turn causes supersaturation of excess silicon atoms in the matrix. R.A. Hartzell, et al [112] have found that supersaturation of excess self-interstitials could increase the free energy of precipitates and tends to inhibit nucleation or slow growth. Consequently, in silicon containing high density of microprecipitates, microprecipitates will grow only at a very slow rate. As the nucleation process continues and growing precipitate particles inject more excess self-interstitials into the silicon matrix, small stacking faults and interstitial dislocation loops are formed. Because microprecipitates can not grow to a sufficiently large size, a large portion of them will be dissolved during the epitaxial deposition process. On the other hand, small extrinsic stacking faults and dislocation loops can not be

dissolved and will grow in size. Unlike bulk stacking faults, the growth of small extrinsic stacking faults is not related to the length of the high temperature cycles. Instead, the total growth is limited by the excess self-interstitial concentration. Therefore, when prolonged preannealing was applied, most of the stacking faults observed were microstacking faults (MSFs).

Figure 38 shows the relationship between average stacking fault length L_{sf} and preannealing time in crystal ingot containing medium oxygen concentration. From Figure 38a, the average stacking fault length in the seed-end and center section decreases with increasing preannealing time. It should be mentioned that most of the stacking faults found in the cross-section are BSFs. In the single-section and tang-end, however, the average length initially increases with increasing preannealing time and decreases after the average length reached is a maximum. From observation, it was found that BSF density is low when no, or a short, preannealing was applied. As the preannealing time increases, BSF as well as MSF density increases. However, for prolonged preannealing only MSFs were found in the cross-section. In the case where the wafers were annealed at $750^{\circ}C$, the average stacking fault length in all sections seems to decrease with increasing preannealing time.

In Figures 39a and 39b total effective gettering length L_{eff} versus preannealing time is plotted. The effective gettering length is defined as the product between the average stacking fault length and the bulk defect density. From the figures, the relationship between the total effective gettering length and preannealing time is similar to that between bulk defect density and preanneal time. This occurs because in general bulk defect size found in the samples is small, so

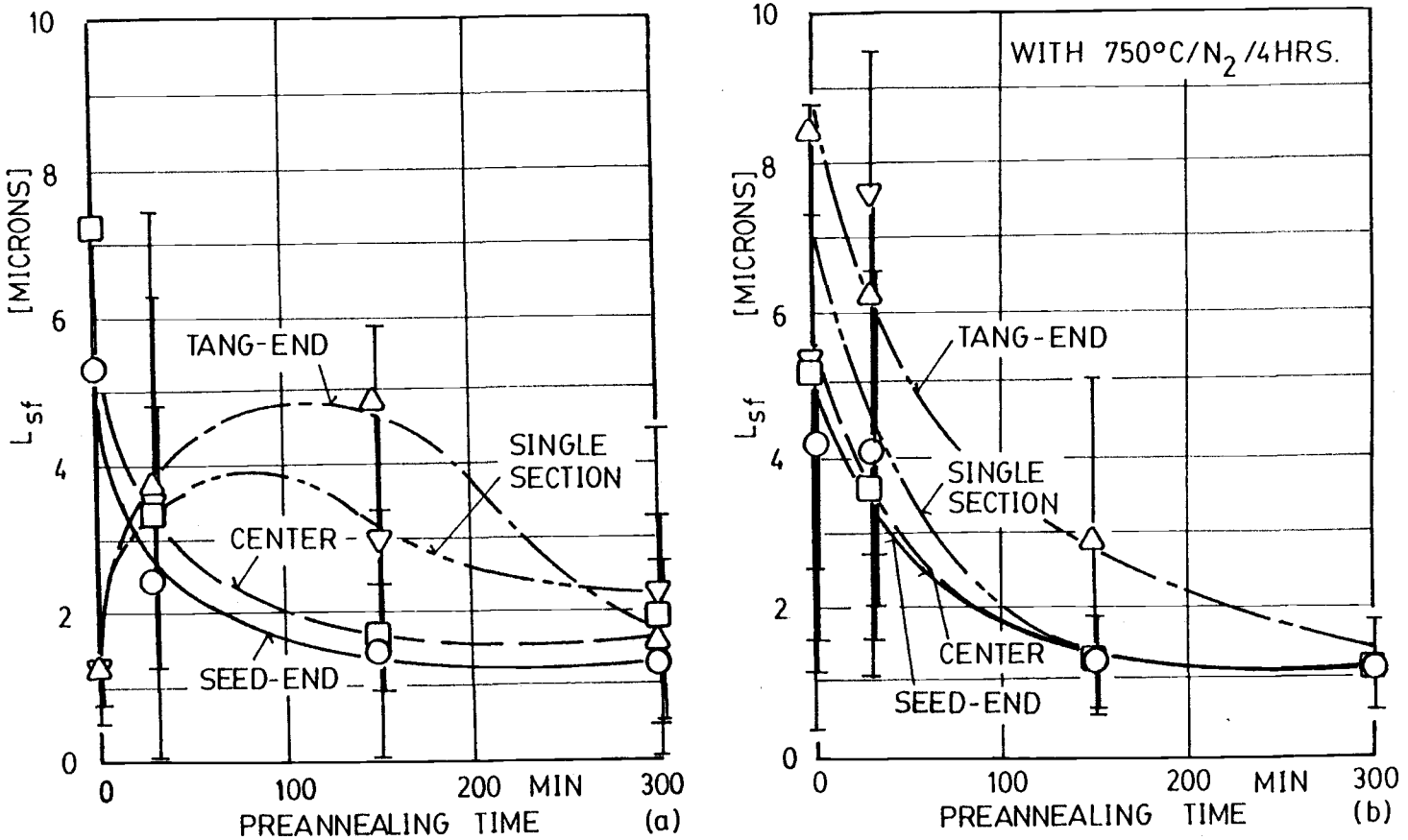

Figure 38: Relationship between Average Stacking Fault Length Lsf and Preannealing
a) Without and b) With Post Epitaxial Deposition Annealing

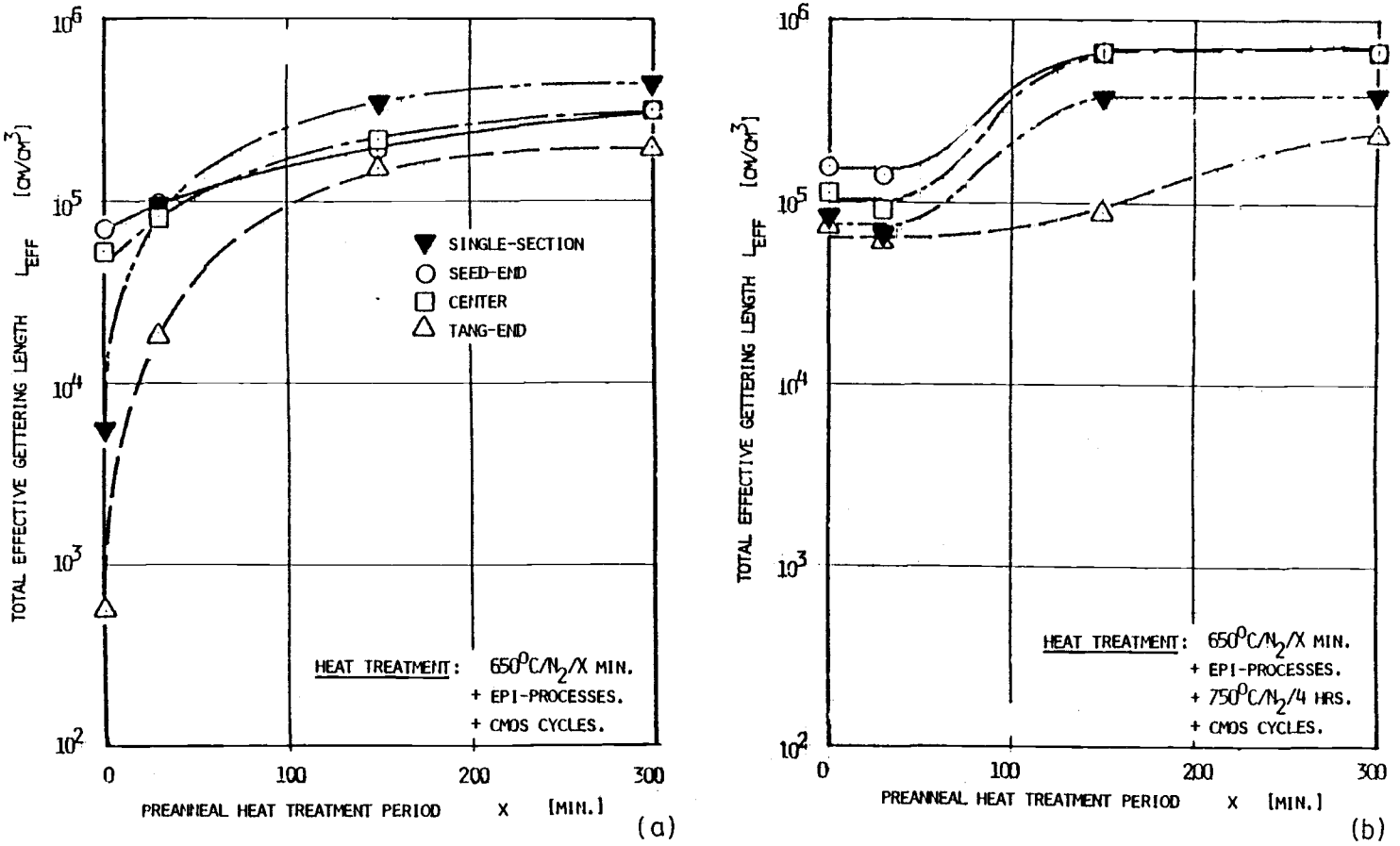

Figure 39: Relationship between Total Effective Gettering Length Leff and Preannealing
a) Without Post-Epitaxial Deposition Annealing
b) With Post-Epitaxial Deposition Annealing

because in general bulk defect size found in the samples is small, so that the average stacking fault length becomes a secondary factor in the product between the average stacking fault length and the bulk defect density.

C. Impact of Epitaxial Deposition Processes on the Growth Kinetics of the Bulk Defects.

Figures 40a and 40b show the bulk defect distribution in both crystals after a one-step heat treatment at 1050 C for 24 hours. It can be seen that the bulk defect distribution obtained from substrate wafers is uniformly distributed throughout the crystals. Except in the seed-end of the crystal containing medium oxygen concentration, where bulk defect density seems to be slightly higher than the average. The average of the bulk defect density in substrate wafers from both crystals is approximately $4X10^{8}$ $[1/cm^{3}]$. In another case, where epitaxial wafers were used, bulk defect density decreases from the seed-end toward the tang-end section. The results for epitaxial wafers are identical to those shown in Figures 35a and 36a. Another observation shows that bulk defect density in the substrate and epitaxial wafers from the seed-end section of both crystals seems to be at the same level.

Figures 41a and 41b show bulk defect density distribution obtained from substrate and epitaxial wafers in both crystals after a two-step heat treatment. In epitaxial wafers, similar results to those shown in Figures 35b and 35b, were also observed. In the case where substrate wafers were used, bulk defect density is highest in the seed-end section and decreases toward the tang-end section. In the seed-end, bulk defect density in the crystal containing medium oxygen

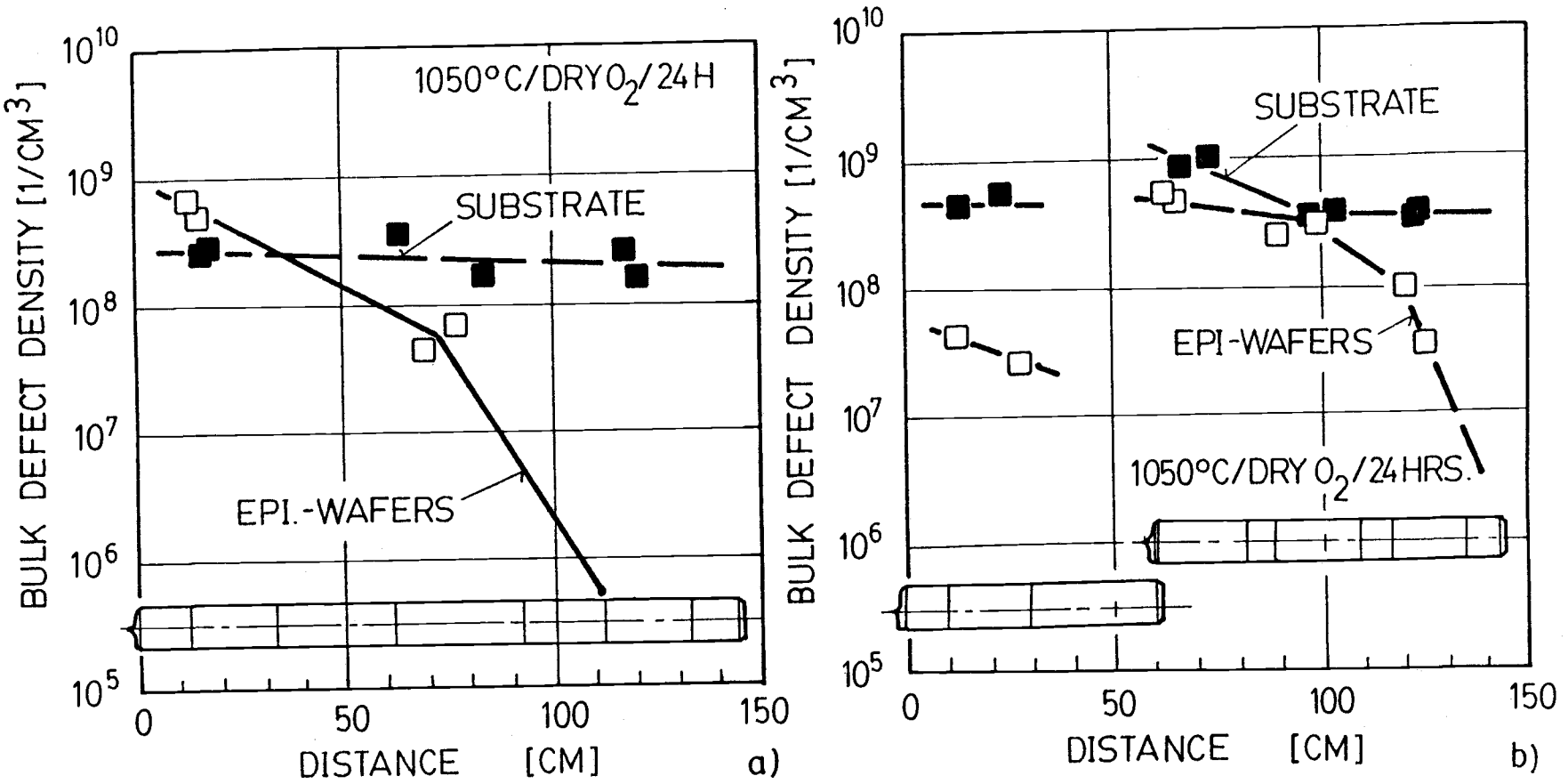

Figure 40: Bulk Defect Distribution after One-Step Heat Treatment in Crystal Ingot Containing
a) Low and b) Medium Oxygen Concentration

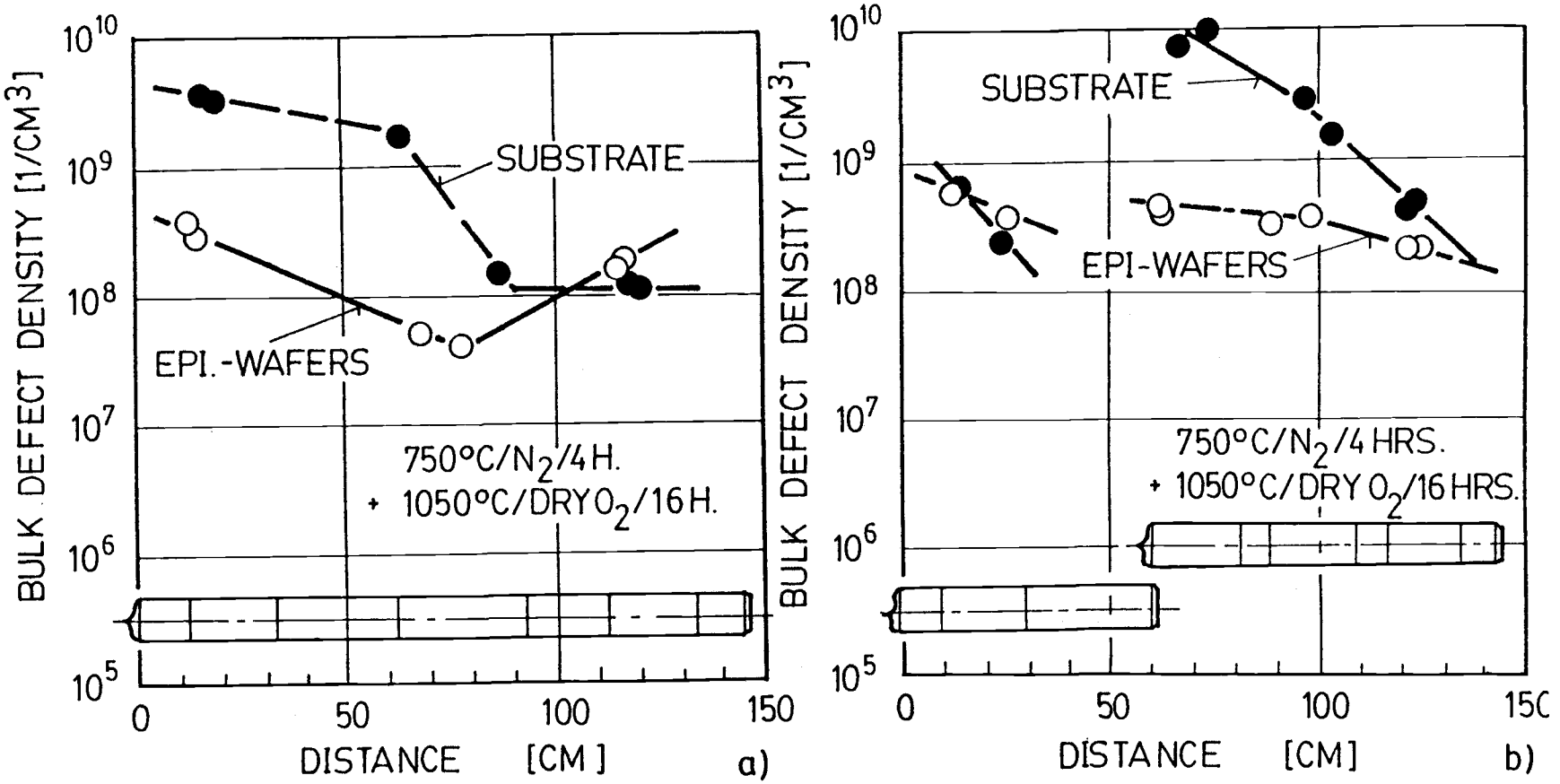

Figure 41: Bulk Defect Distribution after Two-Step Heat Treatment in Crystal Ingot Containing
a) Low and b) Medium Oxygen Concentration

bulk defect density in substrate as well as epitaxial wafers is at the same level.

From these results the following can be seen: Since bulk defects were observed after a one-step heat treatment, microprecipitates must exist in the as grown-crystal. Their density depends strongly on the growth parameter and is less influenced by the initial oxygen concentration (as observed in substrate wafers). Microprecipitates are typically uniformly distributed throughout the crystal ingot. Low bulk defect density in the tang-end section , as observed in eptaxial wafers, indicates the dissolution of microprecipitates during epitaxial deposition process. It is suggested that epitaxial deposition process generates a high concentration of silicon self-interstitials, which leads to retardation of the precipitation processes. This retardation is observed in the tang-end section of the ingot. This can be explained as follows: During the epitaxial deposition process microprecipitates are partially dissolved. Since small size microprecipitates can be found in the tang-end section of the crystal (see Figure 37), total dissolution of microprecipitates occurs during subsequent heat treatment.

The results from substrate and epitaxial wafers are plotted separately in Figures 42 and 43. In substrate wafers (Figure 42a and 42b) nucleation anneal at 750°C has no effect on the formation of the bulk defects in the tang-end section, but significant effect in the seed-end and center sections. This is because large size of microprecipitates can be found in the seed-end section (see Figure 37). Therefore large number of microprecipitates (having larger size than the critical nuclei size) is heterogeneously formed during

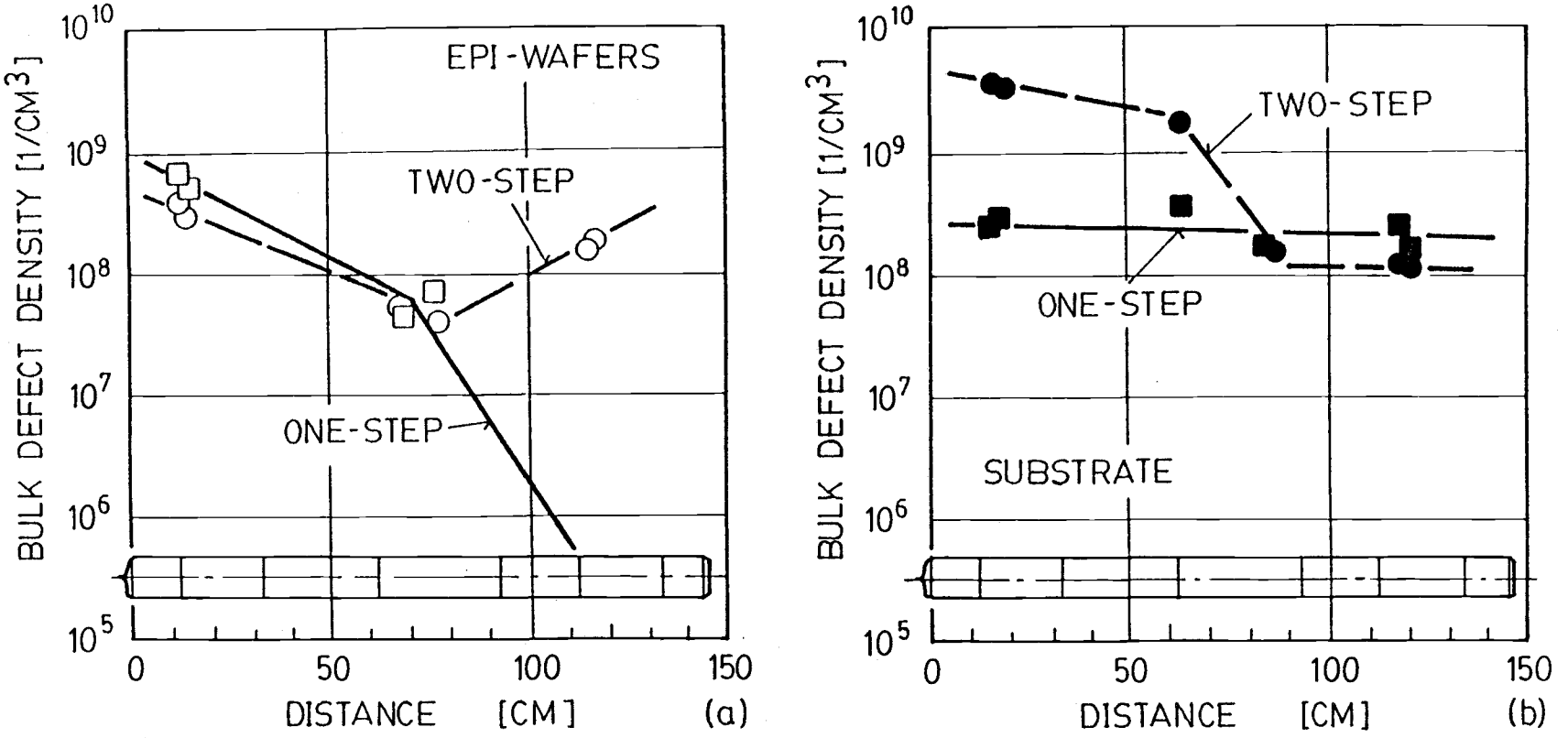

Figure 42: Bulk Defect Distribution in the Crystal Containing Low Oxygen Concentration: a) Epitaxial Wafers and b) Substrate Wafers.

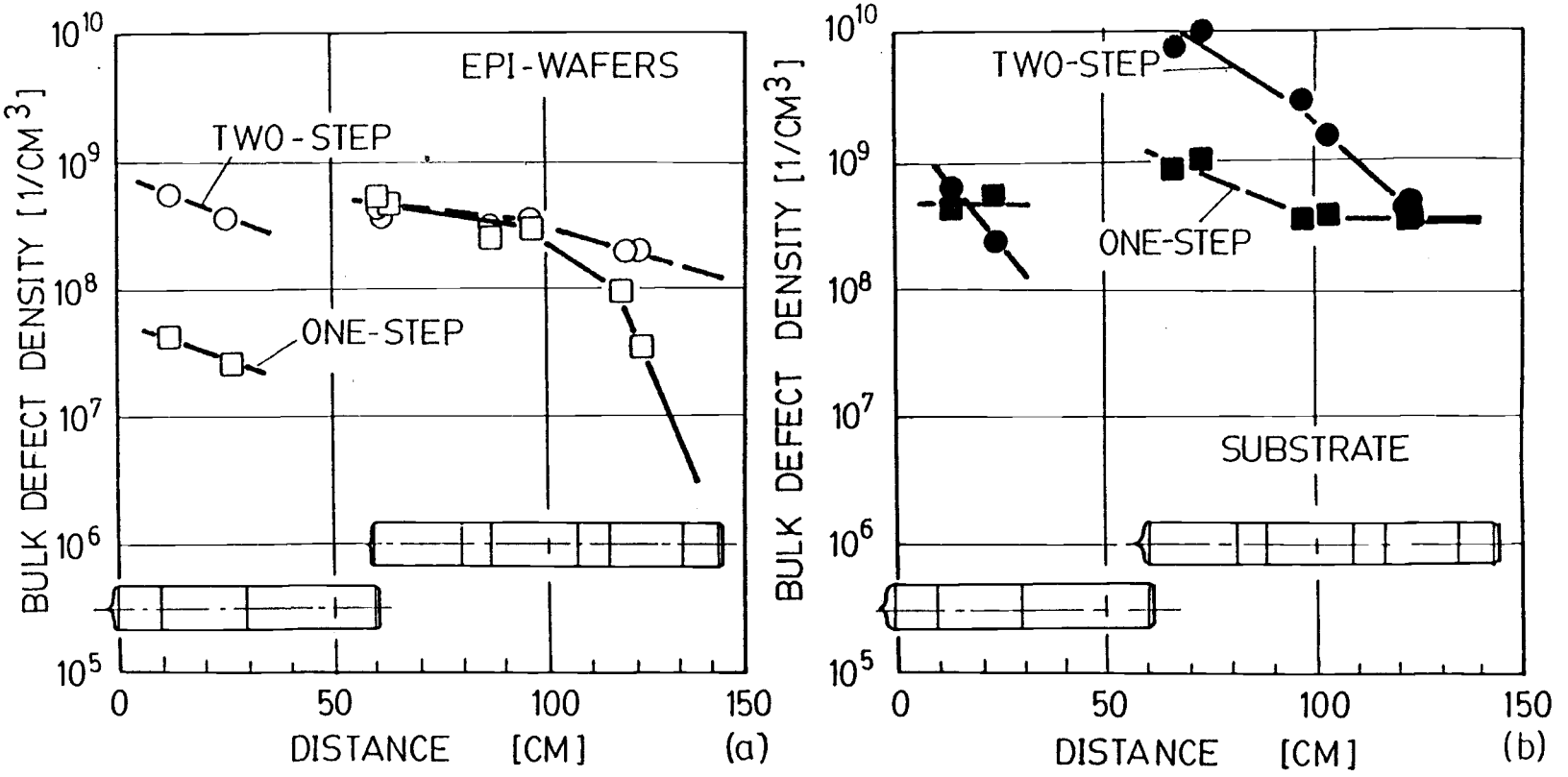

Figure 43: Bulk Defect Distribution in the Crystal Containing Medium Oxygen Concentration: a) Epitaxial Wafers and b) Substrate Wafers.

nucleation anneal. In epitaxial wafers, on the other hand, nucleation anneal has an effect on the formation of bulk defects only in the tang-end section. As explained above, microprecipitates in the tang-end are partially dissolved during epitaxial deposition process and completely dissolved during subsequent heat treatment. Regrowth of microprecipitates took place during nucleation anneal and in turn causes retardation of the total dissolution process.

VII CONCLUSIONS

It has been shown that the thermal history of epitaxial silicon wafers plays a significant role in the nucleation and growth of the oxide precipitates. Ambients influence also the growth of the bulk defects, but not significantly. Both pre- and post-epitaxial deposition annealing enhances the growth process due to heterogeneous nucleation. In general it can be concluded as follows:

A. Post-Epitaxial Deposition Heat Treatment.

In this experiment it has been shown that the ambients can affect the growth of the bulk defects in epitaxial silicon wafers during post-epitaxial heat treatment. The effect of ambients is, however, suppressed by application of nucleation heat treatment prior to post-epitaxial heat treatment. This is because during the nucleation heat treatment, preexisting nuclei increase their size and become stable. Stable nuclei are less affected by the ambients. Denudation of epitaxial silicon material is also affected by the denuding ambients. The mechanism of the denuded zone formation is controlled by oxygen out-diffusion and point defect interaction. The bulk defect formation mechanism, on the other hand, is controlled by the point defects generated during the denuding cycles.

B. Pre-Epitaxial Deposition Heat Treatment.

From the experimental results and observations it is concluded that:

1. The warpage in p/p+(100) epitaxial silicon wafers is not influenced by the oxygen precipitation. Warp decreases after

the heat treatment, and the final warp of the wafers tested in this experiment seems to depend upon the initial warp of the wafers. It can be concluded that oxygen precipitation can not directly result in warp of the epitaxial silicon wafers. Directly warpage is caused by the thermal stresses generated by the film deposited on the wafer surface or during fast push and pull.

2. Three types of bulk defects can be observed after preferential etch in the Wright etch solution ultilizing the scanning electro microscope (SEM): a) Bulk Stacking Faults (BSFs), b) Micro Stacking Faults (MSFs) and c) Precipitate Particles. However, under the optical light microscope at 200x magnification only two types of defects, BSFs and MSFs, can be detected.
3. The bulk defect density increases with increasing preannealing time.
4. Post-epitaxial deposition annealing at 750^{o}C in nitrogen ambient enhances the nucleation rate of the bulk defects, only when no, or a short, preannealing is applied.
5. The bulk defect density in the seed-end section is higher than that in the other sections of the ingot. This behavior is not related to the initial oxygen concentration in the crystal. Bulk defect density can, therefore, not be correlated directly to the oxygen data. However, high oxygen concentration crystal ingot shows higher bulk defect density after heat treatment.
6. Preannealing does not influence the defect distribution in an as-grown stage. Therefore, it is concluded that bulk defects

are formed preferentially by the heterogeneous nucleation process.

7. Two major factors which influence the nucleation and growth of the bulk defects are: a) Thermal history of the ingot and b) Oxygen concentration. For an extended preanneal heat treatment thermal history of the crystal ingot predominates the bulk defect generation process in the epitaxial silicon materials.

VIII. REFERENCES

[1] A. Seeger, K.P. Chik, Phys. Stat. Sol.,29(1968)455.

[2] A. Seeger, M.L. Swansen,in "Lattice Defects in Semiconductors", R.R.Hasiguti,ed., (University of Tokyo Press and the Pennsylvania State University Press, 1968)p.93.

[3] S. Mahajan, G.A. Rozgonyi, and D. Brasen, Appl.Phys.Lett., 30(1977)73.

[4] A.J.R. deKock, P.J. Roksnoer, and P.G.T. Boonen, J.Cryst.Growth, 22(1974)311.

[5] J.I. Chikawa and S. Yoshikawa, Solid State Tech., 23(1980)65.

[6] G.D. Watkins, IEEE 70 CH-1175-9NPS(1976).

[7] T. Abe, H. Harada, and J.I. Chikawa, in"Defects in Semiconductors II", S. Mahajan and J.W. Corbett, eds., (Materials Research Society, Symp. Proc., Vol. 14,1983)p.1.

[8] W. Zulehner and D. Huber, "Crystals: Growth, Properties and Applications", H.C. Freyhardt,ed., (Springer-Verlag,Berlin,1982) p.1.

[9] A. Murgai, W.J. Patrik, J. Combronde, J.C. Felix, IBM J.Res. Develop, 26(1982)546.

[10] W.L. Bond, and W. Kaiser, J.Phys.Chem.Solids, 16(1960)44.

[11] Y. Yatsurugi, N. Akiyama, Y. Endo, and T. Nozaki, J.Electrochem. Soc., 120(1973)9.

[12] W. Kaiser, Phys.Rev., 105(1957)1751.

[13] C.S. Fuller, F.H. Doleiden, and K. Wolfstirn,J.Phys.Chem. Solids, 13(1960)187.

[14] H. J. Hrostowski, and R.H. Kaiser, Phys.Rev.Letters,1(1958)199.

[15] A.R. Bean, and R.C. Newman, J.Phys.Chem.Solids, 33(1972)255.

[16] A.R. Bean, and R.C. Newman, J.Phys.Chem.Solids, 32(1971)1211.

[17] K. Graff, and H. Pieper, J.Electronic Mat., 4(1975)281.

[18] K. Graff, H. Pieper, and G. Goldbach, in"Semiconductor Silicon", H.R. Huff, R.R. Burgess, eds., (The Electrochemical Soc., NY, 1973)p.170.

[19] S.M. Hu and W.J. Patrick, J.Appl.Phys., 46(1975)186.

REFERENCES - Continued

[20] S.M. Hu, Appl.Phys.Lett, 31(1977)53.

[21] K. Yasutake, M. Umeno, H. Kawabe, H. Nakayama, T. Nishino, and Y. Hamakawa, Jpn.J.Appl.Phys., 19(1980)L544.

[22] M. Tajima, A. Kanamori, S. Kishino and T. Iizuka, Jpn.J.Appl. Phys., 19(1980)L755.

[23] M. Tajima, T. Masui, T. Abe, and T. Iizuka, in"Semiconductor Silicon 1981", eds. H.R. Huff, R.J. Kriegler and Y. Takeishi, (The Electrochemical Soc., Pennington, 1981)p.72.

[24] P.M. Grinshtein, G.V. Lazareva, E.V. Orlova, Z.A. Sal'nik, and V.I. Fistul', Sov.Phys.-Semicond., 12(1978)68.

[25] A. Kanamori and M. Kanamori, J. Appl.Phys., 50(1979)8095.

[26] A.C. Bonora, in"Silicon Crystal Growth and Processing Technology: A review," Silicon Processing, ASTM STP 804, D.C. Gupta, ed., American Society for Testing and Materials, 1983, p.5-23.

[27] R.B. Swaroop, Solid State Tech., 26(1983)111.

[28] S. Kishino, M. Kanamori, N. Yoshihiro, M. Tajima, and I. Iizuka, J.Appl.Phys., 50(1979)8240.

[29] H. Walitzki and M. Blaette,in"VLSI Science and Technology/1984", K.E. Bean, and G.A. Rozgonyi, eds, (the Electrochemical Society, Pennington, NJ)p.10.

[30] K.V. Ravi and C.J. Varker, J.Appl.Phys., 45(1974)263.

[31] A.J.R. de Kock, J.Electrochem.Soc., 118(1971)1851.

[32] A.J.R. de Kock, Appl.Phys.Lett., 16(1970)100.

[33] A.J.R. de Kock, Philips Res.Rept., Suppl.No. 1(1973).

[34] L.I. bernewitz, B.O. Kolbesen, K.R. Mayer, and G.E. Smith, Appl. Phys.Lett., 25(1974)277.

[35] H. Foll, U. Goesele, and B.O. Kolbesen,in"Semiconductor Silicon 1977", H.R. Huff, and E. Sirtl, eds., (the Electrochem. Society, Pennington, 1977)p.565.

[36] H. Foll, U. Goesele, and B.O. Kolbesen, J. Crystal Growth, 40(1977)90.

[37] H. Foll, B.O. Kolbesen, and W. Frank, Phys.State.Solidi, (a)29, K83(1975).

REFERENCES - Continued

[38] P.M. Petroff and A.J.R. deKock, J. Cryst. Growth, 30(1975)117.

[39] P.M. Petroff and A.J.R. deKock, J. Cryst. Growth, 36(1976)1822.

[40] P.M. Petroff and A.J.R. deKock, J. Cryst. Growth, 35(1976)4.

[41] K.V. Ravi, in "Imperfections and Impurities in Semiconductor Silicon", (John Wiley & Sons, New York, 1981)p.77.

[42] U. Goesele and W. Frank,in"Defects in Semiconductors",J. Narayan and T.Y. Tan, eds, (Materials Research Society,NY, 1981)p.55.

[43] S.M. Hu, J.Appl.Phys., 45(1974)1567.

[44] B. Leroy, J.Appl.Phys., 50(1979)7996.

[45] H.J. Queisser and P.G.G. Van Loon, J.Appl.Phys., 35(1964)3066.

[46] G.R. Booker and R. Stickler, Phil.Mag., 11(1965)1303.

[47] W.A. Fisher and J.A. Amick, J.Electrochem.Soc.,113(1966)1054.

[48] G.R. Booker and W.J. Tunstall, Phil.Mag., 13(1966)71.

[49] J.M. Silcock and W.J. Tunstall, Phil.Mag., 10(1964)361.

[50] K.V. Ravi and C.J. Varker, J.Appl.Phys., 45(1974)263.

[51] A. Mayer, RCA Review, June 1970, (1970)415.

[52] G.A. Rozgonyi, S. Mahayan, M.H. Read, and D. Brasen, Appl.Phys.Lett., 29(1976)531.

[53] D.A. Antoniadis, A.G. Gonzalez and R. Dutton, J.Electrochem.Soc. 125(1978)814.

[54] K. Taniguchi, K. Karosawa, and M. Kashiwagi, J.Electrochem.Soc., 127(1980)2243.

[55] K.H. Nicholas, Solid State Electronic, 9(1966)35.

[56] G. Masetti, S. Solmi, and G. Soncini, Solid State Electronic, 16(1973)1419; Phil.Mag., 33(1976)613.

[57] R. Francis and P.S. Dobson, J.Appl.Phys., 50(1979)280.

[58] R.N. Ghostagore, Appl.Phys.Lett., 17(1970)137.

[59] P.S. Dobson, Phil.Mag., 24(1971)567.

REFERENCES - Continued

[60] K.V. Ravi, in "Imperfections and Impurities in Semiconductors Silicon", (John Wiley & Sons, New York, 1981)p.101.

[61] D.A. Antoniadis, A.M. Lin, and R.W. Dutton, Appl.Phys.Lett., 33(1978)1030.

[62] R. Conti, G. Corda, R. Mattecci, and G. Ghezzi, J.Mat.Sci., 10(1975)705.

[63] S.P. Murarka and G. Quintana, J.Appl.Phys., 48(1977)46.

[64] S.P. Murarka, Phys.Rev., B 16, (1977)2849.

[65] J.E. Lawrence, J.Appl.Phys., 40(1969)360.

[66] S.M. Hu, Appl.Phys.Lett., 27(1975)165.

[67] H. Shiraki, Jap.J.Appl.Phys., 14(1975)747.

[68] H. Shiraki, Jap.J.Appl.Phys., 15(1976)1.

[69] T. Hattori, J.Electrochem.Soc., 123(1976)945.

[70] C.L. Claeys, E.E. Laes, G.J. Declerck, and R.J. Van Overstraeten, in"Semiconductor Silicon 1977", H.R. Huff and E. Sirtl, eds., (the Electrochemical Society, Princeton,1977)p.773.

[71] Y. Hokari and H. Shiraki, Jap.J.Appl.Phys., 16(1977)1899.

[72] T. Hattori and T. Suzuki, Appl.Phys.Lett., 33(1978)347.

[73] I.R. Sanders and P.S. Dobson, J.Mat.Sci., 9(1974)1987.

[74] U. Goesele and H. Strunk, J.Appl.Phys., 20(1979)265.

[75] Y. Hokari, Jap.J.Appl.Phys., 18(1979)873.

[76] I.R. Sanders and P.S. Dobson, Phil.Mag., 20(1969)280.

[77] R.E. Reed-Hill, in"Physical Metallurgy Principles", 2.ed.,(D. Van Nostrand Co., New York, 1973)p.358.

[78] J.R. Patel, in"Semiconductor Silicon 1981", H.R. Huff, R.J. Kriegler, and Y. Takeishi, (the Electrochemical Society, Pennington, 1981)p.189.

[79] Y.B. Zeldovich, Zh.Eksp.Teor.Fiz., 12(1942)525.

[80] E.A. Irene, E. Tierney, and J. Angilello, J.Electrochem.Soc., 129(1982)2594.

RFERENCES - Continued

[81] N. Inoue, K. Wada, and J. Osaka, in "Semiconductor Silicon 1981" , H.R. Huff, R.J. Kriegler, and Y. Takishi, eds.,(the Electrochemical Society, Pennington, 1981)p.282.

[82] H.J. Hrostowski and R.J. Kaiser, J.Phys.Chem.Sol., 9(1959)214.

[83] J. Osaka, N. Inoue, and K. Wada, Appl.Phys.Lett., 36(1980)288.

[84] P.E. Freeland, K.A. Jackson, C. Lowe, and J.R. Patel, Bull.Am.Phys.Soc., 21(1976)226.

[85] D.M. Maher, A. Staudinger, and J.R. Patel, J.Appl.Phys., 47(1976)3813.

[86] D.I. Pomerantz, J.Electrochem.Soc., 119(1972)255.

[87] J.H. Matlock, in"Defect in Silicon", W.M. Bullis and L.C. Kimerling, eds., (the Electrochemical Society, Pennington,1983) p.3

[88] R.B. Swaroop, Solid State Tech., 6(1983)111.

[89] L.E. Katz, P.F. Schmidt, and C.W. Pearce,J.Electrochem. Soc., 128(1981)620.

[90] G. Keefe-Fraundorf, R.A. Craven and D.E. Hill, IDEM, paper No. EE83-131 (1983).

[91] S.M. Hu, U.S. Patent, 4,653,335(1977).

[92] Y. Hayafuji, T. Yanada, and Y. Aoki, J.Electrochem.Soc., 128(1981)1975.

[93] M. Wright-Jenkins, J.Electrochem.Soc., 124(1977)752.

[94] S.M. Hu, Appl.Phys.Lett., 35(1980)561.

[95] K. Wada, N. Inoue, and J. Osaka, in"Defects in Semiconductors II", S. Mahajan and J.W. Corbett, eds., (Materials Research Society, Symp.Proc., Vol.14, 1983)p.125.

[96] J.R. Mankowski, et al , in"Semiconductor Processing, ASTM STP 850", D.C. Guta, ed., (American Society for Testing and Materials, 1984)p.219.

[97] J. Andrews, in"Defects in Silicon", W.M. Bullis, and L.C. Kimerling, eds., (The Electrochemical Society, Pennington, NJ, 1983)p.133.

REFERENCES - Continued

[98] R.B. Swaroop,in"Semiconductor Processing, ASTM STP 850", Dinesh C. Gupta, ed., (American Society for Testing and Materials, 1984)p.230.

[99] Y. Tarui, Jap.J.Appl.Phys., 19(1980)15.

[100] J.R. Patel, Faraday Soc., 38(1964)201.

[101] M. Stavol and L.C. Snyder, in"Defects in Silicon", W.M. Bullis and L.C. Kimerling, (The Electrochemical Society, Pennington, 1983)p.61.

[102] Y. Kondo, in"Semiconductor Silicon 1981", H.R. Huff, R.J. Kriegler, and Y. Takeishi, eds., (The Electrochemical Society, Princeton, NJ, 1981)p.220.

[103] V.V. Batavin, Sov.Phys.Solid State, 8(1967)2478.

[104] V.V. Batavin, Sov.Phys.Crystallogr., 15(1970)100.

[105] U. Goesele and T.Y. Tan, in"Impurity Diffusion and Gettering in Silicon", R.B. Fair, C.W. Pearce, and J. Washburn, eds., (Materials Research Society, Symp.Proc., Vol.36, 1984)p.105.

[106] I. Yonenaga and K. Sumino, Jap.J.Appl.Phys., 22(1982)47.

[107] A.K. Sinha, H.J. Levinstein, and T.E. Smith, J.Appl.Phys., 49(1978)2423.

[108] R.J. Roksnor and M.M.B. Van de Boom, J. Cryst.Growth, 53(1981)563.

[109] G.A. Rozgonyi, in"Defects in Silicon", W.M. Bullis, and L.C. Kimerling, eds.,(The Electrochemical Society, Pennington, N.J., 1983)p.23.

[110] A. Bourret, J. Thibault-Desseaux, and D.N. Seideman, J.Appl.Phys., 55(1984)825.

[111] F.A. Ponce, T. Yamashita, and S. Hahn, in"Defects in Silicon", W.M. Bullis and L.C. Kimerling,eds., (The Electrochemical Society, Pennington, NJ, 1983)p.105.

[112] R.A. Hartzell, H.F. Schaake, and R.G. Massey, in"Impurity Diffusion and Gettering in Silicon",R.B. Fair, C.W. Pearce, and J. Washburn,eds., (Materials Research Society, Pittsbury, 1984)p.217.